DOI 10.1007/978-1-4899-7413-6_18
Reprinted from *Space Science Reviews* Journal, DOI 10.1007/s11214-013-9972-y

The Dynamic Quasiperpendicular Shock: Cluster Discoveries

V. Krasnoselskikh · M. Balikhin · S.N. Walker · S. Schwartz · D. Sundkvist · V. Lobzin · M. Gedalin · S.D. Bale · F. Mozer · J. Soucek · Y. Hobara · H. Comisel

Received: 19 October 2012 / Accepted: 25 February 2013 / Published online: 28 March 2013

Abstract The physics of collisionless shocks is a very broad topic which has been studied for more than five decades. However, there are a number of important issues which remain unresolved. The energy repartition amongst particle populations in quasiperpendicular shocks is a multi-scale process related to the spatial and temporal structure of the electromagnetic fields within the shock layer. The most important processes take place in the close vicinity of the major magnetic transition or ramp region. The distribution of electromagnetic fields in this region determines the characteristics of ion reflection and thus defines the con-

V. Krasnoselskikh (✉)
LPC2E, CNRS-University of Orleans, Orleans, France
e-mail: vkrasnos@cnrs-orleans.fr

M. Balikhin · S.N. Walker
ACSE, University of Sheffield, Sheffield S1 3JD, UK

S. Schwartz
Blackett Laboratory, Imperial College London, London SW7 2AZ, UK

D. Sundkvist · S.D. Bale · F. Mozer
Space Sciences Laboratory, University of California, Berkeley, CA, USA

V. Lobzin
School of Physics, University of Sydney, Sydney, NSW, Australia

M. Gedalin
Department of Physics, Ben-Gurion University, Beer-Sheva, Israel

J. Soucek
Institute of Atmospheric Physics, Academy of Sciences of the Czech Republic, Prague, Czech Republic

Y. Hobara
Research Center of Space Physics and Radio Engineering, University of Electro-Communications, Tokyo, Japan

H. Comisel
Institute for Space Sciences, Bucharest, Romania

ditions for ion heating and energy dissipation for supercritical shocks and also the region where an important part of electron heating takes place. In other words, the ramp region determines the main characteristics of energy repartition. All these processes are crucially dependent upon the characteristic spatial scales of the ramp and foot region provided that the shock is stationary. The process of shock formation consists of the steepening of a large amplitude nonlinear wave. At some point in its evolution the steepening is arrested by processes occurring within the shock transition. From the earliest studies of collisionless shocks these processes were identified as nonlinearity, dissipation, and dispersion. Their relative role determines the scales of electric and magnetic fields, and so control the characteristics of processes such as ion reflection, electron heating and particle acceleration. The determination of the scales of the electric and magnetic field is one of the key issues in the physics of collisionless shocks. Moreover, it is well known that under certain conditions shocks manifest a nonstationary dynamic behaviour called reformation. It was suggested that the transition from stationary to nonstationary quasiperiodic dynamics is related to gradients, e.g. scales of the ramp region and its associated whistler waves that form a precursor wave train. This implies that the ramp region should be considered as the source of these waves. All these questions have been studied making use observations from the Cluster satellites. The Cluster project continues to provide a unique viewpoint from which to study the scales of shocks. During its lifetime the inter-satellite distance between the Cluster satellites has varied from 100 km to 10000 km allowing scientists to use the data best adapted for the given scientific objective.

The purpose of this review is to address a subset of unresolved problems in collisionless shock physics from experimental point of view making use multi-point observations onboard Cluster satellites. The problems we address are determination of scales of fields and of a scale of electron heating, identification of energy source of precursor wave train, an estimate of the role of anomalous resistivity in energy dissipation process by means of measuring short scale wave fields, and direct observation of reformation process during one single shock front crossing.

Keywords Collisionless shocks · Waves in plasmas · Nonstationarity · Shock scales · Plasma heating and acceleration · Wave-particle interactions

1 Introduction

Collisionless shocks (CS) are ubiquitous in the universe. They play an important role in the interaction of the solar wind with the planets (Russell 1977, 1985; Greenstadt and Fredricks 1979; Ness et al. 1974, 1981), they also are supposed to have vital role in fundamental astrophysical problems such as cosmic ray acceleration (Krymskii 1977; Axford et al. 1977; Bell 1978a, 1978b; Blandford and Ostriker 1978). CS's are of crucial importance for understanding physical processes in the vicinity of such astrophysical objects as supernova remnants (Koyama et al. 1995; Bamba et al. 2003), plasma jets (Piran 2005), binary systems and ordinary stars. In spite of this great variety of CS in the Universe only those shocks in the Solar system can be probed using in-situ observations. Moreover, comprehensive in-situ data exist only for interplanetary shocks and planetary bow shocks, however, it is worth noting that some astrophysical shocks are similar to those in the solar system. As was noted by Kennel et al. (1985) 'The density, temperature and magnetic field in the hot interstellar medium are similar to those in the solar wind, and the Mach numbers of supernova shocks at the phase when they accelerate the most cosmic rays are similar to

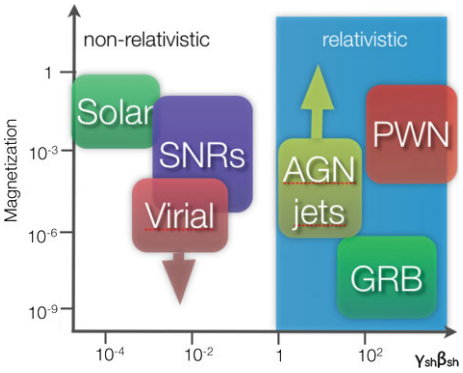

Fig. 1 (Courtesy of A. Spitkovsky) Parametric range of observations of collisionless shocks associated with different astrophysical objects

those of solar wind shocks'. Astrophysical shocks associated with different objects exhibit large differences in the parameters that characterise them. Figure 1 shows the variation of astrophysical shocks as a function of magnetisation (Y-axis), determined as $1/M_A$ where M_A is the Alfvén Mach number (the ratio of the upstream flow velocity to the characteristic velocity of propagation of magnetic perturbations in a plasma or Alfvén velocity) and the characteristic plasma pressure to magnetic pressure ratio (X-axis) where γ_{sh} is the ratio of the upstream flow velocity to the velocity of light and β_{sh} the ratio of total plasma particle thermal pressure to the magnetic field pressure in the reference frame of the upstream flow. Collisionless shocks associated with different astrophysical objects such as Supernovae Remnants (SNR), Active Galactic Nuclei jets (AGN), Pulsar Wind Nebulae (PWN), and Gamma Ray Bursts (GRB) are indicated.

As can be seen from this figure, different 'families' of shocks occupy different regions of parameter space. One can also see that the parameters of SNR shocks are quite similar to those of solar system shocks. It allows one to suggest that the studies of solar system shocks, and in particular Earth's bow shock, represents an interest for wider scientific community than only for geophysics. The majority of astrophysical and Solar system shocks are developed in magnetised plasmas.

Collisional shocks have been studied for many decades, beginning with the earliest observations of Mach (Mach and Arbes 1886; Mach and Salcher 1887). A shock occurs when an obstacle finds itself immersed in a supersonic gas flow. Before reaching the surface of the obstacle the flow should be decelerated to velocities lower than the velocity of sound so that it may flow around the body. This process of flow deceleration and the redistribution of its directed energy occurs over distances of the order of the collisional mean free path of gas particles. The energy taken from the flow during deceleration is mainly transformed into the thermal energy of the gas as it is heated. As a result the sound velocity in the gas increases and, after the shock transition, becomes larger than the remaining directed velocity of the flow so that the motion downstream of the shock is subsonic. Thus the shock represents the transition from supersonic directed motion to subsonic in the reference frame of the obstacle immersed into the flow.

The notion of the collisionless shock was introduced by several authors in the late 50's (Adlam and Allen 1958; Davis et al. 1958; Sagdeyev 1960). The modern form of the description was presented in an almost complete form in the famous review paper by Sagdeev (1966). The first problem to be overcome is related to the the existence of a shock. For collisional shocks (as mentioned above) the shock thickness is related to the mean free path of the gas particles. However, in space plasmas the mean free path can be as large as 5 AU (i.e. similar to the distance of Jupiter from the Sun)! So, how can a shock exist whose width is

much smaller than the mean free path? Historically, a very similar problem first appeared in laboratory devices and only later in space plasmas. However the crucial issue in both cases is exactly the same (Paul et al. 1965; Kurtmullaev et al. 1965, 1967; Ascoli-Bartoli et al. 1966; Goldenbaum and Hintz 1965).

The solution proposed initially relied on the processes of anomalous dissipation, namely, anomalous resistivity. Thin shock transition contains quite strong variations of the magnetic field components perpendicular to its normal. This implies that there is a very intense current inside the shock transition layer. The current carriers, populations of charged particles, move with respect to one another. The plasma state supporting these intense currents is, in general, unstable. The instabilities in the plasma result in the generation of intense waves. Wave generation opens a new channel of impulse and energy exchange between the different populations of plasma particles. For instance, current carrying electrons can emit/generate the waves, and these waves can be absorbed by ions. This generation-absorption exchange using waves as a transmission media between plasma components leads to an exchange of energy and momentum between them. Typically, the characteristic scale of energy exchange between different particle populations can be much smaller than the mean free path of particles. As a result the characteristic scale of the dissipation process can be determined by this anomalous dissipation. Thus the principal difference between collisional and colisionless shocks is the change of the dissipation scale that is determined by additional processes involved, but the nature of the transition and its characteristics remain very similar. In both cases the shock redistributes the directed bulk plasma flow energy to plasma thermal energy. However, the dissipation rate and characteristic scales of collisionless shocks are determined by the anomalous process of energy dissipation. The notion of anomalous resistivity was already well known and widely used in plasma physics. The theory of anomalous resistivity based on current instabilities and the generation of ion-sound waves was directly applied to the theory of collisionless shocks by Galeev (1976). Later this idea was further developed in series of papers by Papadopoulos (1985a, 1985b), who noticed that in the case of currents perpendicular to the magnetic field the ion-sound instability is less efficient than the instability of lower-hybrid waves that propagate almost perpendicular to the magnetic field and the theory of anomalous resistivity in this case should account for these rather than for ion-sound waves.

From the earliest experimental studies of shocks in space and laboratory plasmas it was found that the characteristics of the shocks observed can be quite different even in the range of parameters that correspond to solar system shocks and those in laboratory plasmas. There were observations of quite small scales for the ramp with much longer precursor wave train, there were shocks consisting of a long transition region with large amplitude structures in the magnetic field filling a very large area in space. These early observations gave rise to attempts to classify shocks.

The first systematic classification was proposed by Formisano (1985). He noticed that there are three basic parameters of the upstream flow that are important for the classification. These are the angle between the magnetic field and shock front normal, θ_{Bn}, the plasma beta β, i.e. the ratio of total particle thermal pressure to the magnetic field pressure $\beta = 8\pi nT/B^2$, where T is the total plasma temperature, n is the plasma density, and B the magnitude of the magnetic field; and the magnetosonic Mach number $M_{Ms} = (V_{up}/V_{Ms})$, where V_{up} is the normal component of the velocity of the shock, V_{Ms} is the velocity of the magnetosonic wave propagating in the same direction as the shock. Later this classification was slightly modified and is used in the form proposed by Kennel et al. (1985). This paper divides shocks into two broad classes that are related to the ion dynamics, namely, quasiparallel and quasiperpendicular. The characteristic feature of the first group is that the ions that

are reflected from the shock front can freely propagate to the upstream region. These shocks correspond to the range of angles between the magnetic field and the normal vector to the shock front $\theta_{Bn} < 45°$. In the second group, quasiperpendicular, part of the ion population is reflected. After reflection they turn back to the upstream region and can gain extra energy due to the acceleration by inductive electric field tangential to the shock surface and perpendicular to the magnetic field. Then they can cross the shock front (Woods 1969, 1971; Sckopke et al. 1983). This process can occur when $\theta_{Bn} > 45°$.

Low Mach number shocks can dissipate the necessary energy entirely through some anomalous resistivity within the current-carrying shock layer. The right-hand fast magnetosonic/whistler waves have phase and group velocities that increase with decreasing wavelength beyond the fluid regime. Thus, steepened fast mode shocks are expected to radiate short wavelength waves, and hence energy, into the unshocked oncoming flow. The shortest wavelength capable of standing in the flow then forms a "precursor wavetrain" that has been observed at these sub-critical shocks (Mellott 1985) and as we shall show later this process occurs in supercritical shocks also. However, above a critical Mach number, anomalous resistivity within the layer carrying the limited shock current is unable to convert the required amount of energy from directed bulk flow into thermal energy. At quasi-perpendicular shocks, where the magnetic field in the unshocked region makes an angle $\theta_{Bn} > 45°$ with the shock propagation direction (the shock "normal" $\hat{\mathbf{n}}$), a fraction of the incident ions are reflected by the steep shock ramp as described above. They gyrate around the magnetic field and gain energy due to acceleration by the transverse motional electric field ($-\mathbf{V} \times \mathbf{B}$). Returning to the shock layer they have sufficient energy to pass through into the downstream shocked region (Woods 1969, 1971; Sckopke et al. 1983). The separation of ions onto two groups, crossing front directly and after the reflection, results in the dispersal of particles in the velocity space. Group of reflected particles is separated from the bulk ion population due to an increase in peculiar velocity relative to the bulk motion. This process corresponds to the kinetic "heating" required by the shock jump conditions and it ensures the major part of energy dissipation necessary for directed energy transfer to thermal energy of plasma ion population. The process of ion thermalization takes place on rather large scale downstream of the shock front. The spatial length of the transition to ion thermal equilibrium can be treated in a similar fashion to that of the shock front thickness in collisional shocks. Detailed measurements of ion distributions onboard ISEE mission resulted in establishing all major characteristics of this process (Sckopke et al. 1983). This result is probably one of the most important obtained in this outstanding program. In theory this critical Mach number corresponds to the multi-fluid hydrodynamic limit in which the resistivity and viscosity cannot provide sufficient dissipation (Coroniti 1970). The reflection occurs on sufficiently smaller scales than thermalization due to a combination of magnetic forces and an electrostatic cross-shock potential. The main potential, which corresponds to the frame-invariant $\mathbf{E} \cdot \mathbf{B}$ electric field, is known as the deHoffmann-Teller potential (de Hoffmann and Teller 1950; Goodrich and Scudder 1984). It results directly from the leading electron pressure gradient term in the Generalised Ohm's Law (Scudder et al. 1986b). However in more detailed two-fluid descriptions, the quasiperpendicular shock has fine structure that depends upon the characteristics of the nonlinear shock profile (Galeev et al. 1988, 1989; Gedalin 1997; Krasnoselskikh et al. 2002). In this paper we shall present the results of the studies of quasiperpendicular shocks only. Quasiparallel shocks will be discussed in a paper by Burgess and Scholer (this review).

The basic ideas of shock formation can be understood by considering the propagation and evolution of large amplitude wave. In gas dynamics the wave corresponds to a sound wave whose evolution in terms of gas dynamics leads to the formation of discontinuities. In reality, however, narrow transition regions are formed in which the dynamics

is dominated by dissipative processes. In plasmas, the characteristics of the main shock transition are determined not only by an interplay between nonlinearity and dissipation, but also by another important physical effect, wave dispersion. It is well known that a subcritical shock has a nonlinear whistler wave train upstream of its front (Sagdeev 1966; Mellott 1985). The presence of whistler/fast magnetosonic precursor wave trains in supercritical shocks as well, was experimentally established in Krasnoselskikh et al. (1991), Balikhin et al. (1997b), Oka et al. (2006). These whistler waves have rather large amplitudes and their role in energy transformation and redistribution between different particle populations and in the formation of the structure of the shock front is still an open question. The major transition of such a dispersive shock, the ramp, may behave in a similar fashion to either the largest peak of the whistler precursor wave packet (Karpman et al. 1973; Sagdeev 1966; Kennel et al. 1985; Galeev et al. 1988, 1989; Krasnoselskikh et al. 2002) or the dissipative shock region in which the major dissipation due to current driven instabilities occurs. The nonlinear steepening process can be described as the transfer of energy to smaller scales. The steepening can be terminated either by collisionless dissipation, as described above, or by wave dispersion. Typically the dissipative scale L_d exceeds the dispersive scale L_{disp}, the former is reached first and further steepening can be prevented by the dissipation that takes away energy. When steepening is balanced by dissipation, a dissipative subcritical shock forms. Most subcritical collisionless shocks observed in situ are supposed to be dissipative even though dispersive processes play a role in forming a dispersive precursor wave train. Such a shock is characterized by a monotonic transition in the magnetic field (magnetic ramp) of width L_d. The dissipative length is determined by the most important anomalous dissipative process. Its major features are the generation of intense short-scale waves and their dissipation. This form of the evolution of a nonlinear wave takes place at low Mach numbers. However, if the nonlinearity is strong enough (as determined by the velocity and density of the incoming flow), dissipation is not capable of stopping the steepening, and the gradients continue to grow, then energy transfer to smaller scales continues and the characteristic scale of the transition can become smaller. The next process that comes into play to counterbalance the steepening is dispersion. Dispersion becomes important when the gradients become comparable with the dispersive scale L_{disp}. In this case the shock front structure becomes multi-scale. The steepening is prevented by short-scale dispersive waves which are able to propagate away from the evolving shock front. These waves effectively remove some part of the energy and, most importantly, restrain further growth of the gradients. For perpendicular shocks the phase velocity of the dispersive waves decreases with decreasing scale and a wave train is formed downstream of the magnetic ramp. For shocks with a more oblique geometry (quasiperpendicular shocks) the phase velocity increases with decreasing spatial scale and an upstream wave train is formed. The upstream wave precursor is approximately phase standing in the upstream flow. Its amplitude decreases with the distance from the shock ramp due to dissipation processes as was discussed in the early theoretical papers describing subcritical shocks (Sagdeev 1965a, 1966).

The transition to reflection shock takes place when downstream bulk velocity reaches the downstream ion-sound speed. Supercritical reflection shocks have a more complex structure in comparison to subcritical shocks. In quasi-perpendicular shocks the upstream magnetic field does not allow reflected ions to travel far upstream before turning them back to the shock front. The upstream region in which the beam of reflected ions perform part of their Larmor orbit before being turned back to the shock is called a foot. The foot region is characterised by a 15–20 % increase in the magnitude of the magnetic field. The consideration of a Larmor orbit of a reflected ion gives relatively accurate estimate of the spatial size of the foot $L_f = 0.68 R_{Li} \sin\theta_{Bn}$ where R_{Li} is the gyroradius of ions moving

with the velocity equal to normal component of the velocity of upstream flow (Woods 1969; Livesey et al. 1984). The coefficient 0.68 corresponds the case of specular reflection. For non-specular reflection this relation is slightly modified (Gedalin 1996). Downstream of the quasi-perpendicular shock's main transition the joint gyration of the bulk plasma ions and beam of reflected ions leads to an overshoot-undershoot structure. Again, the size of this overshoot/undershoot can be estimated in a straightforward manner in terms of the ion gyroradius. However, the main transition layer lies between the foot and the overshoot. This is the region where the most dramatic changes in the plasma parameters occur. In a supercritical, quasi-perpendicular shock this layer is characterised by the steepest increase of the magnetic field referred to as the ramp. The change of the electrostatic potential, reflection of ions, and electron thermalisation take place within the ramp and its spatial scale determines the major physical processes within the shock and the mechanisms for the interaction of the shock front with the incoming electrons and ions. For instance, several theoretical models suggest that in the ramp of high Mach number shocks very small scale electric fields can be present (Krasnoselskikh 1985; Galeev et al. 1988, 1989). There are several critical issues regarding supercritical quasiperpendicular shock physics for which alternative explanations for the observational features of the shock front have been proposed. Theoretical considerations (Galeev et al. 1988, 1989; Krasnoselskikh et al. 2002), that treat the supercritical shock front as being similar to a nonlinear dispersive wave, predict that the ramp scales (gradients) should decrease with increasing Mach number, eventually reaching characteristic values as small as several electron inertial lengths $L_e = c/\omega_{ep}$. Moreover, after some critical Mach number corresponding to nonlinear whistler critical Mach number whose value is approximately 1.4 times the linear whistler critical Mach number, the shock should become nonstationary. These critical Mach numbers determine the characteristic flow velocities when they become larger than the maximum velocity of a linear or nonlinear whistler wave propagating upstream along the shock front normal. Many computer simulations (Scholer and Matsukiyo 2004; Matsukiyo and Scholer 2006) come to the conclusion that the thickness of the ramp is determined by dissipative processes due to either the modified Buneman instability (MBI) or the modified two stream instability (MTSI). Both theoretical studies and computer simulations have associated pitfalls. Theoretical models can not accurately take into consideration the presence of reflected ions whilst simulations are carried out with an unrealistic ratio of the plasma frequency to gyrofrequency that strongly changes the ratio of electric to magnetic wave fields and often with an unrealistic ion to electron mass ratio. Both theoretical models and simulations predict the transition to nonstationary dynamics. However, they strongly differ in the determination of the scales of the electric and magnetic fields in the ramp region, in the energy sources for the upstream whistler waves that form the precursor wave train, and in the characteristics of the shock dynamics when it becomes nonstationary. For these reasons experimental studies of these questions are crucial for our understanding of the physical processes in quasiperpendicular collisionless shocks. Our Review aims to report the studies of all these questions making use mainly of Cluster measurements (adding some other data where it is necessary, in particular THEMIS data in studies of magnetic field scales of shocks).

The first critical issue we shall address is magnetic ramp width and spatial scale. The main motivation for the study of the magnetic ramp width L_r is that it is this scale that determines the nature of the shock, i.e., the dominant physical processes that counteract nonlinear steepening. The shock width can be determined either by the solitary structure of nonlinear whistler slightly modified by the presence of reflected ions or by characteristic anomalous resistivity scale associated with one of instabilities mentioned above. For

instance if it is indeed the case that the ramp width increases with increasing Mach number as concluded by Bale et al. (2003), then the evolution of nonlinear whistler waves must be excluded from the processes that are involved in the formation of supercritical shocks. The characteristics of the major transition within the shock in which the flow deceleration and the magnetic field and electrostatic potential variations take place are determined by the interplay between nonlinearity, dispersion and dissipation. The presence of a population of reflected ions makes it difficult to construct a reliable theoretical model based on an analytical or semi-analytical description. However, the establishment of the scales of this transition allows one to determine the characteristics of the dominant physical processes in play. The ramp thickness is also crucial for a redistribution of energy between electrons and ions. An important characteristic involved in this process is the gradient scale of the transition. Two reasons cause the need in introducing this ramp gradient spatial scale. The first is the interaction between the incoming electrons and the electromagnetic field at the shock front. As was shown by Balikhin et al. (1993, 1998), Balikhin and Gedalin (1994), and Gedalin et al. (1995a, 1995b), an important effect of this interaction is the possible violation of adiabaticity even in the case when the width of the magnetic ramp considerably exceeds the formally calculated electron gyroradius. Two very different scenarios of electron heating can occur depending upon if the conditions for adiabaticity are satisfied or violated. This effect is crucially dependent upon the ramp spatial scale. The change between adiabatic/non-adiabatic regimes is related to the ability of the nonuniform electric field within the ramp to rectify the electron motion and increase their effective gyration radius (Balikhin et al. 1993, 1998; Balikhin and Gedalin 1994; Gedalin et al. 1995a, 1995b). The parameter that determines the transition from adiabatic to nonadiabatic motion of the electrons is the inhomogeneity of the magnetic field. The characteristic spatial scale of such a layer may be defined as the product of the change in magnetic field ΔB normalised to the upstream field B_0 and the spatial distance L_{br} over which this change occurs i.e. $l_{gr} = L_{Br}(B_0/\Delta B)$. To illustrate the effect of this parameter, one can consider two cases. For a weak shock for which $(B_d/B_0) \approx 1.2$, here B_d is the magnetic field magnitude after the shock transition (downstream), and whose ramp width is of the order 5–6 R_{Le} (electron Larmor radii) the electron motion will be adiabatic. However, in a stronger shock of similar magnetic ramp width for which the maximum magnetic field observed in the overshoot exceeds that of the upstream field by a factor 5–6 the electron behaviour becomes non-adiabatic. This makes it necessary to carry out the statistical study of the magnetic ramp spatial scale in addition to the ramp width (size). The ramp width and its gradient scale are also important for the problem of stability of the ramp region of the shock front. According to Krasnoselskikh (1985), Galeev et al. (1988, 1989) and Krasnoselskikh et al. (2002), the nonlinear whistler wave structure becomes unstable when the characteristic gradient exceeds some critical value. It was suggested by Krasnoselskikh et al. (2002) that it takes place when the Mach number becomes equal to nonlinear critical whistler Mach number. When this happens, dispersive processes can no longer counterbalance the nonlinearity and the shock front overturns. Thus, the characteristic gradient scale provides a rather universal characteristic of the degree of steepness of the shock front. Thus its determination completed a comprehensive statistical study of the magnetic ramp spatial gradient scale in addition to the ramp width (size). Many papers have been devoted to the magnetic field structure of collisionless shocks (e.g. Russell et al. 1983; Krasnoselskikh et al. 1991; Farris et al. 1991; Newbury and Russell 1996; Hobara et al. 2010; Mazelle et al. 2010). In particular, the spatial scales of its various regions have been comprehensively investigated (Balikhin et al. 1995; Farris et al. 1993; Hobara et al. 2010; Mazelle et al. 2010). ISEE and AMPTE measurements of the magnetic field profiles of

the shock front structure led to evaluation of the scale sizes of the foot and overshoot regions that were supposed to be of the order of ion inertial length c/ω_{pi} and $3c/\omega_{pi}$ respectively, here ω_{pi} is the ion plasma frequency. The ramp scale has been estimated to be less than an ion inertial length with reports of one or two very particular shocks whose ramp scale was sufficiently smaller, of the order $0.1c/\omega_{pi}$ (Newbury and Russell 1996; Walker et al. 1999b). We report here the statistical studies of scales based on papers by Hobara et al. (2010) and Mazelle et al. (2010). Another critical issue we shall address hereafter is the electric field distribution inside the ramp region. The energy transfer to smaller scales due to steepening can achieve the scales comparable to electron inertial scale where the whistler waves become quasi-electrostatic. In nonlinear-dispersive scenario of the shock front description the field can have multiple short scale electric field spikes. The experimental study can answer the question whether they exist or not and to determine their characteristics. Studies of the magnetic field profile across the terrestrial bow shock significantly outnumber those based on electric field measurements. Despite the fundamental effect that the electric field has on the plasma dynamics across collisionless shocks, the complexity of the interpretation of electric field data has impeded studies of the electric field structure within the shock front. It is worth noting that only a handful of studies are dedicated to the electric field structure within the shock front (Heppner et al. 1978; Formisano 1982; Scudder et al. 1986a; Wygant et al. 1987; Balikhin et al. 2002, 2005; Bale and Mozer 2007; Walker et al. 2004; Hobara et al. 2008; Dimmock et al. 2012; Bale et al. 2008). There have been very few reports regarding the scale lengths of features observed in the electric field at quasi-perpendicular shocks. The scale size over which the potential varies at the front of a quasi-perpendicular bow shock is an issue that should be resolved in order to gain a full understanding of the physical processes that are occurring in the front. Several different points of view have been published on the relationship between the scale size of the magnetic ramp and that over which the change in potential is observed. Some studies (Eselevich et al. 1971; Balikhin et al. 1993, 2002; Formisano and Torbert 1982; Formisano 1982, 1985; Krasnoselskikh 1985; Leroy et al. 1982; Liewer et al. 1991; Scholer et al. 2003) have proposed that the spatial scale of electrostatic potential is of the same order or smaller than that of the magnetic ramp under certain conditions. Such shocks have been observed in numerous experimental and numerical studies of quasi-perpendicular supercritical shocks. On the other hand Scudder (1995) claimed that the potential scale length is larger than that of the magnetic scale length. Actual measurements of the electric field variations within the bow shock are very sparse. The main reason for this is due to the difficulties encountered when making electric field measurements. Only a small number of space-based measurements of the electric field during the shock front crossing have been reported. Heppner et al. (1978) reported observations of a short lived spikes in the electric field making use of ISEE measurements. However, being short duration, these features were not observed at every shock crossing. Subsequent investigations by Wygant et al. (1987) have shown the existence of spike-like features in the electric field both at the shock ramp and in the region just upstream. From the study of spin averaged ISEE-1 data, Formisano (1982) determined that the increase in the observed electric field intensity began just upstream of the magnetic ramp and lasted longer than the ramp crossing itself. Whilst the electric-field intensity in the regions upstream and downstream of the shock could be interpreted as due to the $V \times B$ motion of the plasma the enhancement observed during the shock crossing must be due to the processes occurring within the shock front itself. In laboratory experiments, where the conditions are not exactly the same as in space plasmas, Eselevich et al. (1971) reported that the major change in potential across the shock occurs within the magnetic ramp region.

Using data of numerical simulations, Lembège et al. (1999) analysed the scale size of both the magnetic ramp region L_{Br} and the scale of the major change in potential L_ϕ inside and around the ramp. They concluded that the scale lengths were of the same order, i.e. $L_{Br} \approx L_\phi$. This view is supported by the simulations of Scholer et al. (2003). The latter authors also show that during the shock reformation process, the main potential drop occurs over several ion inertial scales in the foot region and they noticed that the steepened magnetic ramp region also contributes a significant fraction of the change in total potential over much smaller scales, typically 5–10 Debye lengths. Despite the simulation shocks parameters are still rather far from observations (see Sect. 3 for more details) the tendencies in majority of simulations are well pronounced and are similar to those in laboratory experiments. Hereafter we report the observations of electric field spikes observed onboard Cluster satellites first reported by Walker et al. (2004) and the statistical study of their characteristics. The third important problem of quasiperpendicular shock physics addressed in this Review is the problem of electron heating. In contrast to the ion heating problem which has been well advanced through to detailed studies of data from ISEE, the electron heating problem has remained controversial. The action of shock quasistatic electric and magnetic fields on the electron population (which can have thermal speeds far in excess of the shock speed) is to inflate and open up a hole in the phase space distribution by accelerating (decelerating) incoming (escaping) electrons (Scudder et al. 1986c; Feldman et al. 1982). This inflation in itself is reversible thus it is not dissipation or heating if other processes would not be involved. Irreversibility may be imposed if additional scattering would take place infilling the hole. If adiabatic invariant of electrons is conserved while electrons cross the shock front it can not happen. One should conclude that some non-adiabatic process should occur inside the shock front. One of the possibilities can be related to Debye-scale electric fields (Bale et al. 1998). Another possibility is to suggest that the phase space inflation is indeed accompanied by instabilities which could scatter the electrons. Demagnetisation of the electrons due to the strong gradients in the electric field as it was mentioned above (Balikhin and Gedalin 1994) or nonlinear wave phenomena (Krasnoselskikh et al. 2002) combined with wave particle interactions can offer an alternative scattering processes. Thus the partition of energy between ions and electrons is a complex, self-consistent multi-scale interplay between electron heating, magnetic/electric field profile, shock potential, and ion reflection. This interplay remains poorly understood despite 40 years of research. That research has included detailed case studies (Scudder et al. 1986b), statistics of the inferred potential and electric field structures (Schwartz et al. 1988; Walker et al. 2004), theoretical studies (Galeev et al. 1988; Gedalin 1997; Krasnoselskikh et al. 2002) and increasingly sophisticated numerical simulations (Lembège et al. 2004; Scholer and Burgess 2006). Direct measurements of the thickness of the shock transition layer combined with the rapid simultaneous measurements of the electron distribution function can allow solving this long standing opened problem in shock physics. If the electron heating can be attributed to kinetic instabilities, the shock thickness will be measured in ion inertial lengths (c/ω_{pi}) (Papadopoulos 1985b; Matsukiyo and Scholer 2006). If such instabilities prove ineffective, above a second critical Mach number the shock steepening is expected to be limited by whistler dispersion and/or be unstable to shock reformation (Krasnoselskikh et al. 2002). Recent studies of the shock thickness (Hobara et al. 2010; Mazelle et al. 2010) do show scales comparable to whistler wavelengths. These contrasted an earlier study (Bale et al. 2003) reporting scalings that matched the gyro-scales of reflected ions. To date, studies have relied on the high temporal cadence available from magnetic or electric field experiments. However, field profiles provide only indirect evidence of the shock dissipation scales. A recent study (Lefebvre et al. 2007) used sub-populations of electrons

to determine the electrostatic potential profile at one shock, suggesting that it rose in concert with the magnetic field. In the work reported here, first published in Schwartz et al. (2011), the electron distribution function major characteristics are measured at sufficient cadence to reveal directly for the first time the scale of the electron temperature profile. Many shock crossings by Cluster satellites take place on the flanks of the magnetosphere that creates quite favourable conditions for the studies of the relatively narrow shock transitions allowing one to have many measurements on small spatial scale. Hereafter we present unprecedently rapid measurements of electron distribution moments that allow to shed new light on electron heating problem and its scales.

The fourth problem presented in the Review, which is closely related to the problem of magnetic and electric field scales, is determination of the source of waves forming upstream precursor wave train. The presence of whistler/fast magnetosonic precursor wave trains in supercritical shocks was experimentally established by Balikhin et al. (1997a), Krasnoselskikh et al. (1991), Oka et al. (2006). These whistler waves have rather large amplitudes and their role in energy transformation and redistribution between different particle populations and in the formation of the shock front structure is still an open question. The energy source responsible for the generation of these waves is the subject of active debate in shock physics (see Galeev et al. 1988, 1989; Krasnoselskikh et al. 2002; Matsukiyo and Scholer 2006; Comişel et al. 2011). Often the precursor waves are almost phase-standing in the shock frame. However, if they are generated by the ramp region as the dispersive precursor their group velocity can still be greater than zero in the shock reference frame, which would allow energy flow in the form of Poynting flux to be emitted towards the upstream of the shock transition. On the other hand, if the waves are generated by instabilities related to reflected ions, their energy flux will be directed from the upstream region towards the shock ramp. The goal of Sect. 4 is to address this problem, to present the direct measurement of the Poynting flux of the upstream whistler waves aiming to establish the direction of the Poynting flux. There are two different points of view on this subject also. It has been suggested that the shock front structure of quasi-perpendicular supercritical shocks is formed in a way similar to that of subcritical shocks (Galeev et al. 1988, 1989; Krasnoselskikh et al. 2002). In such scenario the precursor wave train is a part of the shock front structure emitted by the ramp region upstream due to positive dispersion of whistler waves. The observed dynamic features of shocks have also been studied extensively using computer PIC or hybrid simulations, often with focus on the precursor wave activity and reflected ions (Hellinger and Mangeney 1997; Hellinger et al. 2007; Matsukiyo and Scholer 2006). From a kinetic viewpoint, however, it may be argued that the shock-reflected ions change the physical picture and that the principal scales, temporal and spatial, could be determined by the characteristics of the reflected ion population (Bale et al. 2003). Upstream waves can then be generated due to counterstreaming ions and electrons in the shock front region, forming unstable particle distributions with respect to some wave modes (Papadopoulos 1985b; Hellinger et al. 2007; Scholer and Matsukiyo 2004; Matsukiyo and Scholer 2006). While this is probably the case for some higher frequency waves, we present here an analysis that leads to the conclusion that the source of the upstream low frequency whistler waves is indeed related to the presence of the nonlinear ramp transition, emitting smaller scale dispersive waves towards the upstream flow. The existence of phase-standing upstream whistler waves depends on the value of the upstream flow speed Mach number relative to the phase velocity. If the Mach number of the shock does not exceed the nonlinear whistler critical Mach number $M_w = V_{w,max}/V_A = 1/2\sqrt{m_i/m_e}\cos\theta_{Bn}$, where $V_{w,max}$ represents the highest possible velocity of nonlinear whistler wave, then phase-standing (nonlinear) whistler wave trains can exist upstream of the shock (Galeev

et al. 1988, 1989; Krasnoselskikh et al. 2002). The results we report here were first published by Sundkvist et al. (2012). Similar results were reported making use the Time Domain Sampling instrument (TDS) onboard Wind satellite (Wilson et al. 2012) for three of four crossings of interplanetary shocks. In one case the polarization of waves was found to be different from whistler wave. Unfortunately, single satellite measurements do not allow one to establish unambiguously the reason of this anomaly, it could be associated with some particular perturbation in the solar wind.

The fifth problem intimately related to previous is the problem of nonstationary dynamics of high Mach number shocks. Shock waves are usually considered to be nonlinear waves that cause irreversible changes of state of the media and from macroscopic point of view they are stationary (for a review, see, e.g. Tidman and Krall 1971). However, in the very beginning of the collisionless shock physics Paul et al. (1967) hypothesized that high-Mach-number shocks can be nonstationary, and the first unambiguous evidence of the nonstationarity was obtained by Morse et al. (1972) in laboratory experiments. New evidence of shock front nonstationarity was found in the 1980s. In particular, Vaisberg et al. (1984) reported low frequency oscillations of the ion flux in the Earth's bow shock. Later Begenal et al. (1987) observed a similar phenomenon in the Uranian bow shock. In the very beginning of computer simulations of the collisionless shocks Biskamp and Welter (1972) have observed the process of shock dynamic behaviour. The inflowing ions formed vortices in the phase space and dynamics of the front was definitely nonstationary. Later, numerical simulations performed by Leroy et al. (1982) using 1-D hybrid code showed that the front structure of perpendicular shocks varies with time, for instance, the maximum value of the magnetic field exhibits temporal variations with a characteristic time of the order of ion gyroperiod, the magnitude of these variations being about of 20 % if the parameters are typical for the Earth bow shock ($M_A = 8$ and $\beta_{e,i} = 0.6$, where M_A is the Alfvén Mach number, $\beta_{e,i}$ is the ratio of the thermal electron/ion and magnetic pressures). They also found that for $M_A = 10$ and $\beta_{e,i} = 0.1$ the ion reflection was bursty, oscillating between 0 and 70–75 %. Hybrid simulation of perpendicular shocks with very high Mach numbers carried out for the first time by Quest (1986) have shown that the ion reflection in the shocks can be periodic, the stages with 100 % ion reflection alternating with the stages of 100 % ion transmission. As a result, instead of a stationary structure, he observed a periodic wave breaking and shock front reformation. Later Hellinger et al. (2002) reexamined the properties of perpendicular shocks with the use of the 1-D hybrid code and observed the front reformation for a wide range of parameters if upstream protons are cold and/or Mach number is high. Scholer et al. (2003) and Scholer and Matsukiyo (2004), Matsukiyo and Scholer (2006) in their 1-D full-particle simulations with the physical ion to electron mass ratio reproduced the reformation of exactly and approximately perpendicular high-Mach-number shocks in plasmas with $\beta_i = 0.4$ and demonstrated an importance of modified two-stream instability for the reformation process. Krasnoselskikh (1985) and Galeev et al. (1988, 1989) proposed models describing the shock front instability due to domination of nonlinearity over dispersion and dissipation. This instability results in a gradient catastrophe within a finite time interval. Several aspects of the model, including the role of nonlinear whistler oscillations and existence of a critical Mach number above which a nonstationarity appears, were developed in further detail and more rigorously by Krasnoselskikh et al. (2002) and complemented by numerical simulations with the use of the 1-D full particle electromagnetic code with a relatively small ratio of electron and ion masses, $m_e/m_i = 0.005$. It was also shown that the transition to nonstationarity is always accompanied by disappearance and re-appearance of the phase-standing whistler wave train upstream of the shock front. Moreover, for large Mach numbers the nonstationarity manifests itself as a periodic ramp reformation, which

influences considerably the ion reflection, in particular, the reflection becomes bursty and sometimes the ions are reflected from both old and new ramps simultaneously. The four-spacecraft Cluster mission gave much more new opportunities for experimental studies of the shocks. The first examples of some aspects of shock nonstationarity were presented by Horbury et al. (2001). These authors analyzed magnetic field data for two quasiperpendicular shocks with moderate and high Alfvén Mach number. While for moderate M_A the shock profiles measured by different spacecraft were approximately the same, with the exception of a small-amplitude wave activity in the foot, for high M_A the amplitude of the fluctuations attains 10 nT, making profiles considerably different for different spacecraft. However, the authors argued that these fluctuations stop before the ramp and do not appear to disrupt the shock structure; on the other hand, they didn't reject an opportunity that the fluctuations observed may represent the signatures of the unsteady shock reformation. Hereafter we report the first direct observation that clearly evidence the shock front reformation observed onboard Cluster mission on 24th of January 2001. This material was first published by Lobzin et al. (2007).

The sixth problem we discuss in this Review is important for the definition of the relative role of dissipative and dispersive effects, namely the problem of anomalous resistivity. The problem of electron heating mentioned above is considered for many years to be 'solved' for subcritical shocks and conventional solution proposed and widely accepted is formulated in terms of magic words 'anomalous resistivity'. This notion was introduced first by Sagdeev (1965b) and then analyzed in more detail by Galeev (1976), who made estimates of the characteristic scale of the shock transition relying on ion-sound instability. Papadopoulos (1985a) has noticed that in case of quasiperpendicular shocks the most important instabilities should be related to lower hybrid waves and has revised the model taking these effects into account. However there were no measurements that might be used to confirm or reject theoretical models of the dissipation due to anomalous resistivity. It is worth noting that this problem is very important for the determination of energy redistribution between electrons and ions, especially for the electron heating and electron acceleration. We can not present here theoretical studies of anomalous resistivity, an interested reader can find general ideas in the review papers by Galeev and Sudan (1989) and Papadopoulos (1985a). The second important problem for which short scale length waves are important is an energization of electrons within a collisionless shock. It requires the transfer of a portion of the energy associated with the incoming upstream plasma flow to the electron population. In order for this energy transfer to occur, there has to be some media that can channel energy from the incoming ion population to the electrons. One mechanism that has commonly been proposed, both for solar systems and particularly for astrophysical applications is based on excitation of lower-hybrid waves (Papadopoulos 1981; Laming 2001; Krasnoselskikh et al. 1985). The increased level of electric field fluctuations in the frequency range 10^2–10^3 Hz observed in the vicinity of a quasiperpendicular shock front is usually attributed to either ion-sound or whistler waves. One of the most comprehensive studies of the plasma waves in this frequency range was conducted by Gurnett (1985). His main conclusion was that waves observed above local electron cyclotron frequency are Doppler shifted ion-sound waves whilst those below are whistler mode waves.

The main reason of the lack of measurements of ion sound and lower hybrid waves is related to technical difficulties of small scale electric field measurements. Recently two papers were published that represent first attempts to create the experimental basis for the anomalous resistivity studies in collisionless shocks. We present in this section a short summary of the results obtained by Balikhin et al. (2005), Walker et al. (2008). The rapid changes that are observed in the plasma at the front of a supercritical, quasi-perpendicular shock

and described in previous sections lead to the creation of multiple free energy sources for various plasma instabilities. Twin satellite missions, such as ISEE or AMPTE, have provided data for a number of comprehensive surveys of the waves observed in the frequency range (10^{-2}–10^{1} Hz) of the plasma turbulence encountered at the shock front. The use of multisatellite data for wave identification and turbulence studies is limited to the analysis of those waves whose coherence lengths are of the same order of magnitude as the satellite separation distance. Plasma wave modes such as the ion-sound or lower-hybrid, that are supposed to play an important role at the shock front, possess coherence lengths that are very short in comparison with any realistic satellite separation distance (Smirnov and Vaisberg 1987). For majority of these waves the coherence length is either comparable to or a few times greater than their wavelength. In such cases the waves observed by different satellites in a multisatellite mission will be uncorrelated. This will make it impossible to apply wave identification methods based on intersatellite phase delays (Balikhin et al. 1997a; Balikhin et al. 2003) or k-filtering (Pinçon and Glassmeier 2008). Nevertheless the identification of waves with short wavelengths and study of their dynamics remains very important because of their potential role in the transfer of energy associated with the upstream directed motion into other degrees of freedom. In the classical model of a quasiperpendicular low β shock anomalous resistivity occurs due to ion-sound turbulence in the shock front (Galeev 1976). Lower hybrid waves also may play an important role at the shock front since they also can be involved in resonance interactions both with electrons and ions and so may be extremely efficient at channelling the energy exchange between the two species. In order to assess the importance of ion-sound, lower hybrid and other waves with relatively short wavelengths within the plasma dynamics of the shock front the mode of the observed waves should first be identified. The strong Doppler shift that results from the large values of wavevector $|k|$ precludes the reliable use of the observed frequency for correct identification as was done in many previous studies. Here we show that the data from a single spacecraft can be used to determine propagation modes of waves observed in the frequency range 10^{2}–10^{4} Hz at the front of the terrestrial bow shock. A similar approach has been used by Tjulin et al. (2003) in a study of lower-hybrid waves in the inner magnetosphere.

The lower-hybrid wave is an electrostatic plasma wave mode whose plasma frame frequency is in the vicinity of the lower-hybrid resonance frequency $\omega_{lh} \sim \sqrt{\Omega_{ci}\Omega_{ce}}$, where Ω_{ci} and Ω_{ce} are the ion and electron gyrofrequencies respectively. The wave has linear polarisation and propagates almost perpendicular to the magnetic field ($\cos(\theta_{kB}) \sim \sqrt{m_e/m_i} \sim 89°$). The maximum growth rate γ_{max} occurs when $k_\parallel/k \sim \omega_{pi}/\omega_{pe}$, where $k_\parallel$ is parallel component of the wavevector. Since the waves are propagating in a plasma that is moving with respect to the satellite, their frequencies will be Doppler shifted in the spacecraft frame. The magnitude of this shift can be estimated using the resonance condition of the Modified Two Stream Instability (MTSI) $2V_A M_A k = \omega_{lh}$. This gives a maximum estimate for the correction in observed wave frequency due to the Doppler shift, $kV_{sw} \sim \omega_{lh}/2$, here V_{sw} is the velocity of the solar wind supposed to be equal to normal component of the upstream flow velocity.

Current models of wave turbulence that determines anomalous resistivity in the front of quasiperpendicular shocks are based on the occurrence of lower hybrid waves at a shock front being generated due to counter-streaming populations of ions and relative motion of reflected ions (Leroy et al. 1982) and bulk electrons and ions at the front via the modulational two-stream instability (MTSI) (Papadopoulos 1985b; Matsukiyo and Scholer 2006) or modified Buneman instability. These models are often used to explain the electron acceleration observed at various astrophysical shocks such as supernova remnants (Laming 2001). However, there is currently no substantial experimental evidence that these waves do indeed exist in the fronts of supercritical, quasiperpendicular, collisionless shocks. The results

of data analysis from the Intershock electric field experiment, in which wave activity was observed at frequencies of a few Hertz, has been used to argue for the existence of lower hybrid waves (Vaisberg et al. 1983). An alternative explanation, however, has been proposed in which Intershock may have simply observed the electric field component of whistler wave packets propagating in the foot region (Krasnoselskikh et al. 1991; Balikhin et al. 1997a; Walker et al. 1999a). Electric field observations of Comet Halley also showed evidence for waves observed in the vicinity of the lower hybrid frequency (Klimov et al. 1986). However, their exact wave mode was not determined. The natural way to differentiate these modes is to examine their polarisations. Whistler mode waves are elliptically polarised whilst lower hybrid waves, as mentioned above, are linearly polarised. We present here the summary of direct observations of the ion-sound (Balikhin et al. 2005) and lower-hybrid waves (Walker et al. 2008) that we complete by estimates of characteristic effective collision frequencies.

The paper is organized as follows. In Sect. 2 we present the statistical studies of quasiperpendicular shock ramp widths. Section 3 is dedicated to electric field scales of the ramp of quasiperpendicular shocks. In Sect. 4 the results of evaluation of the Poynting flux of oblique whistler waves upstream of the shock front are outlined. Recent results on electron heating scale at High Mach number quasiperpendicular shocks are presented in Sect. 5. In Sect. 6 we use the data of measurements of lower hybrid and ion sound waves intensities to evaluate the characteristics of anomalous resistivity aiming to determine its role in the shock front formation. In Sect. 7 we present results of direct observations onboard Cluster satellites of nonstationarity and reformation of high-Mach number quasiperpendicular shock. In Sect. 8 we summarise the results of experimental observations and discuss the conclusions that follow from Cluster and THEMIS observations. In Appendix A we present some short comments concerning comparison of computer simulations with the observations. Appendix B contains a notation table defining the notations used in this paper.

2 Statistical Studies of Quasi-Perpendicular Shocks Ramp Widths

As was discussed in the Introduction the characteristics of the major transition within the shock in which the flow deceleration and the magnetic field and electrostatic potential variations take place are determined by the interplay between nonlinearity, dispersion and dissipation. The presence of a population of reflected ions makes it difficult to construct a reliable theoretical model based on an analytical or semi-analytical description. However, the establishment of the scales of this transition allows one to determine the characteristics of the dominant physical processes in play. Single satellite missions provide very poor possibilities for the reliable identification of the shock width and evaluation of the characteristic scales of structures within it. In such cases the spatial size of the foot or overshoot have been used (Balikhin et al. 1995) to evaluate the thickness of the ramp region. The first shock crossings by two satellites were studied in the frame of ISEE and AMPTE projects. These missions provided the first insight into the thickness of the shock transition. The decrease of the shock width and consequent increase of gradients as a function of increasing Mach number was clearly demonstrated by Farris et al. (1993). In their study the Mach number was normalized to the critical Mach number that determines the transition from sub-critical to supercritical shocks. Figure 2 (from Farris et al. 1993) shows magnetic field magnitude measurements made by ISEE 1 for five low beta quasiperpendicular shocks ordered by the ratio of their Mach number to critical Mach number increasing from top to bottom. The increase in the gradient of the shock transition is clearly independent of the differences in the angles between the normal to the shock front and the magnetic field and of the value of beta.

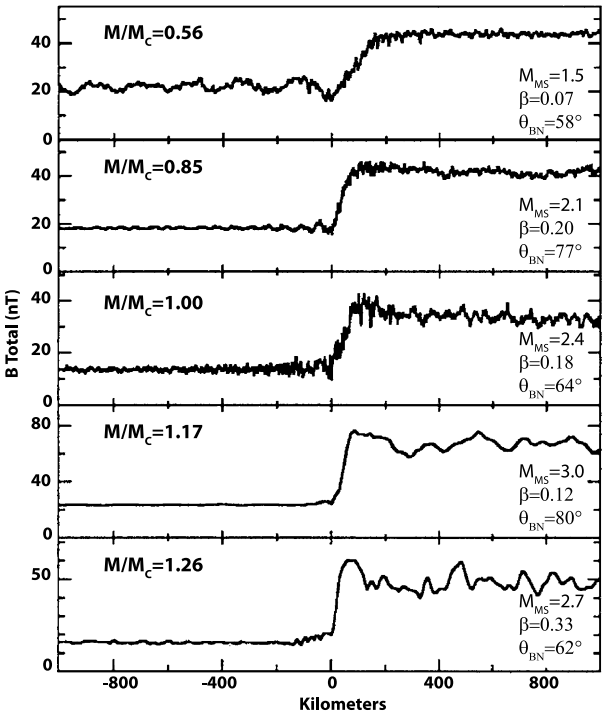

Fig. 2 The total magnetic field strength as a function of distance through five low beta, quasi-perpendicular shocks in order of increasing ratio of criticality. The Mach number, β, and θ_{Bn} for each shock are displayed. The data are shown at the highest temporal resolution available. The sampling rate for the first three shocks is 16 Hz and 4 Hz for the last two (Adapted from Farris et al. 1993)

Several studies have been dedicated to the investigation of structural elements of the shock front making use of ISEE 1,2 magnetometer data. Scudder and co-authors (Scudder et al. 1986a, 1986b, 1986c) carried out the detailed study of the shock crossing on 7th November 1977. This is presumably the most detailed study of a single event, in which all the elements of the structure were put together and compared with detailed measurements of the particle distribution functions. These authors succeeded in relating the evolution of the ion distribution function to the characteristic features of the magnetic field structure and in the determination of the major macro-features of structure of the shock front. This study concluded that the size of the magnetic field transition was determined by the dissipative process related to reflection of ions. Twin satellite measurements by ISEE provided the first indications that some shocks have quite narrow fronts (Newbury and Russell 1996; Newbury et al. 1998). Newbury and Russell (1996) reported the observation of an extremely thin, quasiperpendicular shock whose ramp width was determined to be $0.05L_i$ (where L_i is ion inertial length), i.e. of the order of electron inertial length. Figure 3 shows this particular shock crossing (bottom panel) together with a second shock, observed under similar solar wind conditions, whose ramp width was $0.89L_i$.

Cluster and THEMIS have provided new opportunities for a comprehensive study of the shock ramp scales. Recently, there have been two papers dedicated to studies of the ramp scales of the magnetic field transition (Hobara et al. 2010; Mazelle et al. 2010). They have used slightly different definition of the ramp thickness and scale and applied different methodology, however they came to very similar conclusions about statistical characteristics of the scales of the ramp transition. Hereafter we present the summary of results reported in these papers.

The article by Hobara et al. (2010) is devoted to statistical studies of the magnetic field spatial scales in the ramp region of the shock front based on Cluster and THEMIS ob-

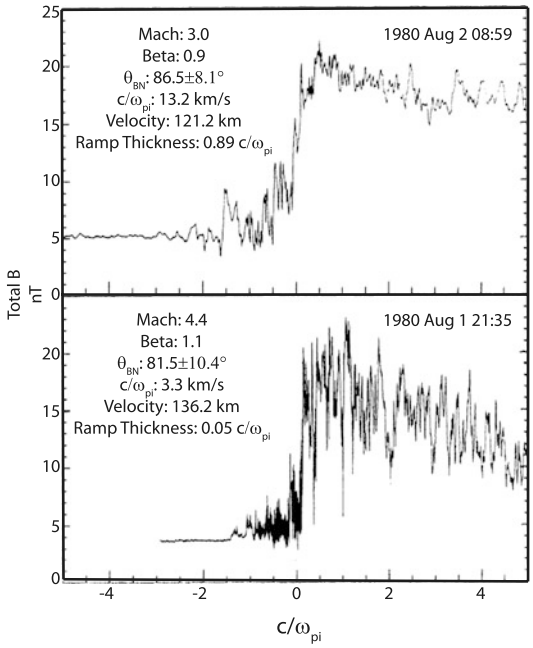

Fig. 3 These shocks formed under similar solar wind conditions, but there is great disparity between their ramp widths (Adapted from Newbury and Russell 1996)

servations. Due to their highly inclined orbit, the Cluster satellites enable the observation of shock crossings away from ecliptic plane. These shocks typically exhibit Mach numbers that are in the lower range of the whole space of terrestrial Mach numbers, since the shock normal deviates from the sunward direction. To increase the range of available Mach numbers, THEMIS shock crossings were added to the set of Cluster observations. Magnetic ramps cannot be always treated as uniform. Nonlinear substructures have been observed and reported within the ramp in several cases (e.g. Balikhin et al. 2002; Walker et al. 2004). The study of spatial-temporal characteristics of such substructures requires at least two point measurements separated by a distance that is sufficiently smaller than the inter satellite distances of both THEMIS and Cluster missions, thus the authors restricted themselves with the study of the ramp spatial scales only.

2.1 Criteria for Choosing Shocks and Definition of Notions "Size" and "Scale"

Hobara et al. (2010) have used the data from Cluster and THEMIS for a statistical study of the spatial size of the ramp. Both these missions assembled a huge stockpile of shock crossings. These data sets complement each other because of the difference in the orbits of Cluster and THEMIS satellites. The THEMIS orbit is close to equatorial plane providing an opportunity to sample the terrestrial bow shock in the vicinity of the subsolar point. Cluster crossings of the terrestrial bow shock occur mainly on the flanks. The solar wind flow in the vicinity of the terrestrial orbit is almost along Sun-Earth line, so that the Mach numbers of flank shocks are relatively low due to the greater deviation of the local shock normal from the sunward direction. Therefore, the combination of THEMIS and Cluster crossings allowed to cover a greater dynamical range of Mach numbers available for the analysis than each of these missions provides separately. Cluster crossings for two time intervals, February–April 2001 and February–March 2002, were used in the study. THEMIS shock crossings included in the study took place from the beginning of July 2007 to the end of August 2007.

The magnetic field data used in the present paper came from Cluster and THEMIS fluxgate magnetometers (FGM) (Balogh et al. 1997; Auster et al. 2008). Another reason to use the THEMIS data from the initial phase of the mission was that THEMIS C and D spacecraft separation was not very large.

The set of shocks that have been used by Hobara et al. (2010) for the study of statistical properties of the ramp width and gradient scale in the paper included 77 individual crossings of the terrestrial bow shock (30 by THEMIS and 47 by Cluster). In order to determine the spatial scale of the shock ramp by means of transformation from temporal to spatial variables an estimate of the relative shock spacecraft velocity along the shock front normal was used. These estimates are very sensitive to shock normal definition. That's why to perform reliable identification of the local normal to the shock front one of them (Hobara et al. 2010) compared normals found making use of four different methods, using the model shape of the terrestrial bow shock similar to Farris et al. (1991), using timing differences methods between the 4 Cluster spacecraft shock crossings, minimum variance and coplanarity theorem. In order to validate the results the evolution of the magnetic field component along the normal direction B_n was used. The reliability of the shock normal identification served as the only shock selection criteria. Those shock crossings, for which the calculated normal could not be considered reliable (because of the B_n evolution or due to large discrepancy in the shock normal directions found by different methods), have been excluded from consideration. The relative shock spacecraft velocity V_{ss} has been calculated using the shock normal direction, satellite separation vectors and time delay between two subsequent shock crossings.

The second recent study dedicated to the same problem (Mazelle et al. 2010) was also based on Cluster magnetic field measurements during spring seasons of 2001 and 2002 corresponding to small interspacecraft separation (100 to 600 km typically). The shock parameters (angle between upstream magnetic field and local shock normal θ_{Bn}, Alfvénic Mach number M_A and ion beta β_i) were computed from the data of Cluster and ACE.

Mazelle et al. (2010) selected the shocks for the statistical study according to following criteria. First, in order to restrict the study by almost perpendicular shocks the shocks with θ_{Bn} as close as possible to 90° were chosen. The other criteria were the existence of well-defined upstream and downstream intervals for the 4 s/c, the stability of the upstream averaged field from one s/c to another, the validity of the normal determination by checking the weak variability of the normal field component B_n around the ramp and low value of B_n upstream for θ_{Bn} to be close to 90°. Only 24 from 455 crossings of Cluster satelite quartet in 2001 and 2002 were left with all criteria validated. This means that 96 individual shock crossings were analyzed. Selected θ_{Bn} values were chosen to be in the range from nearly 90° to 75° but about 80 % of the shocks selected were above 84°. Mach numbers M_A were found to be equally distributed from 2 to 6.5 and corresponding β_i between very low values to 0.6 but with 67 of values less than 0.1.

The major difference between two works consists in using different methods of the determination of the shock ramp thickness. If the beginning of the ramp region was defined quite similarly as the beginning of the monotonous increase of the magnetic field, the end of ramp or exit from the ramp region was determined differently. Hobara et al. (2010) defined the ramp crossing duration as a time interval between the upstream edge of the ramp and the maximum of overshoot. The spatial size (width) of the magnetic ramp has been estimated as a product of V_{ss} and the duration D_t of the ramp crossing. Mazelle et al. (2010) determined at first a stationary asymptotic level of the magnetic field that might be considered as satisfying to Rankine-Hugoniot conditions. To this end a downstream interval where the magnetic field magnitude is quite steady was used. It is then considered as giving an approximate estimate of the value of the magnetic field corresponding to exit from the ramp/entry

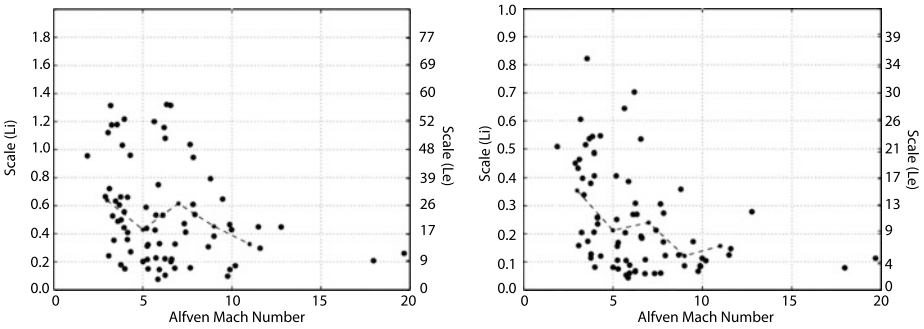

Fig. 4 Scatterplot of experimentally derived shock size (*left panel*) and shock spatial scale (*right panel*) normalized to the ion inertial scale length c/ω_{pi} (*left axis*) and electron inertial scale c/ω_{pe} (*right axis*) as a function of Alfvén Mach number. The *dashed line* represents the averaged values of shock width averaged over shocks with Alfvén Mach number in the ranges 2–4, 4–6, 6–8, 8–10, 10–12. The *vertical lines* represent the statistical *error bars* for each of these Mach number ranges. (Adapted from Hobara et al. 2010)

in the overshoot. From the initial values of the entry in and exit from the ramp a linear fit of the data points inside the estimated time interval is made and this later on is allowed to vary. The choice of a linear fit allows excluding any pollution of the ramp region by a part of the extended foot. The same analysis was repeated for all four satellites for each shock crossing. The steeper slope found for the ramp defines the 'reference satellite'. The times of the middle of the four samples of ramps for one shock crossing are then used to compute both the shock normal and velocity in the GSE frame by the 'timing-method' described in Horbury et al. (2002). This makes it possible to derive the 'apparent' width (along each satellite trajectory) and compare between the 4 s/c. Then, the velocity vector of the shock in each s/c frame is computed. Its angle with the shock normal allows reconstructing a local profile along the normal and determining the real local spatial width of each shock substructure. Readers interested in more technical details can find them in Mazelle et al. (2010) and Hobara et al. (2010).

A scatterplot of the spatial sizes of the ramp as a function of Alfvén Mach number is shown in the left hand panel of Fig. 4. The left hand panel shows the scale sizes in terms of the ion inertial length whilst the right hand panel shows the width in terms of the electron inertial length. The width of the magnetic ramp varies by about an order of magnitude from $L_r = 1.4L_i$ ($\approx 60L_e$) to $0.1L_i$ ($\approx 4L_e$). The general trend in Fig. 4 indicates that the magnetic ramp becomes thinner with increasing of Alfvénic Mach number. This trend is evident even without taking into account two shock crossings with peculiarly high Mach numbers M in the range 17–20 that correspond to the two markers in the bottom right corner of the scatterplot. The figure also shows a distinct decrease in the maximum width of the shock front with increasing Mach number. To make these tendencies more clear the characteristic width of the magnetic ramp averaged for the shocks with Alfvénic Mach numbers in ranges 2–4, 4–6, 6–8, 8–10 and 10–12 (dashed curve) are presented.

The vertical lines on Fig. 4 (left panel) represent the statistical error bars for each range of Mach numbers 2–4, 4–6, 6–8, 8–10 and 10–12. The decrease of statistical errors with the Mach number is in complete agreement with the significant decrease of the maximum shock width, while the minimum shock width undergoes much smaller changes.

The right hand panel of Fig. 4 shows the scatterplot of the spatial gradient scale of the magnetic ramp. It clearly demonstrates the same characteristic features as were evidenced in the left hand panel for the ramp width, namely a quite wide range of values, especially

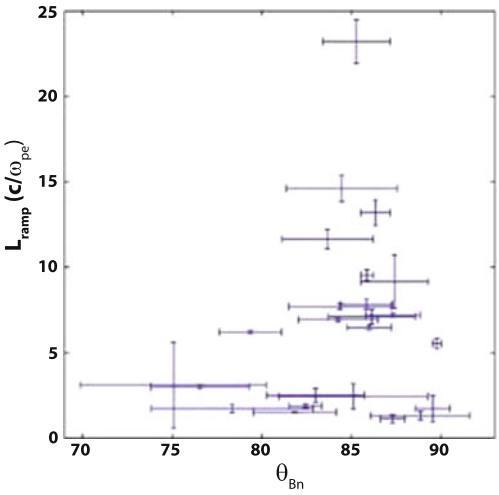

Fig. 5 Thinnest ramps observed versus shock θ_{Bn}. Reprinted with permission from Mazelle et al. (2010). Copyright 2010, American Institute of Physics

for low Mach number shocks and the trend toward shorter scales with the increase of the Mach number as well as the decrease of the maximum gradient scale while Mach number increases. As the change of the magnetic field for all chosen shocks exceeds upstream magnetic field B_0 (for many of them quite significantly) the values of the gradient scale are smaller then the width of the corresponding shocks. The ramp gradient spatial scale varies in the range 0.05–0.82L_i (2–35L_e).

2.2 Statistical Analysis (Mazelle et al. 2010)

Figure 5 displays the thinnest ramp found among each quartet of crossings for each individual shock versus θ_{Bn}. There were no simple relation found. However, it is unambiguously established that many observed thinnest ramps are less than 5 c/ω_{pe} thick and there was found an apparent trend for lower values as $\theta_{Bn} \rightarrow 90°$.

The histogram of all ramp thicknesses in Fig. 6 reveals the predominance of narrow ramp width with a Gaussian-like regular decrease towards an asymptotic limit that is still less than c/ω_{pi}.

The authors came to conclusion that their analysis confirms statistically that the magnetic field ramp of the supercritical quasi-perpendicular shock often reaches a few c/ω_{pe}.

So, the results of two independent studies by two different groups come to the same conclusion, the ramp width for quasiperpendicular high Mach number shocks as seen in magnetic field is of the order of several c/ω_{pe} and is in a perfect agreement with estimates determined from the dispersive scale of a nonlinear whistler wave, modified by the presence of reflected ions (Galeev et al. 1988, 1989; Krasnoselskikh et al. 2002).

3 Electric Field Scales of the Ramp of Quasiperpendicular Shocks

As mentioned in the introduction, there have only been a few reports regarding the scales and structure of the electric field transition at quasi-perpendicular shocks. Based on laboratory experiments, in which the conditions are not exactly the same as in space plasmas, Eselevich et al. (1971) reported that the major change in potential across the shock occurs within the magnetic ramp region.

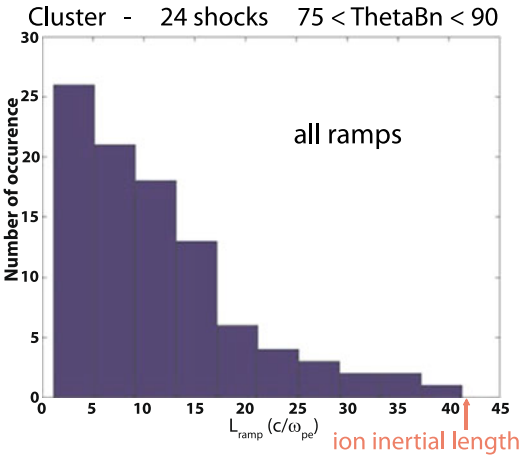

Fig. 6 Histogram of the 96 shock ramp thicknesses. Reprinted with permission from Mazelle et al. (2010). Copyright 2010, American Institute of Physics

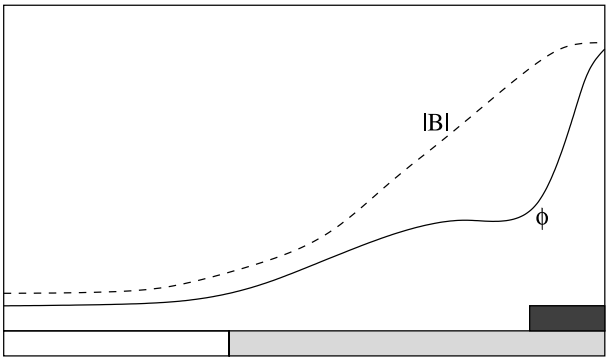

Fig. 7 Sketch of the changes observed in the magnetic field and electrostatic potential during the crossing of a quasi-perpendicular shock (based upon the experimental results of Eselevich et al. 1971)

Figure 7 is a sketch (based on the results of Eselevich et al. 1971) of the change in the magnitude of the magnetic field and the accompanying change in the electrostatic potential. These authors interpreted it as a viscous subshock similar to isomagnetic jump. From Fig. 7 it can be seen that there are two different length scales that may be associated with the change in the electrostatic potential as the shock is crossed. The first, indicated by the lightly shaded bar at the foot of the plot, shows that overall the potential changes on scales similar to that of the magnetic ramp region in agreement with the results of Lembège et al. (1999). This corresponds to an enhancement of the electric field observed as the shock is crossed. The second scale, indicated by the darkly shaded bar, corresponds to a region within the shock front in which a large increase in the potential is observed over a small spatial scale. Such changes in the potential result from large amplitude spike like features in the electric field.

The results reported here present a study of the large amplitude, short duration features in the electric field observed by the Cluster satellites during a number of crossings of the quasi-perpendicular bow shock published in Walker et al. (2004). These features contribute significantly to the overall change in potential observed at a shock crossing but their short duration implies that they are very localised. The aim of the study was to determine their scale size and amplitudes. These parameters were studied in relation to the upstream shock parameters.

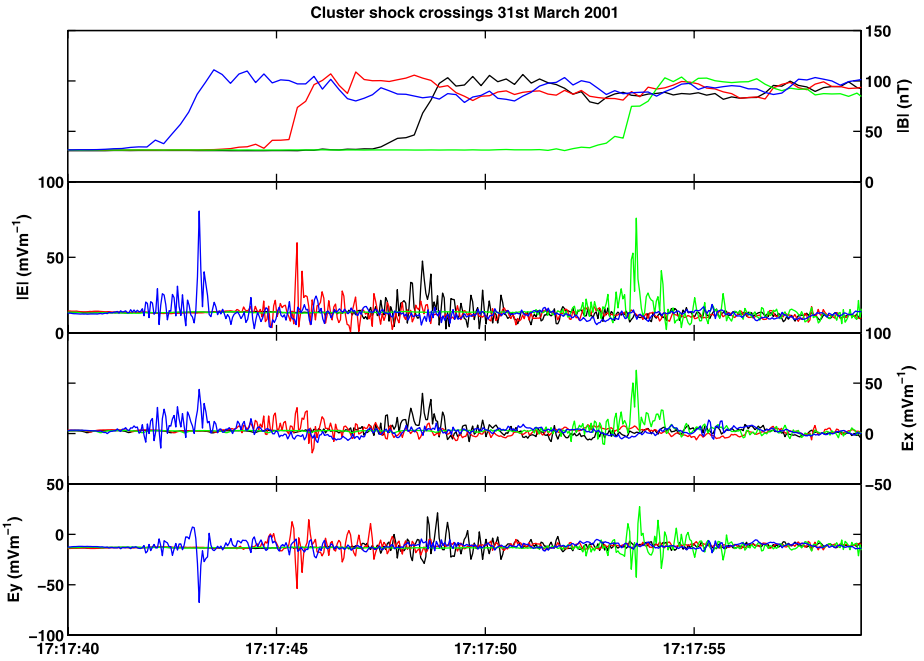

Fig. 8 Overview of the shock crossing on March 31st, 2001 at 17:18 UT. The *top panel* shows the magnitude of the magnetic field measured by FGM. The *second panel* shows the magnitude of the electric field measured in the satellites spin plane. The *lower two panels* show the spin plane components E_x and E_y (Adapted from Walker et al. 2004)

A total of 54 shock crossings, occurring on 11 separate days were investigated but not all could be analysed fully for various reasons such as unavailability of certain data sets, or the accuracy of the shock normal determination. In this section we present a case study of the electric field within the shock front, namely the crossing that occurred on 31st of March 2001 at around 17:18 UT. On this day the conditions in the solar wind were some what abnormal due to the passage of a CME. Measurements in the solar wind by Cluster indicated that the magnitude of the magnetic field was of the order of 30 nT, the normal for this shock (based upon FGM crossing times) is $n_B = (0.94, -0.17, 0.293)$ (in the GSE frame), and the shock velocity was determined to be 48.92 km s^{-1}. Other relevant parameters are $\theta_{Bn} \approx 87°$- and a density $n \sim 19$ cm^{-3}. The high value of the field resulted in an unusually small $\beta \sim 0.07$. The Alfvén Mach number for this shock ($M_A \sim 3.6$) lies close to the First Critical Mach number and to the whistler critical Mach number so the conditions of the solar wind are quite favourable for the formation of quasi-electrostatic sub-shocks at the shock front (Balikhin et al. 2002). Figure 8 (adopted from Walker et al. 2004) shows an overview of the magnetic and electric field measurements made by FGM and EFW respectively during this shock crossing. The top panel shows the magnitude of the magnetic field measured by FGM. Initially, all four Cluster spacecraft are in the solar wind just upstream of the outward moving bow shock which subsequently swept over the satellites in the order C4 (17:17:43.5), C2 (17:17:45.5), C1 (17:17:48.5), and finally C3 (17:17:53.5). The magnetic field profiles show a set of clean shock crossings that possess clearly discernible foot, ramp and overshoot regions. The second panel shows the magnitude of the electric field measured by EFW in the spin plane of each satellite ($|E|^2 = E_x^2 + E_y^2$). In the solar wind, the typical magnitude

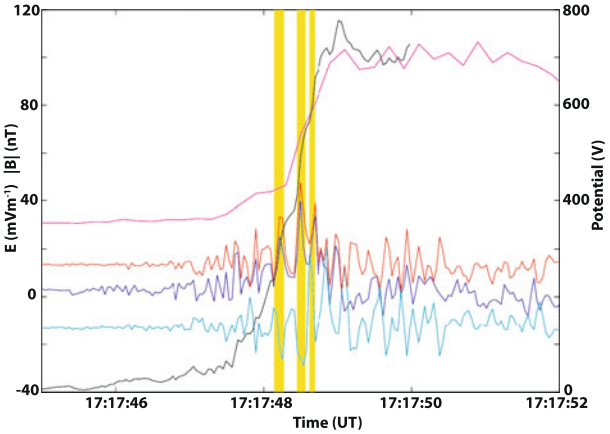

Fig. 9 The FGM magnetic and EFW electric fields measured by Cluster 1 on 31st of March 2001 around 17:18 UT. The magnetic field magnitude is shown by the *magenta line*. The spin plane electric field magnitude, and E_x and E_y components are shown in *red*, *blue* and *cyan* respectively. The *yellow regions* highlight the periods when large amplitude short duration spikes in the electric field are observed. The *black line* (Y scale of RHS) represents the change in potential within the shock (Adapted from Walker et al. 2004)

of the electric field is around 14 mV m^{-1} in the satellite spin plane. It is possible to estimate the E_z component of the upstream electric field assuming that $\mathbf{E} \cdot \mathbf{B} = 0$. This assumption is valid for estimating the field upstream and downstream of the shock but not within the shock region itself. Upstream of the shock, $E_z \approx 5$ mV m^{-1}. This value is higher than the measured E_x component ($\sim$2.5 mV m^{-1}) and less than the E_y component (-13 mV m^{-1}). Comparing the top two panels it can be seen that the disturbances measured in the electric field begin in the foot region of the shock and continue until the satellites are downstream of the overshoot/undershoot. These general disturbances have amplitudes generally in the range 5–30 mV m^{-1}. During their crossings, each of the satellites recorded a number of large amplitude, short duration features in the electric field. The largest of these spikes have maximum amplitudes of approximately 30, 40, 60, and 65 mV m^{-1} for satellites 1, 2, 3, and 4 respectively above the field measured in the solar wind just upstream of the shock front. These values represent lower limits of the strength of the electric field since the component perpendicular to the spin plane is not considered. They are seen to occur within the ramp region but there is no strong feature within the FGM data with which they correlate. It is also observed that the largest electric field peaks observed on each satellite appear to occur in pairs which may suggest field rotation. The two lower panels show the components of the electric field measured in the satellite spin planes. Both panels show that the components of the field exhibit a twin peaked structure, similar to that observed in the field magnitude and that the direction of rotation is the same for both peaks. Thus the overall structure is not due to a single rotation of the field. Our goal is a statistical study of the widths of these short living, large amplitude features.

Using the four point measurements one can determine the occurrence time of these peaks in the electric field and hence compute a normal. Examining the E_x component, the time differences between the observations of the first peak in the electric field are $\Delta t_{12} = -3.01$ s, $\Delta t_{13} = 5.03$ s, and $\Delta t_{14} = -5.35$ s. When coupled with the respective positions of the satellites this yields a normal direction $n_E = (0.946, -0.155, 0.283)$ and a velocity of $\sim$50 km s^{-1}. The difference between this normal n_E and that determined from the magnetic field (n_B) is less than a degree. Thus it appears that the electric field spikes correspond to layers within the overall shock structure. Figure 9 shows the results from Cluster 1 in greater detail. The magenta line shows the magnitude of the magnetic field. The foot region was entered around 17:17:47.3 UT whilst the ramp was crossed between 17:17:48.3 and 17:17:48.9 UT. Several large spikes in the electric field are observed in the region of the foot and shock ramp. The three largest occur around 17:17:48.2 (20 mV m^{-1}),

17:17:48.5 (30 mV m^{-1}), and 17:17:48.6 (15 mV m^{-1}). Their short duration implies that their scale size is of the order 3–5c/ω_{pe}. The black line in Fig. 9 represents an estimation of the electrostatic potential measured in the normal direction. This was calculated by removing an average of the field measured in the region just upstream of the shock from the field measured within the shock region and then integrating the projection of this electric field along the normal direction. Whilst the actual potential cannot be calculated due to the incomplete vector measurements, it can be estimated by assuming that the field perpendicular to the spin plane $E_z = 0$. This assumption is valid because for this particular shock, the normal lies very close to the spin plane. This calculation can be used to show that the largest jumps in the potential coincide with the spikes observed in the electric field and that these occurrences contribute a significant fraction of the total potential change observed at the shock. During this period, the electric field enhancements contribute around 40 % of the total change.

3.1 Scale Size

The preceding sections have presented evidence for localized increases in the electric field strength measured as the satellite traverses a quasi-perpendicular bow shock. All shocks analyzed show evidence for an enhancement in the background electric field. In most cases, the region in which this field enhancement occurs lasts longer than the crossing of the magnetic ramp. The field typically increases of the order 1–3 mV m^{-1} above that measured in the solar wind. However, as has been noted above, the turbulence in this region is dominated by spike-like fluctuations lasting a few milliseconds and with magnitudes of typically 4–20 mV m^{-1} with a maximum magnitude of the order of 70 mV m^{-1}. This existence of large gradients in the electric field has repercussions for processes involved in the heating of electrons. In the presence of strong electric field gradients the electron gyration frequency can deviate from its classically calculated value (Cole 1976; Balikhin et al. 1998), leading to an increase in its Larmor radius and the possibility of a breakdown in adiabaticity (Cole 1976; Balikhin et al. 1998). Having shown that the spikes observed in the electric field at the front of a quasiperpendicular shock appear to be physical structures that form a layer within the shock front as opposed to being the result of noise in the data or motion of the shock a statistical study of these features was performed to investigate their relationship to the properties of the shock front. Now we shall present statistical study of the data collected from a number of such spike-like features.

Figure 10 shows the distribution of the scale sizes determined from the event duration and the shock velocity evaluation of these features in terms of the electron inertial length. The scale size of these events will be unaffected by the incomplete vector measurements of the electric field. The vast majority of crossings have scale sizes of the order of 1–5c/ω_{pe}. The data that form tail of the distribution at longer scale sizes typically comprise events that have a multi-peak structure. This type of event represents an upper limit to the scale size of these short-lived events. In comparison, the typical scale of the magnetic ramp is characterized by the ion inertial length (Newbury and Russell 1996) although these authors also report one particular shock as having a ramp scale as small as 0.05c/ω_{pi} or 2c/ω_{pe}.

Figure 11 shows the relationship between the Mach number and scale size of the spikes observed in the electric field. From the figure, it is clear that the scale size has a lower limit that decreases as the Mach number increases. One should notice that these results represent the tendency rather than the proof, the number of points at high Mach numbers is not sufficient for valuable statistical study.

Figure 12 shows a scatter plot of the relationship between θ_{Bn} and the scale size of the electric field enhancements. In general there appears to be a broad range of scales. However,

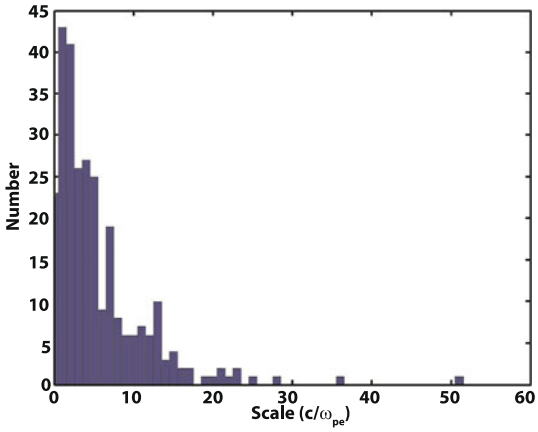

Fig. 10 Histogram of the scale sizes for the spike-like enhancements observed during a number of crossings of the quasi-perpendicular bow shock (Adapted from Walker et al. 2004)

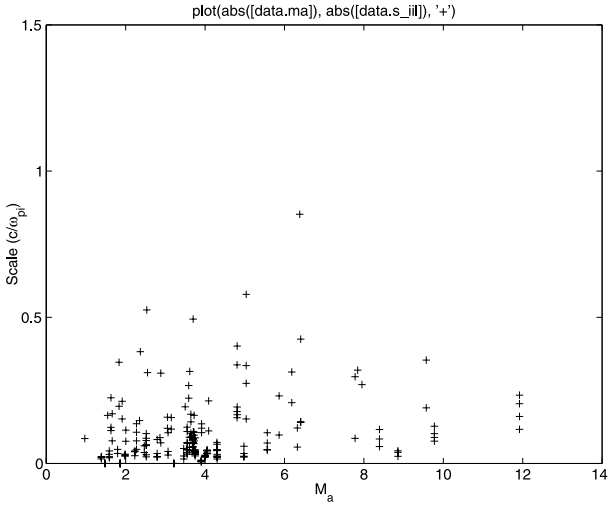

Fig. 11 Dependence of scale size on upstream Mach number (From Walker et al. 2004)

as θ_{Bn} approaches 90°—the scale length decreases. For the shocks analysed with θ_{Bn} close to 90°—the scale lengths are of the order of $2c/\omega_{pe}$. This compares favourably with theoretical estimates that for shocks close to perpendicular the scale width is estimated to be of the order of the electron inertial length as proposed by Karpman (1964), Galeev et al. (1988). This tendency corresponds exactly to dispersion dependence upon the angle θ_{Bn}.

3.1.1 Amplitude

The examples presented above show that the increase in the electric field ($\Delta E = E_{spike} - E_{upstream}$) observed during encounters with these spike-like structures varies between 4 and 70 mV m^{-1} above the average field that is measured in the solar wind just upstream of the shock. In this section the relationship between this change (ΔE) and the shock Mach number, and the angle θ_{Bn} is presented. Figure 13 shows a scatter plot of the peak amplitude observed in the electric field spike event (ΔE) as a function of the shock Mach number M_A.

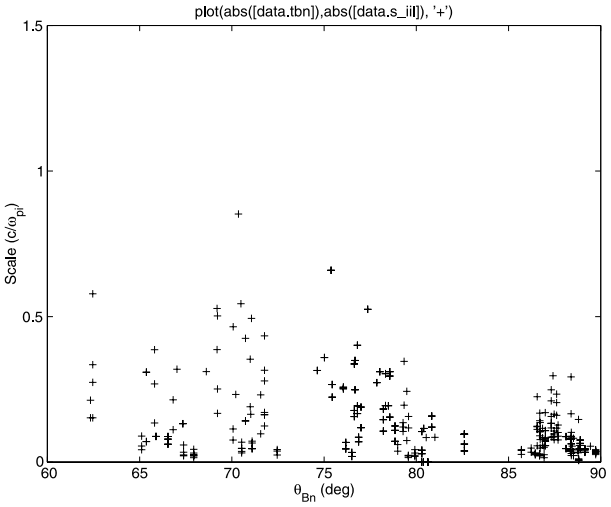

Fig. 12 Dependence of scale size on θ_{Bn} (From Walker et al. 2004)

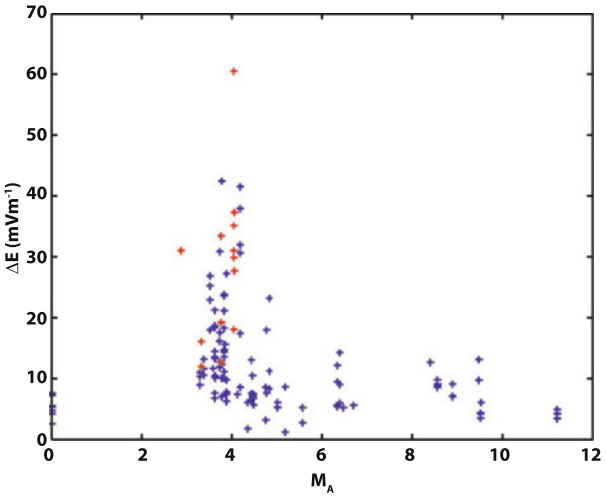

Fig. 13 Scatter plot showing the relationship between the amplitude of the electric field spikes as a function of Mach number. The *red crosses* are used to highlight the data for the shocks that occurred on 31st of March 2001 (Adapted from Walker et al. 2004)

For shocks whose Mach number $M_A > 5$ there is a fairly constant trend in which $\Delta E < 15\ \mathrm{mV\,m^{-1}}$. In the Mach number range $3 < M_A < 5$ the range of observed amplitudes varies between 5 and 60 $\mathrm{mV\,m^{-1}}$. It appears that in this Mach number range the electric field potential becomes more important than for low and high Mach number shocks that corresponds to dependence of the electrostatic potential upon the Mach number (Dimmock et al. 2012). The red crosses highlight the shocks observed on 31st of March 2001. All of these shocks fall into this range of Mach numbers. This set of shocks seems to possess Mach numbers corresponding to supercritical range and having large number density, at about 7 %, of alpha particles (Maksimovic, private communication). Their structure seems to resemble that of electrostatic sub-shocks similar to those observed in laboratory plasmas (Eselevich et al. 1971). A characteristic signature of sub-shocks is the occurrence of small scale electrostatic fluctuations such as those observed on this particular day. Ion sound sub-shocks have been observed in laboratory plasmas with scales of the order of 100 Debye

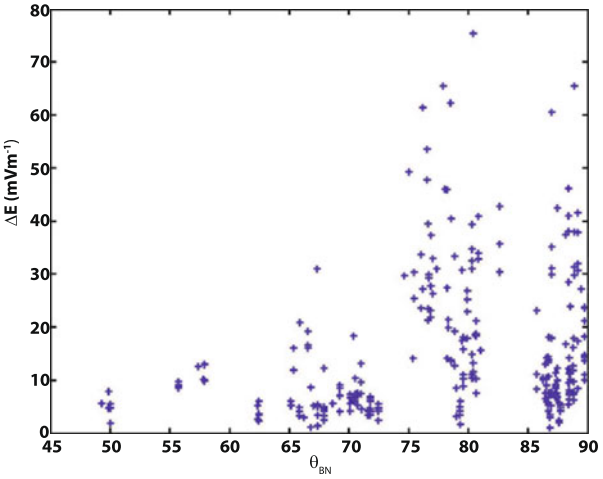

Fig. 14 The relationship between ΔE and θ_{Bn} (Adapted from Walker et al. 2004)

lengths. For the shocks observed in 31st of March 2001, the scale is closer to characteristic scale of the fast magnetosonic mode (Balikhin et al. 2002).

The relationship between ΔE and θ_{Bn} is shown in Fig. 14. It clearly shows that as θ_{Bn} approaches 90°—the range of the observed amplitudes of the electric field spikes increases.

3.2 Conclusions

In this section we presented the changes observed in the electric field during the crossing of a number of quasi-perpendicular bow shocks. It is shown that the electric field is enhanced during the crossing of the shock and that the scale size over which this enhancement is observed is larger than that of the macroscopic magnetic ramp region. Within the whole shock region, short lived electrostatic structures are observed that are intensified in the ramp region. The scale size of these structures is of the order of a few c/ω_{pe}: and was shown to decrease as θ_{Bn} approaches 90°—which corresponds to the dependencies following from theoretical model based on consideration of the shock as mainly dispersive nonlinear structure (Galeev et al. 1988; Krasnoselskikh et al. 2002). The amplitudes of these structures are typically of the order of 5–20 mV m^{-1}: but under special circumstances may reach as high as 70 mV m^{-1}. The highest amplitudes appear to be observed for shocks whose Mach number is in the range 3 to 5. This may be an indication that such shocks have quasi-electrostatic sub-shocks inside the main ramp transition. It was also demonstrated that these small scale structures make a substantial contribution to the overall change in potential observed across the shock and that the potential change is not linear.

4 Dispersive Nature of High Mach Number Shocks: Poynting Flux of Oblique Whistler Waves

It is well known that a subcritical shock has a nonlinear whistler wave train upstream of its front (Sagdeev 1966; Mellott 1985). The major transition of such a dispersive shock, the ramp, behaves as the largest peak of the whistler precursor wave package (Karpman et al. 1973; Kennel et al. 1985; Galeev et al. 1989; Krasnoselskikh et al. 2002). The presence of whistler/fast magnetosonic precursor wave trains in supercritical shocks was

experimentally established in Balikhin et al. (1997b), Krasnoselskikh et al. (1991), Oka et al. (2006). These whistler waves have rather large amplitudes and their role in energy transformation and redistribution between different particle populations and in the formation of the shock front structure is still an open question. The energy source responsible for the generation of these waves is the subject of active debate in shock physics (see Galeev et al. 1988, 1989; Krasnoselskikh et al. 2002; Matsukiyo and Scholer 2006; Comişel et al. 2011). Often the precursor waves are almost phase-standing in the shock frame. However, if they are generated by the ramp region as the dispersive precursor their group velocity can still be greater than zero in the shock reference frame, which would allow energy flow in the form of Poynting flux to be emitted towards the upstream of the shock transition. On the other hand, if the waves are generated by instabilities related to reflected ions their energy flux will be directed from the upstream region towards the shock ramp. The goal of this section is to address this problem, to present the direct measurement of the Poynting flux of the upstream whistler waves aiming to establish the direction of the Poynting flux.

Below we establish the energy source of the waves by calculating the Poynting flux of the waves in the Normal Incidence Frame (NIF) of the shock, using multi-satellite Cluster data from crossings of the Earth's bowshock (Escoubet et al. 1997; Bale et al. 2005). Two events with supercritical Alfvénic Mach numbers are analyzed. In both cases it is found that the shocks show dispersive behaviour with the Poynting flux directed in upstream direction.

Poynting flux is not a Lorentz invariant and therefore depends on the frame of reference. To evaluate the value and direction of the Poynting flux with respect to the the shock we transform the electric field to the Normal Incidence Frame (NIF). The normal $\hat{\mathbf{n}} = +\hat{\mathbf{x}}$ which also serves as the x-coordinate direction in the NIF system is obtained by four-spacecraft timing, $\hat{\mathbf{z}}$ is the direction of maximum varying magnetic field obtained from a minimum variance analysis, and $\hat{\mathbf{y}}$ is the direction of the convection electric field which completes the right-handed system.

The transformation from the spacecraft frame to the NIF is given by $\mathbf{E}_{NIF} = \mathbf{E}_{sc} + \mathbf{v} \times \mathbf{B}$. The total velocity required for this transformation is defined by $\mathbf{v} = \mathbf{v}_{sh} + \mathbf{v}_{NIF}$ where $\mathbf{v}_{sh} = v_{sh}\hat{\mathbf{n}}$ is the shock velocity, $\mathbf{v}_{NIF} = \hat{\mathbf{n}} \times (\mathbf{v}_u \times \hat{\mathbf{n}})$ is the NIF velocity and $\mathbf{v}_u$ is the solar wind velocity.

A general shift of reference frame, coordinate transformation, and evaluation of the complete Poynting vector requires knowledge of the full six-dimensional electromagnetic field (three electric and three magnetic components). The Cluster spacecraft, however, only measures the two components of the elecric field in the spin-plane of the spacecraft, while the third component normal to the spin-plane is not measured. To reconstruct the third component we use the assumption that for the wave electric and magnetic fields the condition $\mathbf{E} \cdot \mathbf{B} = 0$ holds. While this is a true condition for the cross-shock (DC) electric field, it holds well for whistler wave electric fields at lower frequencies.

We study two quasi-perpendicular high Mach number shocks encountered by the Cluster multi-spacecraft mission (Escoubet et al. 1997). The first shock was observed around 04:53:40 Universal Time (UT) on 20th of January 2003, and the second around 07:07:00 UT on 24th of January 2001. We use data from the EFW (electric field) (Gustafsson et al. 1997), FGM (DC magnetic field) (Balogh et al. 1997) and STAFF (wave magnetic field) instruments (Décréau et al. 1997) from spacecraft 2 (for the 2003 shock) and spacecraft 3 (for the 2001 shock). The shock normal $\hat{\mathbf{n}}$ is established by assuming a planar shock and using the time of crossing of the four spacecraft and their relative positions (Paschmann and Daly 1998).

The first shock analyzed had an upstream $\theta_{Bn} \sim 85°$ and an Alfvénic Mach number $M_A \sim 5.5$. The electric and magnetic fields in the shock front region are characterized by

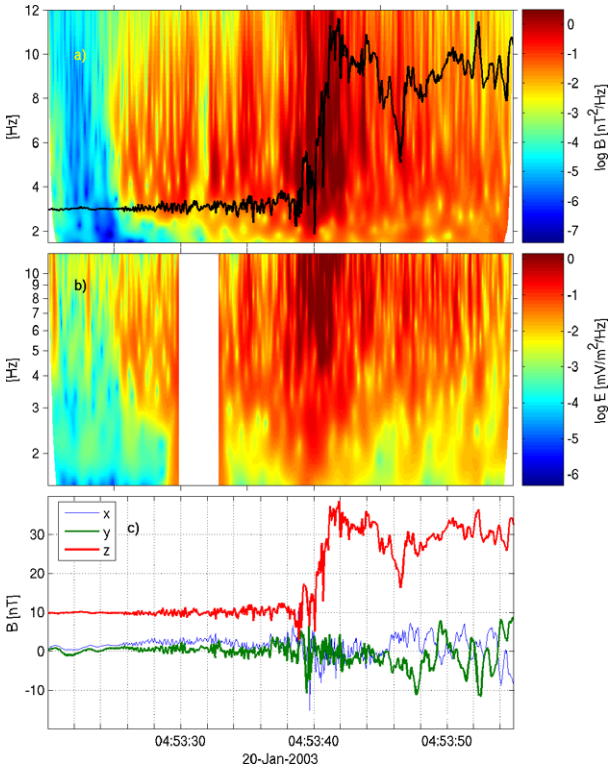

Fig. 15 Magnetic and electric fields in the Normal Incidence Frame (NIF) of a high Mach number shock. (**a**) Power spectra of the magnetic field (STAFF). The *black line* is the DC total magnetic field, included to show the waves in relation to the shock ramp structure. (**b**) Power spectra of the electric field (EFW). The data gap is due to instrumental interference. (**c**) The magnetic field in NIF coordinates B_{NIF} (Adapted from Sundkvist et al. 2012)

waves, with stronger amplitudes closer to the ramp, see Fig. 15. The waves have frequencies $f_{cp} < f$, where $f_{cp} \sim 0.1$ Hz is the proton gyrofrequency, and right-handed polarization looking along the magnetic field vector and thus belong to the magnetosonic/whistler mode. The direction of the wave-vector $\hat{\mathbf{k}}$ was determined by the Means method (Means 1972), which uses the imaginary part of the three-dimensional magnetic field spectral matrix. The angle θ_{kB} between the wave vector and the local ambient magnetic field is shown as a function of frequency in Fig. 16(b). The average value $\langle\theta_{kB}\rangle$ in the shock front region is ∼10–50° (right-hand scale). The whistler waves are thus oblique with respect to the local magnetic field, as well as to the shock normal. The angle increases continously as the shock front is approached and $\theta_{kB} \rightarrow 90°$ at the ramp, reflecting the quasi-perpendicular nature of the shock. This smooth transition stresses the nature of the shock as a dispersive nonlinear whistler wave.

Since Poynting flux is a second-order quantity the electric and magnetic fields in the NIF were wavelet transformed (Morlet width 5.36) and the cross-product $\mathbf{S}_f = 1/\mu_0 \mathbf{E}_f \times \mathbf{B}_f$ formed in frequency space. The calculated Poynting flux is therefore distributed in both time and frequency. The projection of the Poynting flux distribution along the magnetic field $S_{\parallel} = \mathbf{S}_f \cdot \mathbf{B}_0/|\mathbf{B}_0|$ using an instantaneous value of $\mathbf{B}_0$ is plotted in Fig. 16(a), where the colors red (upstream) and blue (downstream) show the direction of the flux. We note that in the front region of the shock the Poynting flux is everywhere directed upstream (red), away from the shock. In the downstream area there is a mixture of blue, green and red, where there is more turbulence and the waves are no longer coherent. The upstream and slightly oblique direction of the Poynting flux is further quantified in the instantaneous angle $\theta_{S,B}$ between the Poynting flux and the ambient magnetic field, plotted in Fig. 16(c). Figure 17

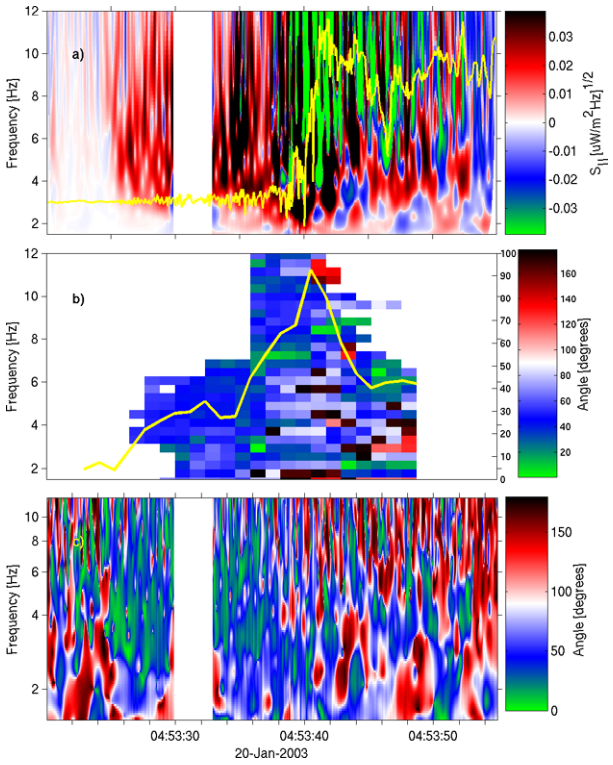

Fig. 16 Poynting flux in the Normal Incidence Frame (NIF) of the same shock as in Fig. 15. (**a**) Poynting flux $S_{\|}$ projected on the local $\mathbf{B}_0$ in the NIF, where red corresponds to the upstream flux away from the shock. (**b**) Angle $\theta_{k,B}$ between $\hat{\mathbf{k}}$ and magnetic field $\mathbf{B}_0$. The *yellow line* represents the average over all frequencies (*right scale*). (**c**) Angle between Poynting flux $\mathbf{S}$ and $\mathbf{B}_0$ (Adapted from Sundkvist et al. 2012)

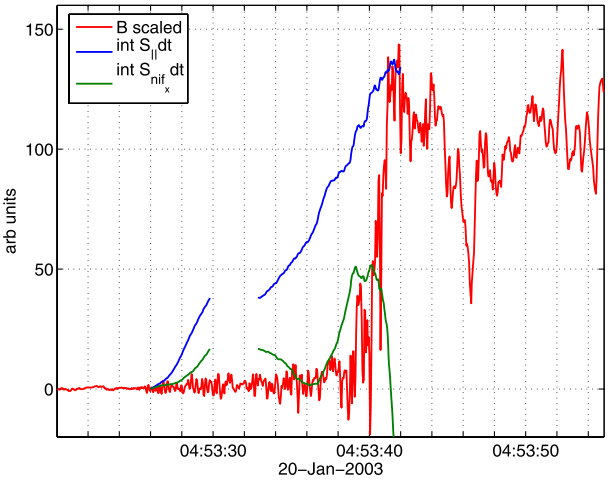

Fig. 17 Poynting flux integrated along the spacecraft trajectory. The *blue line* is a projection along the ambient magnetic field $\int S_{\|}dt$ and the *green line* is a projection on the shock normal $\int \mathbf{S}\cdot\hat{\mathbf{n}}dt$. The *red line* shows the scaled magnetic field B_0 for reference (Adapted from Sundkvist et al. 2012)

shows the Poynting flux along the spacecraft trajectory, with integrated power over frequencies corresponding to the waves in Fig. 16(a), $2 < f < 10$ Hz. In this figure the slope is the important characteristic. Positive slope means Poynting flux carried upstream, and negative slope downstream. From the figure it is evident that the source of the Poynting flux is associated with the shock ramp. The data gap and associated plateau are due to instrumental interference.

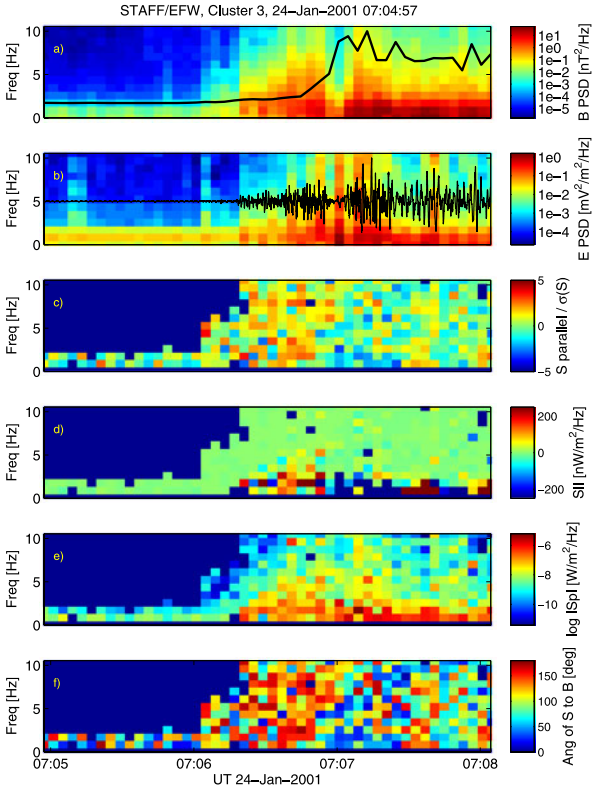

Fig. 18 Poynting flux derived from electric and magnetic fields for a high Mach number shock. (**a**) Wave magnetic field and averaged B_0. (**b**) Wave electric field. (**c**) $S_\parallel$ normalized by its standard deviation (*yellow* and *red* corresponds to upstream flux). (**d**) $S_\parallel$. (**e**) $\log_{10} S_\parallel$. (**f**) Angle of S to $\mathbf{B}_0$ (*red* meaning upstream) (Adapted from Sundkvist et al. 2012)

Another important characteristic established is that the Poynting flux direction is oblique with respect to the shock normal as well as the background magnetic field. This can be explained by analyzing how the phase velocity for whistler waves depends on this angle. The phase velocity of a wave propagating in the plane of the shock normal $\hat{\mathbf{n}}$ and background magnetic field $\mathbf{B}_0$, having an angle α with respect to the shock normal is $V_{ph} = \frac{1}{2}\sqrt{\frac{m_i}{m_e}}\cos(\theta_{Bn} - \alpha)$. Its projection on the direction of the shock normal is $V_{ph,\hat{\mathbf{n}}} = V_{ph}\cos\alpha = \frac{1}{2}\sqrt{\frac{m_i}{m_e}}\cos(\theta_{Bn} - \alpha)\cos\alpha$. Its maximum value can be found to be equal to $\max(V_{ph,\hat{\mathbf{n}}}) = \frac{1}{4}\sqrt{\frac{m_i}{m_e}}(1 + \cos\theta_{Bn})$, thus the projected phase speed can be larger than the whistler critical velocity given above. The above analysis also explains the observation of oblique whistler wave trains found in computer simulations of purely perpendicular shocks (Hellinger et al. 2007). So even in the case of shocks having Mach numbers larger than the whistler critical Mach number, whistler waves oblique with respect to the shock normal can remain quasi-standing.

The second analyzed shock crossing on 24th of January 2001 is shown in Fig. 18. This is a reforming high Mach number shock ($M_A \sim 11$) and has been analyzed in detail in Lobzin et al. (2007). Both of the shocks discussed by were analyzed using wavelet as well as Fast Fourier Transform (FFT) dynamic spectra techniques. We present the second shock using the FFT analysis, to show that the conclusions are not technique dependent. The upstream whistler waves, Figs. 18(a), (b), again have an overall Poynting flux upstream, away from the shock in the normal incidence frame, evident from the red and yellow (upstream) colors

of $S_{\|}$ (Fig. 18, panels (c) through (f)). For this shock the ambient magnetic field was directed in the opposite direction, so that 180° (red) means upstream in Fig. 18.

The power flux given by the Poynting vector shows unambiguously that they carry energy over a broad frequency range from the shock ramp towards the upstream solar wind, starting from the position of the shock front. This leads to conclusion that the results of the analysis are consistent with a theoretical model (Galeev et al. 1988; Krasnoselskikh et al. 2002) that considers the shock steepening to be balanced by the effect of dispersion in addition to dissipation. As the shock steepens, nonlinearities transfer energy to shorter wavelengths of the spectrum, and is ultimately carried away from the shock as dispersive whistler wave trains. This analysis demonstrates that for high Mach number shocks, dispersive effects are dominant for the formation and stability of the shock front. Since the whistler waves are strongly damped upstream of the shock, we infer that they can play the role of an intermediate step in the energy re-partition problem, with the energy ultimately being dissipated through wave-particle interaction.

5 Electron Heating Scale at High Mach Number Quasiperpendicular Shocks

From the discussion in the previous sections the energy repartition amongst particle populations in quasiperpendicular shocks is a multi-scale process related to the spatial and temporal structure of the electromagnetic fields within the shock layer. While the major features of the large scale ion heating are known, the electron heating and smaller scale fields remain poorly understood and controversial. In this section we will discuss the scale of the electron temperature gradient based on the possibility of obtaining unprecedented high time resolution electron distributions measured in situ by the Cluster spacecraft recently discussed by Schwartz et al. (2011). The authors discovered that approximately half of the electron heating coincides with a narrow dispersive layer several electron inertial lengths (c/ω_{pe}) thick. Consequently, it gives one more argument that the nonlinear steepening is limited by wave dispersion. The DC electric field associated with the electron pressure gradient must also vary over these small scales, strongly influencing the efficiency of shocks as cosmic ray accelerators.

The 4 Cluster spacecraft (Escoubet et al. 1997) are unique in their ability to remove the time-space ambiguity in time series data taken by in situ space plasma instrumentation. By timing the passage of an event at each corner of the tetrahedron formed by the 4 spacecraft, the planar orientation and speed of the event can be determined. We employ this technique to convert the time series of data to distance along the shock normal Schwartz (1998). Figure 19 illustrates the identification of the steep shock ramp that we use as event times.

The electron instrument on Cluster measures fluxes at several energies in a half-plane containing the spacecraft spin axis. These measurements form an azimuthal wedge divided

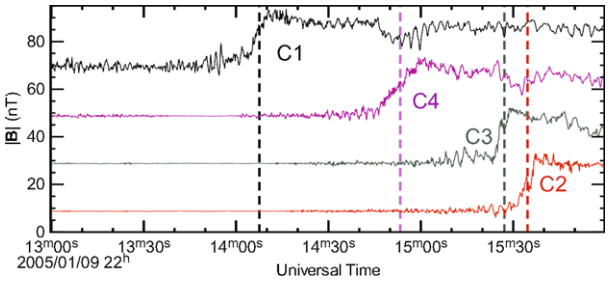

Fig. 19 Magnetic field data at a crossing of the Earth's bow shock by the 4 Cluster spacecraft on 9th of January 2005. Traces have been shifted by 20 nT for clarity. The *dashed lines* show the times of the steep ramp (Adapted from Schwartz et al. 2011)

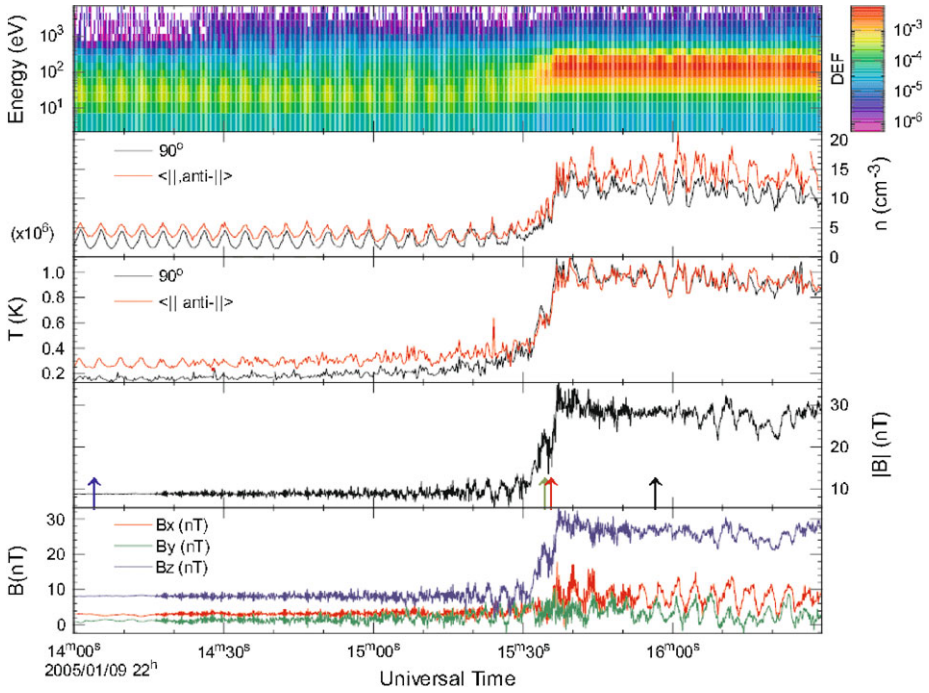

Fig. 20 Overview of data from Cluster 2 on 9th of January 2005. From top to bottom: Omni-directional electron energy-time spectrogram @ 250 ms resolution, electron pseudo-density, electron pseudo-temperatures (see Method), magnetic field magnitude, and field components. *Arrows* in the fourth panel show locations of the cuts presented in Fig. 22 (Adapted from Schwartz et al. 2011)

into 12 polar directions from aligned to anti-aligned with the spin axis, and are repeated at 125–250 ms intervals. A full 3D distribution covering all azimuths is thus built up over 1 spin (∼4 s). However, when the magnetic field is roughly aligned with the spin axis, each wedge contains a full set of pitch angles from 0° to 180°. Under these circumstances, and assuming gyrotropy, the full pitch angle distribution function is available at ≤250 ms resolution.

We rebin the raw electron data into pitch angles α relative to the instantaneous magnetic field. We calculate pseudo-densities and temperatures for each pitch angle bin as if the distribution were isotropic, e.g., $n(90°) = 4\pi \int f(v, \alpha = 90°)v^2 dv$. These pseudo-moments better characterise the phase space distributions in the $\parallel, \perp$ directions than the full $T_{\parallel,\perp}$ moments (cf. Fig. 9 of Mitchell et al. 2012).

5.1 Results and Conclusions

An overview of the data for 9th of January 2005 is shown in Fig. 20. The transition from unshocked solar wind plasma to the shocked magnetosheath occurs around 22:15:30. Although the solar wind flow is a factor of 10 slower than the electron thermal speed, some residual modulation at the spin period is evident in the data. We have averaged the parallel and anti-parallel ($\alpha = 0, 180°$) moments so that the second and third panels of Fig. 20 reveal the pseudo-parallel and perpendicular moments. Note that the pseudo-densities $n(\alpha)$ are not, and from their definition above need not be, equal. The bottom two panels show increasing oscillations and a gradual "foot" ahead of a steeper magnetic "ramp" region. The dominant

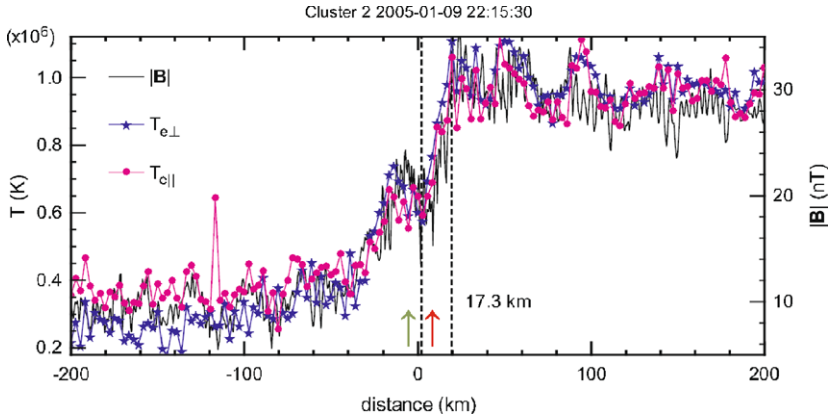

Fig. 21 Magnetic field (*solid*) and electron temperature (*symbols*) as a function of distance from the shock ramp. Roughly half the temperature rise occurs within the region 17.3 km wide between the *dashed vertical lines* corresponding to 6.4 electron inertial lengths (c/ω_{pe}) (Adapted from Schwartz et al. 2011)

$\hat{\mathbf{z}}$ magnetic field component is nearly aligned with the spin axis, enabling the parallel and perpendicular moments to be available in every 0.25 s wedge as described above. Figure 20 already suggests the main result namely that the rise in electron temperature closely follows even the steepest ramp of the magnetic field.

Figure 21 shows that both the parallel and perpendicular electron temperatures closely track the steep rise in magnetic field, with half the electron heating taking place on a scale of 17.3 km, corresponding to 6.4 electron inertial lengths and a small fraction (0.15) of an ion inertial length. Although much of the electron dynamics is linked to the DC electric and magnetic fields within the ramp (Feldman et al. 1983; Goodrich and Scudder 1984; Scudder 1995; Lefebvre et al. 2007) and is therefore reversible (the distribution function in this limiting case might be dependent upon energy and adiabatic invariant in de Hoffmann-Teller reference frame), the fact that both $T_{e\|}$ and $T_{e\perp}$ rise together suggests an inflation of the particle phase space distribution that is not reversible, due primarily to the filling in and/or entrapment of electrons in regions of phase space that would otherwise be inaccessible.

This infilling can be seen in the cuts of the distributions shown in Fig. 22. Within the steep ramp, the inflated distribution is evident, with the flat-topped infilled region already at its downstream level. This supports the notion that the temperature profiles shown in Fig. 21 really do represent irreversible heating. Interestingly, Fig. 22 shows that features previously reported with the ramp, e.g., the beam vestige of the solar wind peak (Feldman et al. 1983), are present only in the more gradual initial rise that precedes the steep ramp. That beam has been totally eroded by the time this electron scale ramp is encountered.

Thus the electron heating occurs over scales that are significantly smaller than the convected proton gyro-scale V_n/Ω_{ci} invoked in Bale et al. (2003) and also smaller than the ion inertial length that might be anticipated due to micro-instabilities within the shock current layer (Papadopoulos 1985b; Matsukiyo and Scholer 2006).

Recent statistical studies (Hobara et al. 2010) argued that previous fits to a proxy of the plasma density profile (Bale et al. 2003) mixed contributions from the more extended foot region governed by reflected gyrating ions. Restricting the measurements to just the steep ramp, they report widths in the range 3–55 c/ω_{pe} with a decreasing trend as the Mach number increases. They interpreted their work in terms of shock steepening limited by the

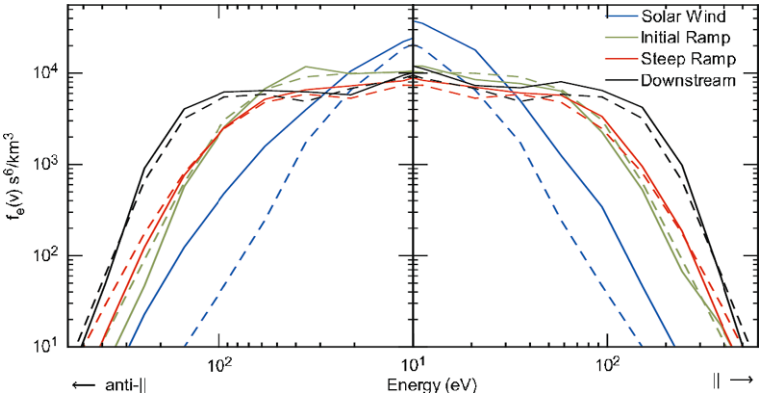

Fig. 22 Cuts of the electron distribution functions in the solar wind, initial ramp, steep ramp, and downstream along (*solid*) and perpendicular (*dashed*) to the magnetic field. The locations of the cuts are indicated along the axes in Figs. 20 and 21. Note the solar wind halo drift evident in the anti-aligned direction and the absence of features within the steep ramp (Adapted from Schwartz et al. 2011)

dispersion of electron whistler waves, with dispersion relation $\omega = \Omega_{ce} \cos\theta_{Bn} (k^2 c^2/\omega_{pe}^2)$. The limiting case of a wave capable of phase standing in the incident flow has a wavelength that can be written

$$\frac{\lambda}{c/\omega_{pe}} = 2\pi \frac{\cos\theta_{Bn}}{M_A} \sqrt{\frac{m_i}{m_e}}$$

The results from Table 1 yield a value of 9.2 for this ratio, comparable to the 6.4 electron inertial lengths given above. The fact that supercritical shocks steepen to this whistler limit suggests that dissipation processes are insufficient to broaden the transition further.

It should come as no surprise that the steepening of a fast mode (right-handed) wave results in a right-handed whistler signature. Indeed, the non-coplanar component of the magnetic field (Thomsen et al. 1987), responsible for the difference in the shock electrostatic potential when viewed in different shock rest frames (Goodrich and Scudder 1984), is right-handed. There is new evidence (Sundkvist et al. 2012) that the wave Poynting flux is directed away from the ramp region upstream as expected for dispersion-limited steepening.

The present study measures directly the actual temperature profile of the electrons. The result confirms that nonlinear steepening proceeds down to scales limited by whistler dispersion. We have argued that this represents irreversible heating, implying that dissipation is operative on this, or probably smaller, scales.

We have attempted a similar analysis on other shock crossings observed by Cluster, with consistent findings. Suitable events are rare, since they require the combination of a slowly moving shock and favorable magnetic field orientations. Future space missions need to be proposed to target electron physics and hence should provide numerous examples for statistical studies.

What process(es) are actually responsible for (sub-)whistler-scale dissipation? The overall inflation in phase space is linked to the action of the cross-shock electrostatic potential in concert with the magnetic mirror forces. Some or all of the potential may be concentrated in intense spikes (Bale and Mozer 2007) that may break the adiabaticity of electron phase space trajectories despite a ramp thickness which, in our example, is 20 times the local electron gyroradius. It is worth noting that the localized spikes of the electric field are present inside the ramp region. Figure 23 represents 10 second interval of electric field measurements

Table 1 Shock parameters 2005 Jan 9 @ 22:15

Parameter	Value	
V_{shock}	+10.8	km s^{-1}
Unshocked magnetic field $\mathbf{B}_u$ †	(3.07, 1.35, 8.14)	nT
Unshocked electron density	4.0	cm^{-3}
Location (Earth radii)	(12.3, 13.3, −6.7)	R_e
$\hat{\mathbf{n}}$ shock normal (timing)	(0.855, 0.418, −0.307)	
$\hat{\mathbf{n}}$ (model) Schwartz (1998)	(0.904, 0.383, −0.189)	
$V_n \equiv \mathbf{V} \cdot \hat{\mathbf{n}}$ (shock rest frame)	373	km s^{-1}
Alfvén Mach no. M_A	3.8	
Magnetosonic Mach no. M_{ms}	3.0	
$\theta_{Bnu} \equiv \angle \mathbf{B}, \hat{\mathbf{n}}$	83	°
Plasma ion β_i	0.4	
Plasma electron β_e	0.34	
Electron inertial length c/ω_{pe}	2.7	km
Ion inertial length c/ω_{pi}	117	km
V_n/Ω_{ciu} ††	443	km
V_n/Ω_{cis}	139	km
Whistler wavelength λ	24.8	km
Electron Larmor radius $r_{Le\,u}$	1.01	km

† All vectors are in the GSE frame of reference. Subscripts "s" ("u") denote quantities in the (un)shocked region

†† $\Omega_{ci} \equiv eB/m_p$ is the proton gyrofrequency

inside the ramp by Cluster 2, from 22:15:30 to 22:15:40 that is relatively short time with respect to time of the shock crossing but corresponds to ramp region (courtesy of F. Mozer). One can clearly see quite intense bursts of the electric field having amplitudes as large as 20–30 mV m^{-1}. These bursts are very similar to those reported in Sect. 2. Such electric field bursts can be one of the possible sources of electron heating and scattering.

Another candidate processes (e.g. Balikhin and Gedalin 1994) responsible for in-filling regions of phase space, in some of which electrons are trapped, include wave scattering (Scudder et al. 1986c; Veltri and Zimbardo 1993) and demagnetization (Balikhin and Gedalin 1994); these will require further analysis and simulations.

Our discovery of short scale electron heating has an important consequence for electron and ion acceleration. Gradient drift and surfing mechanisms are sensitive to the scale of the field transitions (Zank et al. 1996), becoming very efficient at scales comparable to those reported here.

6 Can Anomalous Resistivity Account for Energy Dissipation and Electron Heating

The major results reported in this section were first published in Balikhin et al. (2005), Walker et al. (2008).

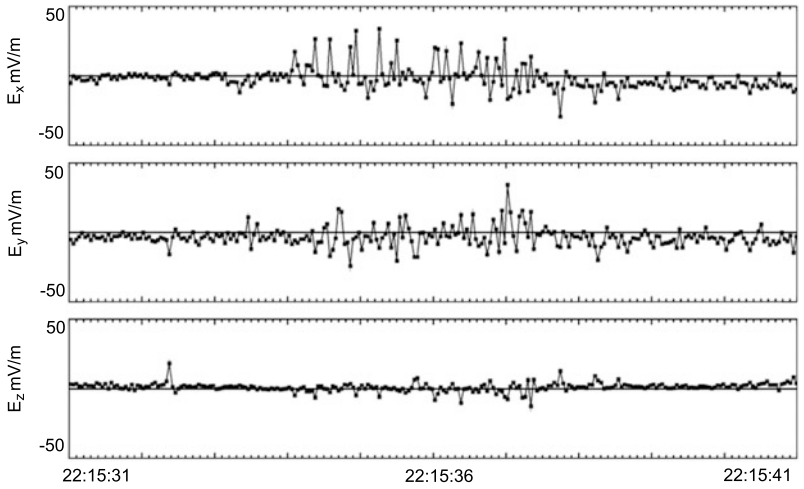

Fig. 23 Electric field measured onboard Cluster 2 satellite from 22:15:31 to 22:15:41. Electric field bursty spikes having amplitudes of 20–40 mV m^{-1} having duration of the order of 0.1 s are clearly seen during ramp crossing. Figure is provided by F. Mozer

6.1 Ion Sound Wave Packets at the Quasiperpendicular Shock Front

The data used in both articles presenting observations of short scale waves were collected by the EFW instrument on board Cluster satellites. EFW uses two pairs of spherical probes in the satellite spin plane situated on the ends of wire booms whose length is 44 m as shown in the left hand panel of Fig. 24. Thus, the distance between probes adjacent/opposite to one another is ∼62/88 m respectfully. Normally, the EFW instruments return the electric field calculated as the difference in probe potentials between probes 1 and 2 (E_{12}) and 3 and 4 (E_{34}) with a sampling rate of either 25 Hz (normal science mode) or 450 Hz (burst science mode). The individual probe potentials are also available with a time resolution of 5 Hz. In addition to these standard modes, there is a triggered internal burst mode. Using this mode, data for a short time period may be captured with a much higher sampling rate. The EFW data that has been analysed in this study consists of internal burst mode data comprising the four individual probe potentials sampled at 9 kHz for periods of around 10 seconds. Since the internal burst data is captured and stored depending upon some criteria, it may be that although the shock region was targeted for data collection, the waveforms returned may not have been captured in the shock front itself. To this end, a search was made to find possible candidate events by cross referencing the list of Cluster shock crossings for 2002 with the list of periods for which internal burst data are available. This resulted in a list of 10 possible events. Of these events, a comparison between the FGM magnetic field measurements and the time periods for which EFW internal burst data were available showed that there were only two shocks for which the period of internal burst data lay solely in the foot region of the shock. Of these, one shock possessed a magnetic profile that was highly turbulent and difficult to interpret and was also eliminated from further analysis. This left just one clean shock on which to perform the analysis.

The internal burst data sets are the only ones generated by EFW that contain the individual probe potentials at a high enough sampling rate to investigate waves and turbulence at frequencies around the lower-hybrid frequency in the vicinity of the terrestrial bow shock

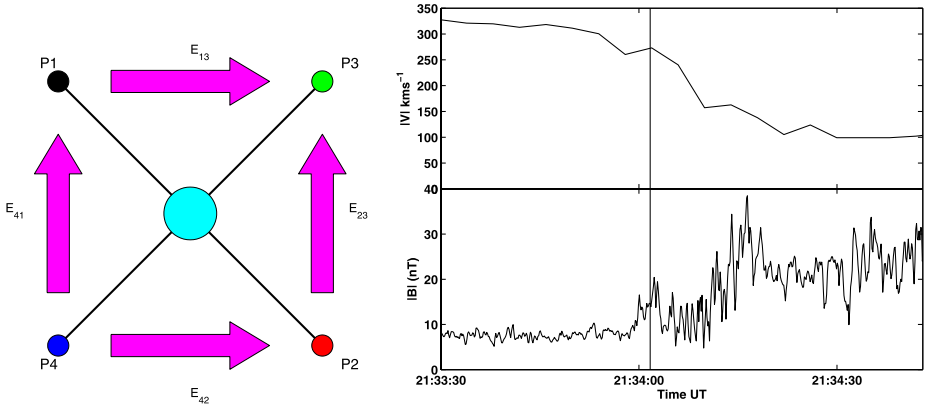

Fig. 24 The *left panel* shows the configuration of the EFW electric field probes and illustrates the electric fields calculated from them. The *right hand panel* shows the magnitude of the magnetic field (*bottom*) and ion bulk flow (*top*) measured during the shock crossing that occurred on 26th of February 2002 at 21:34 UT (Adapted from Balikhin et al. 2005)

(10–30 Hz). By using the individual probe potentials it is possible to compute two parallel electric field components one on either side of the satellite. For example, the probe pairs 1, 3 and 4, 2 maybe used to compute electric field components E_{13} and E_{42} whose directions are parallel and are spatially separated by a distance of ∼62.2 m. This technique has previously been used by Balikhin et al. (2005) and Tjulin et al. (2003) to study small scale electric field structures and waves and is similar to the short baseline interferometry techniques employed in the analysis of data from sounding rockets (Pinçon et al. 1997). Since the probe potentials can be used to calculate two parallel electric field vectors it is possible to use the phase differencing technique to determine the wave vector **k**. This method may also be used to examine the polarisation characteristics of the wave in question. In this case, the phase differencing algorithm is applied to a pair of perpendicular components of the electric field (as opposed to the parallel field components mentioned above). The resulting histogram of the phase difference as a function of frequency yields a vertical line of constant phase difference with respect to frequency at a phase difference of zero for a linearly polarised wave and $\pm\pi/2$ for a circularly polarised wave. Thus, this technique may be used to help distinguish between a linearly polarised lower hybrid wave and a circularly polarised whistler mode wave, both of which have been observed at these frequencies. This method is used in preference to an examination of the coherency (see for example Krasnoselskikh et al. 1991) due to the short duration of the wave packets.

The magnetometer data, used to put the electric field measurements into context within the shock front and compute the lower hybrid resonance frequency, come from the FGM instruments (Balogh et al. 1997) and made publically available through the Cluster Active Archive. These measurements typically have a sampling rate of 22 Hz.

All the data presented in this section were recorded during one shock crossing on February 26th, 2002 at around 21:34 UT during the time intervals marked on Fig. 25 by vertical lines. Red lines mark the periods of registration of ion sound waves, green lines the periods of registration of lower hybrid and whistler waves.

During this period the Cluster satellites were situated in the foot region of a quasiperpendicular shock ($\theta_{Bn} \sim 55°$, $M_A \sim 4.3$). The EFW instrument onboard Cluster 3 was triggered to operate in internal burst mode for a few seconds.

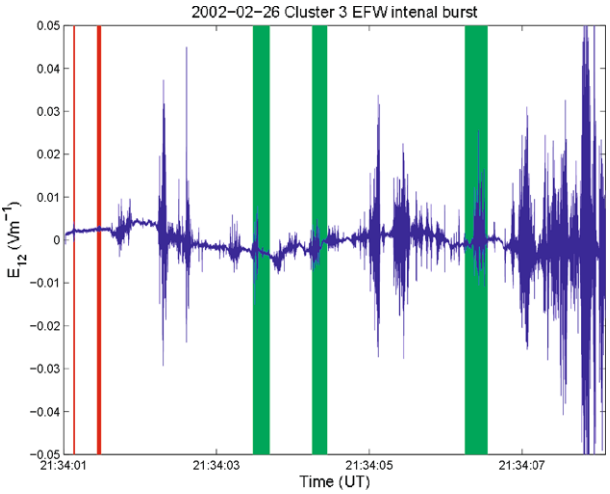

Fig. 25 Waveforms of electric field measurements during shock front crossing on 26th of February 2002 at 21:34 UT. The *vertical lines* mark periods where the waves were registered. As it will be shown later *red vertical lines* mark periods where the waves were identified as ion-sound, two *first green columns* as lower-hybrid electrostatic waves, *third green column* as whistler waves in lower hybrid frequency range

Two parallel electric field vectors of these electric field measurements lie in the same direction and have a perpendicular separation of ∼62.2 m in the direction P_2 to P_3. The availability of two closely spaced, simultaneous measurements enables the use of phase differencing techniques (Balikhin et al. 1997a) for the identification of propagation modes for waves with coherence lengths down to a few Debye lengths based upon single satellite measurements. Since there is no component measured normal to the spin plane, the separation between temporal and spatial variations is possible only in the spacecraft spin plane. As a consequence, phase differencing methods are limited to the determination of the projection of the **k**-vector in the spin plane. In most cases, however, this can provide enough information to identify the plasma wave mode. This approach was implemented in these studies. Plasma measurements were obtained from the CIS HIA (ions) and PEACE (electron) instruments. Magnetic field data were obtained from FGM. It should be noted that the spin vector of the Cluster satellites is almost coincident (to within 5°) with the z GSE axis.

The ion bulk velocity (top panel) and the magnitude of the magnetic field (lower panel) as measured by Cluster 3 spacecraft are plotted in the right hand panel of Fig. 24. Initially, the spacecraft was in the solar wind. The foot region was encountered just before 21:34 UT and the shock ramp was crossed around 21:34:12.5 UT. The plasma bulk velocity began to decrease around 21:33:50. Shortly before 21:34 low frequency oscillations were observed in the magnetic field, a feature commonly observed in the foot region of supercritical shocks. The beginning of the foot region is characterised by a large amplitude, nonlinear structure similar to those previously reported by Walker et al. (1999a). A comparison of magnetic field and plasma data show that this structure is not a partial penetration of the ramp. The present study is limited to the short interval at the beginning of the internal burst mode indicated by the vertical line and coincides with the foot region.

The electric field component E_{31} as measured during the initial part of the internal burst mode interval is shown in the upper left panel of Fig. 26 and its Morlet wavelet spectra is shown in the lower left panel. The electric field fluctuations show a pair of well defined wave packets centered around 21:34:01.6 and 21:34:02.05 UT. Their frequency ranges are 100–800 Hz and 250–2000 Hz respectively. We present here the results of the identification of these wave packets to illustrate the use of the technique and its results.

The f–k_{23} spectrum, as shown in the center and right hand panels of Fig. 26, is a histogram representation of the distribution of wave energy in frequency-k space for the first

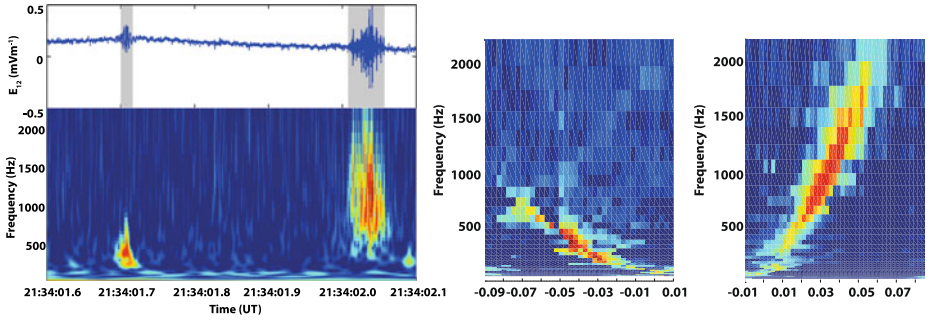

Fig. 26 *Left*: The waveform (*top panel*) and wavelet spectrogram (*bottom panel*) of the electric field computed from the difference in potential between probes 3 and 1. *Centre* and *right*: Examples of the f–k spectrograms for the first (*left*) and second (*right*) wave packets (Adapted from Balikhin et al. 2005)

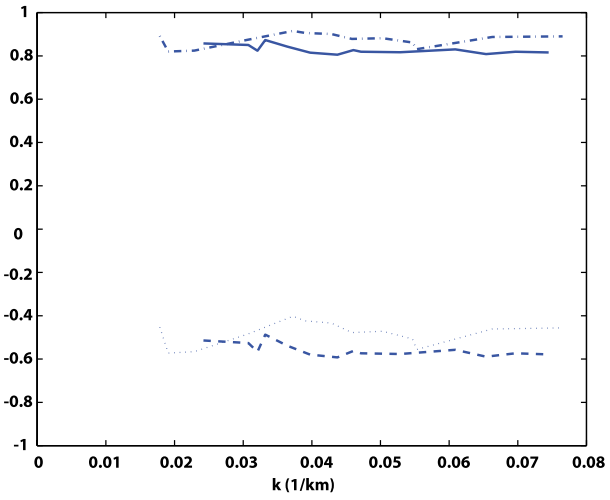

Fig. 27 A comparison of the wave vector directions for the two wave packets. The *dotted* and *dashed lines* represent the X component of wave vector for events 1 and 2 respectively. The corresponding Y components are shown by the *dash-dotted* and *solid lines* (Adapted from Balikhin et al. 2005)

wave packet (Balikhin et al. 1997a). The f–k spectrum shows a well developed ridge like maxima, the shape of which indicates the wave dispersion relation projected along the k_{23} direction. This result may be combined with a similar dispersion along the k_{13} to yield the wave vector projection in the satellite spin plane.

Since the angle between the spacecraft spin plane and the GSE XY plane is small, we will consider that the projection into the spin plane is the same as that into the GSE XY plane. The projection of the dispersion relation into the GSE XY plane is shown as the solid line in Fig. 27 for the first (centre anel in Fig. 26) and second (right on previous figure) wave packets. The observed frequency range of the first wave packet (100–800 Hz) corresponds to approximately 0.25–$1.9\Omega_{ce}$, and the magnitude of wave vector projection is in the range $0.015 < k_1 < 0.075$ m^{-1}. For this interval the electron temperature is $T_e \sim 17$ eV and plasma density $n_i = 9.7$ cm^{-3}. This leads to an estimate for the Debye length of $\lambda_d \approx 10$ m. Thus the observed values of for the projection of k correspond to $\approx$8–40λ_d.

The satellite frame dispersion relation in the satellite spin plane is shown by the solid line in Fig. 27. It's phase velocity is in the range 40–70 km s^{-1}. The Doppler shift can be estimated as the scalar product of the solar wind velocity and spin plane wave vector

component. This estimation of the Doppler shift term is shown as a dashed line. It has the same sign as the phase velocity and is always greater than the observed wave dispersion indicating that in the plasma frame the waves propagate in the direction opposite to that of the solar wind, but are convected Earthwards by the plasma flow. This convection reverses the direction of propagation in the satellite frame. The average angle between the spin plane projections of wave vector and the magnetic field is about 20°.

The second wave packet analysed was observed ≈0.3 seconds after the first. The electric field waveforms (not shown) again indicate a good correlation between the corresponding electric field components measured by different probe pairs. The f–k_{23} spectrum calculated for this wave packet is shown in the right panel of Fig. 26. The ridge like maxima in these spectra correspond to the projections of the wave dispersion relation in the direction k_{23}. The resulting dispersion relation is shown as the solid line in Fig. 27. Its frequency range is 250–2000 Hz (≈ 0.6–$4.9\Omega_{ce}$), and the magnitude of wave vector projections is in the range ≈0.018–0.075 m^{-1}. For this wave packet, the satellite frame phase velocity is in the range 150–160 $\mathrm{km\,s}^{-1}$. The range of wave vectors and angle of propagation with respect to the magnetic field for the second wave packet coincide with those determined for the first. Even more surprising is the fact that the angle between the two wave vector projections is less than 5°. The dashed line in Fig. 27 shows the estimation of the Doppler shift. It can be seen that the Doppler shift term for the second wave packet is less than that of the observed frequency and so the second wave packet propagates in the same direction in both the satellite and plasma frames. Therefore the first and second wave packets propagate in opposite directions in the plasma frame. While for the second wave packet the satellite frame phase velocity is the sum of of its plasma frame velocity and the solar wind convection speed for the first wave packet it is their difference. That explains why in the satellite frame the second wave packet propagates faster than the first one. The use of multipoint measurements enables one to separate temporal and spatial variations. In the current study it is possible to distinguish which of these two wave modes was observed. Thus we have a method that is independent of using the observed frequency criterion formulated by Gurnett (1985). For this interval $|B| \sim 14.8$ nT and hence the local electron cyclotron frequency $f_e = \Omega_{ce}/2\pi \sim 415$ Hz. As can be seen from the f–k spectra shown in Fig. 26 that the maximum wave energy of the first wave packet occurs at a frequency lower than f_e. According to the classification used by Gurnett (1985) this should be a whistler wave packet whose dispersion relation may be written as (neglecting thermal corrections) $\omega^2 = \Omega_{ce}^2 \cos^2\theta_{Bk} k^2 c^2/(k^2c^2 + \omega_{pe}^2)$, where θ_{Bk}, Ω_e, ω_{pe} are the angle between the wave vector and the magnetic field, the electron cyclotron and electron plasma frequencies respectively. The wave vectors for the first wave packet lie in the range $(kc/\omega)^2 \sim 30$–150 and therefore correspond to the electrostatic limit of the mode for which the plasma frame frequency should be $\sim \omega_e \cos\theta_{Bk}$. If we estimate the angle θ_{Bk} using the angle between the projections of wave vector and the magnetic field in the spin plane, the plasma frame frequency can be estimated as $f_e \cos\theta_{Bk} \sim 280$ Hz. For the wavevectors found, $0.015 < k < 0.0075$ m^{-1} the electrostatic whistler phase velocity varies in the range $24 < v_{ph} < 112$ $\mathrm{km\,s}^{-1}$ in the plasma rest frame. In the spacecraft frame the slowest waves would reverse their direction of propagation, so that waves propagating in both directions would be observed. However, it has been shown earlier that all waves are propagating in the same direction. Moreover, for the strongly dispersive electrostatic whistler the phase velocity should vary by a factor of two or more over the observed range of wavevectors, while the actual variation is within 20 % only. These arguments exclude the possibility that the observed mode is the whistler in the electrostatic regime.

The other possibility is the ion-sound mode. Since we are limited to spin plane measurements of wave vectors only order of magnitude estimations of the wave parameters can be

made. For such crude calculations we will disregard the factor $\theta_{Bk} \sim 18°$ in dispersion of ion-sound waves and use the simplified form $\omega = k v_{is}/\sqrt{1 + k^2\lambda_D^2}$ where $v_{is} = \sqrt{k_b T_e/m_i}$ is the ion-sound velocity and k_b is Boltzmann's constant. During the time interval in which both waves packets were observed $v_{is} \approx 40$ km s^{-1}. Thus, in the plasma rest frame the wave phase velocity should be in the range $0.80 v_{is} < v_{ph.pf} < 0.99 v_{is}$. This velocity dispersion is very close to the observations. If observed waves are indeed ion-sound waves their plasma frame frequency should be in the range ≈75–100 Hz, much lower than the observed frequency. This disagreement can be attributed to the Doppler shifts estimated as $\frac{|k|}{2\pi} V_{sw} \sim 600$–$3000$ Hz. In reality the Doppler shift is smaller due to the angle between the wave vector and the solar wind velocity.

The above arguments indicate that the first wave packet consists of ion-sound waves. As previously mentioned, the wave vectors for the second packet have exactly the same range as the first. Therefore, all arguments used above to deduce the wave mode of the first wave packet are valid for the second. The main difference between these two wave packets is in the sign of the Doppler shift. For the first wave packet, the observed frequency is the difference between the Doppler shift and the plasma frame frequency whilst for the second it is their sum. It can be seen that they almost coincide for the whole range of observed waves. The angle between the averaged propagation directions of these wave packets is <5°. This coincidence in the parameters for these two wave packets, observed at clearly distinct periods of time can only be explained by their simultaneous generation at the same location. The generation of ion-sound waves at the shock front are usually attributed either to electric currents or the strong electron temperature gradients in the ramp. Both waves packets were observed upstream of the ramp and carried by the solar wind flow towards it. Since there appear to be no strong gradients in the electron temperature in the foot these waves are probably generated by electric currents. The very short duration of these waves indicates that the current layer might be localized in space and time. Such small scale current layers have been predicted by a nonstationary model of the shock front (Krasnoselskikh 1985, Galeev et al. 1988, 1989; Balikhin et al. 1997b; Walker et al. 1999a). In this model quasiperiodic steepening of and overturning of the shock ramp takes place leading to the ejection of a nonlinear whistler wave into the upstream region. The amplitude of these nonlinear structures can be comparable to the $|B|$ changes in the ramp itself (Walker et al. 1999a) and will be associated with localised currents responsible for the ion-sound waves.

6.2 Observations of Lower-Hybrid Waves

The data set used in this study was collected by the EFW instrument in the same burst mode regime as in previous case onboard the Cluster satellites using onboard timing provided by the DWP instrument (Woolliscroft et al. 1997).

Figure 28(1) shows an overview of the magnetic profile of the shock encountered on February 26th at 21:34 UT. From Fig. 28(1) it can be seen that Cluster 3 first encountered the foot region of the shock just before 21:34 UT, finally crossing the ramp and entering the downstream region at approximately 21:34:15 UT. Here the EFW internal burst data selection was triggered at 21:34:01.922 UT and lasted for a period of 10.47 seconds as indicated by the shaded region in the figure.

The analysis presented here was performed on data recorded on 26th of February 2002 just after 21:34 UT on spacecraft 3. This quasi-perpendicular shock crossing took place on an inbound pass at a position (12.0, −1.60, 8.07) R_E. As can be seen from Fig. 28(1) the whole period of internal burst data was collected in the foot region of the shock. The initial

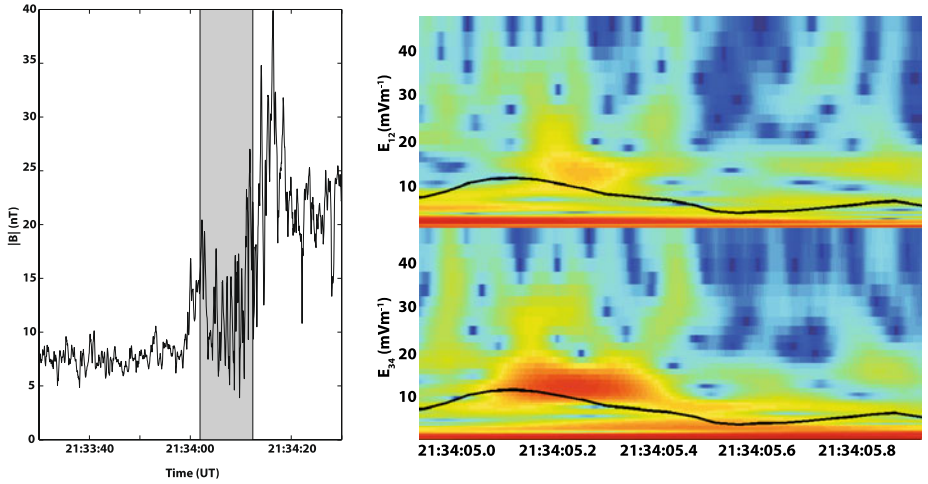

Fig. 28 Panel (*1*): The magnetic profile of the bow shock crossing observed by Cluster 3 on 26th of February 2002 just after 21:34 UT. The period for which EFW internal burst mode data is available is indicated by the *shaded region*. Panel (*2*): The wavelet dynamic spectrogram of electric fields E_{12} (*top*) and E_{34} showing a the occurrence of oscillations just above the lower-hybrid resonance frequency (*black line*) for event 1 (Adapted from Walker et al. 2008)

increase in the magnetic field profile at around 21:34 UT as has been shown above and published in Balikhin et al. (2005) to be part of the foot region rather than a partial ramp crossing.

During the 10.5 second period for which EFW internal burst data is available there were several short periods when the electric field measurements indicated that there were oscillations occurring at or just above the local lower-hybrid resonance frequency. In the following subsections the properties of the waves observed are discussed.

The first event occurred just after 21:34:05 UT. Figure 28(2) shows a dynamic spectrogram of the electric fields E_{12} (top) and E_{34} measured between probes P_1 and P_2 and probes P_3 and P_4 respectively calculated using a Morlet wavelet transform. The black line represents the lower-hybrid resonance frequency. It is clearly seen that at around 21:34:05.2 and there is a packet of waves at a frequency between 10–20 Hz, whose lower edge is just above the lower-hybrid resonance frequency. The duration of this wave packet is around 3 ms corresponding to a few wave periods. Having identified a possible occurrence of lower hybrid waves, the phase differencing technique was applied to parallel electric field vectors in an attempt to compute the dispersion relation of the waves and hence provide an unambiguous identification of the wave mode. However in this case using the spin plane electric field components E_{13} and E_{42} in the frequency range of interest (10–20 Hz) no measurable dispersion of the waves was observed on scales of the separation distance of the probe pairs (62.2 m), see Fig. 29(1).

This implies that the wave travels over the spacecraft at rather high speed so that there is virtually no difference in the phase of the wave measured at the two points on either side of the satellite. This was also evident in the waveform of the electric field signals. A comparison of the waveforms (Fig. 29(2)) shows that the two measurements which are observed to vary in phase which indicates that whatever passed over the satellite has a scale much larger than the individual probe separation distances.

So, one should conclude that the phase differencing method appears to be unable to show any dispersion in the parallel electric field vectors that means that this method cannot be used

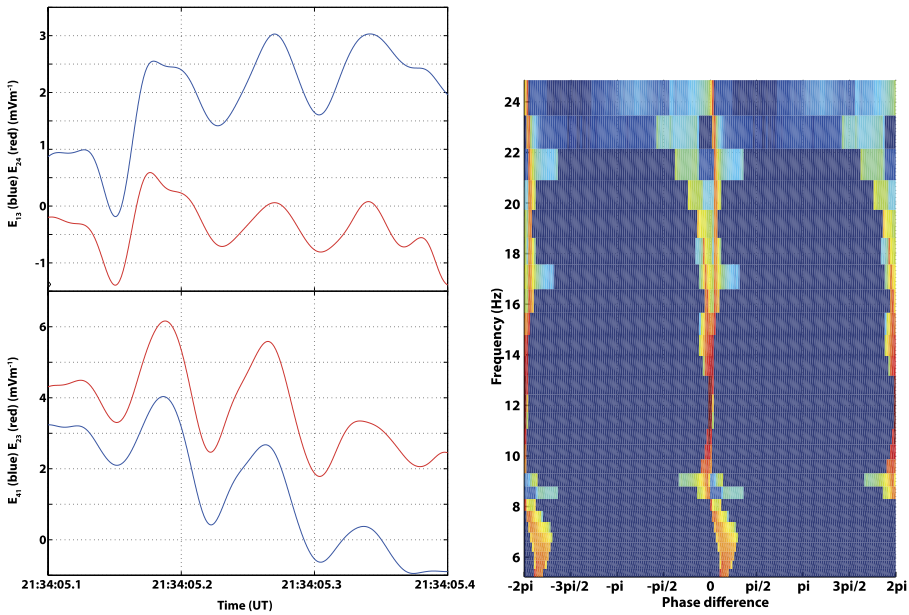

Fig. 29 Panel (*1*): The ω–k joint spectrum calculated from the phase differences measured between the two parallel electric field components E_{13} and E_{42} for event 1. Panel (*2*): The electric field waveforms E_{13} and E_{42} (*top panel*) and E_{41} and E_{23} (*lower panel*) for the first event (Adapted from Walker et al. 2008)

to reliably identify the wave packet as being lower hybrid. As a result, one needs to investigate some other wave properties of the wave packet to determine if they are compatible with the lower hybrid mode. As it was mentioned above that by applying the phase differencing method to perpendicular components of the electric field it should be possible to determine whether the wave packet is linearly or circularly polarised. To this end one should calculate the phase difference between two pairs of probes. The result of this calculation gives the estimate that in the frequency range 10–20 Hz the value of the phase difference is around zero. This result indicates that the wave possesses linear polarisation. This leads to the conclusion that the wave mode that is observed in this case corresponds to a lower-hybrid mode.

Similar analysis of the second event occurred around 21:34:04.5 on 26th of February 2002 shown the very same result, namely, it shows the phase difference of zero which again indicates that the wave is propagating with a large phase speed over the satellite and the wave packet possesses a linear polarisation and it exhibits properties that are consistent with propagation in in the lower hybrid mode.

The third event highlighted by the authors of the paper Walker et al. (2008) occurred between 21:34:07.3 and 21:34:07.45 UT on 26th of February 2002. The wavelet dynamic spectrogram analysis showed a wave packet in the frequency range 10–15 Hz that lies just above the lower hybrid resonance frequency. This wave packet was observed to drift in frequency as time increases. This change in frequency mirrors the change in the lower hybrid resonance frequency as calculated from the magnetic field. Analysis of parallel electric field components using the same phase differencing method again indicated zero phase difference between the components. However, a comparison of perpendicular electric field components indicated that a phase difference between two signals is equal to $\pi/2$. This leads to conclu-

sion that the wave packet possesses circular polarisation and is thus not propagating in the lower hybrid mode. The circular polarisation indicates that this particular wave packet is propagating in the whistler mode.

6.3 Estimates of Efficient Collision Frequency Using Direct Measurements of Ion-Sound and Lower-Hybrid Waves

A definition of the problem of conductivity relies on exchange of momentum between electrons and waves assuming the current is mainly carried by electrons. The conventional formula for plasma conductivity reads

$$\sigma = \frac{ne^2}{m_e \nu}$$

where n is the plasma number density and ν is the collision frequency of electrons with scattering centers, usually ions or neutrals with respect to momentum loss. When electrons excite some oscillations or waves as a result of instability development they also loose the momentum and this loss is referred as the anomalous momentim loss. In order to find effective collision frequency ν_{eff} one has to use the momentum conservation law in the system consisting of electrons and waves. In the case of instability this momentum exchange can be written as follows

$$\nu_{eff} m_e n_0 \overrightarrow{u}_{ed} = \frac{2}{(2\pi)^3} \int d^3k \gamma_k W_k \left(\frac{\overrightarrow{k}}{\omega_k} \right)$$

where $\overrightarrow{u}_{ed}$ is the relative velocity of electrons carrying current, γ_k is the instability increment, W_k is the wave energy density that is defined as $W_k = \frac{\varepsilon_0 |E|^2}{2}$, $|E|$ is the turbulent electric field amplitude. We have in the left hand side the rate of the electron momentum loss per unit time, and in the right hand side we have the momentum gain by waves due to instability. It follows then that

$$\nu_{eff} = \frac{2}{(2\pi)^3 m_e n |\overrightarrow{u}_{ed}|} \left| \int d^3k \gamma_{ke} W_k \left(\frac{\overrightarrow{k}}{\omega_k} \right) \right|$$

If one would like to evaluate the efficient collision frequency from direct measurements it is necessary to have an estimate of the wave energy. Using this estimate one can evaluate the shock thickness that shock might have if it would be determined by the anomalous collisions using the characteristic length of the momentum loss:

$$L_{an} = \frac{V_{sw}}{\nu_{eff}}.$$

The comparison of the thickness obtained from this estimate with the real shock thickness can be used to evaluate the relative role of the efficient collisions.

The standard estimate of the efficient collision frequency for ion sound mode (Galeev and Sagdeev 1984) reads

$$\nu_{eff} = \omega_{pe} \frac{W}{n_0 k_B T_e}$$

Taking the estimate of the averaged electric field intensity $\langle E \rangle^2 \approx 10^{-5}$ calculated making use the data of measurements (it varies from % 1×10^{-5} to 2×10^{-5} V/m) and density

and temperature from observations $n = 9.7\ \mathrm{cm}^{-3}$, $T_e = 17$ eV, $\omega_p = 1.7 \times 10^5\ \mathrm{s}^{-1}$, one can find $W = 4.5 \times 10^{-17}$, $W/(nk_BT_e) = 1.8 \times 10^{-6}$,

$$\nu_{eff}^{is} = 0.3\ \mathrm{s}^{-1}, \qquad L_{an} = \frac{V_{sw}}{\nu_{eff}^{is}} \approx 1200\ \mathrm{km}$$

where ν_{eff}^{is} is anomalous collision frequency due to ion-sound wave activity, L_{an} is the characteristic scale of anomalous energy exchange between electrons and ions. It is sufficiently larger than the electron inertial scale $c/\omega_{pe} = 1.76$ km, and comparable with the thickness of the foot region.

Another group of waves, namely lower hybrid has maximum amplitudes of the order of 10 mV m^{-1} and average electric field energy density of the same order of magnitude as ion sound waves (from 1×10^{-5} to 4×10^{-5} V/m). In order to evaluate the efficient collision frequency for these waves one should take into account the properties of lower-hybrid drift waves. To this end we shall rely on the study of lower hybrid drift instability published by Davidson et al. (1977). The maximum growth rate for these waves can be estimated as

$$\gamma_{LH} \approx \alpha \Omega_{LH}$$

where Ω_{LH} is lower hybrid frequency, coefficient $\alpha < 1$, typically $\alpha \sim 0.1$, and can reach values up to 0.3. Taking maximum of the linear growth rate we can evaluate the upper limit of the effective collision frequency. The phase velocity of waves around the maximum of increment is of the order of ion thermal velocity of ions, and the drift velocity of electrons that carry the current can be estimated evaluating current velocity from macroscopic gradient of the magnetic field. This estimation gives the value comparable with ion thermal velocity. Thus the estimate of the efficient collision frequency in this case can be written as follows:

$$\nu_{eff} \approx \alpha \Omega_{LH} \frac{m_i}{m_e} \frac{W}{nk_BT_i}$$

In the region of observations where $B = 14$ nT and lower hybrid frequency is approximately equal to 56 s^{-1}, thus the efficient collision frequency for these waves is found to be of the of the order of

$$\nu_{eff} \approx \alpha \Omega_{LH} \frac{m_i}{m_e} \frac{W}{nk_BT_i} \sim 0.1 \times 2 \times 10^3 \times 56 \times 10^{-6} \simeq 10^{-2}\ \mathrm{s}^{-1}$$

that is sufficiently smaller than the efficient collision frequency for ion sound waves. The characteristic dissipation scale

$$L_{an} \approx \frac{350}{10^{-2}}\ \mathrm{km} \approx 3.5 \times 10^4\ \mathrm{km}$$

and is sufficiently larger than the major characteristic scales of the shock front.

This leads to the conclusion that the anomalous resistivity observed can not account for the important dissipation rate. The characteristic scales of the dissipation are too large compared to the shock transition features observed.

7 Nonstationarity and Reformation of High Mach Number Quasiperpendicular Shocks: Cluster Observations

In this section, using Cluster observations, we provide convincing evidence that high-Mach-number quasiperpendicular shocks are indeed nonstationary, and moreover, quasi-periodic shock front reformation takes place. Most of the material of this section was first published in Lobzin et al. (2007).

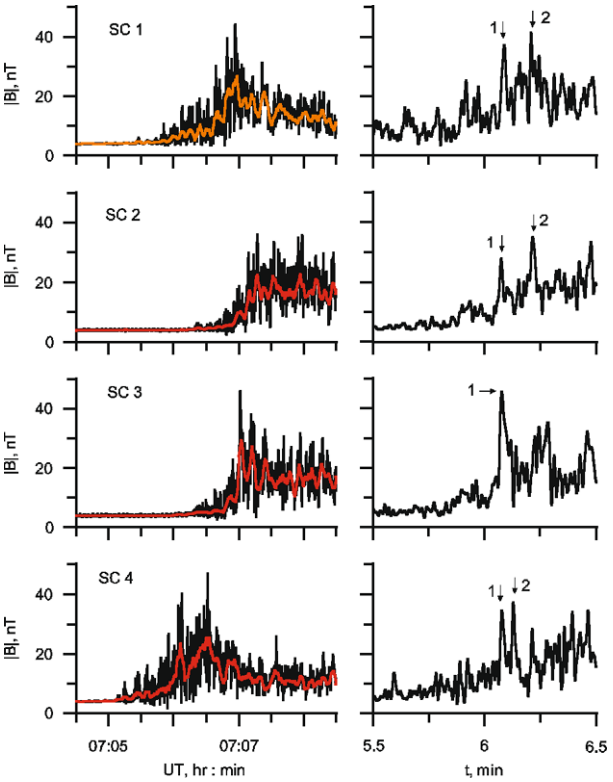

Fig. 30 The magnetic field profiles obtained by FGM experiments aboard four Cluster spacecraft during the Earth's bow shock crossing on 24 January 2001. (*left*) High-resolution magnetic field data (*black line*) and the data obtained by sliding averaging over 4 s time intervals (*red line*). (*right*) Vicinity of overshoots, with large peaks in the magnetic field magnitude. Oscillations with frequencies higher than 2 Hz were removed. To emphasize the similarity and differences of the profiles, the data for the first 3 spacecraft are shifted with respect to that for the 4th one (Adapted from Lobzin et al. 2007)

7.1 An Example of a Typical Crossing of Nonstationary Quasiperpendicular Shock Wave

A number of magnetic field profiles of the quasiperpendicular terrestrial bow shock observed by Cluster triaxial flux gate magnetometers (FGM) (Balogh et al. 1997) in the period January–May 2001 were studied. It was found that nonstationarity seems to be typical for shocks with relatively high Mach numbers. Both from numerical simulations and experiments it follows that the details of this nonstationary behaviour of the shock front may depend strongly not only on the fast magnetosonic Mach number, M_f, but also on the upstream $\beta_{e,i}$ and the angle between the upstream magnetic field and the shock normal, θ_{Bn}. For a detailed case study, a shock was chosen that could be considered as a typical quasiperpendicular, supercritical, high-Mach-number shock wave, namely the shock crossing that occurred on 24th of January 2001 at 07:05:00–07:09:00. Indeed, from the available experimental data and with the use of the multi-spacecraft timing algorithm described by Schwartz (1998) the following estimates were obtained: $\beta_e = 1.7$, $\beta_i = 2.0$, $\theta_{Bn} = 81°$, $M_A = 10$, and $M_f = 5$.

Figure 30 shows the magnetic field profiles measured by the Cluster FGM instruments on 24th of January 2001. The panels on the left show the full resolution data, sampled at 67 Hz (black line) and the result of averaging this data using a 4 second sliding window (red line). The panels on the right show the result of low pass filtering the data at 2 Hz. This process enhances any large peaks in the magnetic field measurements. All the profiles can be considered as quite typical for high-Mach-number quasiperpendicular shock waves. From the averaged data shown by the red lines we observe that the shock front consists of a foot, a ramp, and at least one overshoot-undershoot cycle, i.e. large amplitude

peak of the magnetic field at the end of the ramp region and following after it minimum. The small-scale oscillations of large amplitude are superimposed on this large-scale structure. To check whether these fluctuations are consistent with plane wave activity, the degree of polarization for the magnetic field waveforms obtained from STAFF experiment (Cornilleau-Wehrlin et al. 1997). By definition, the degree of polarization approaches a unity if and only if most of the energy is associated with a plane wave (Samson and Olson 1980). It was found that between the forward edge of the shock and the magnetic overshoot the oscillations in the frequency range 3–8 Hz have a high degree of polarization greater than 0.7 and that this polarization is elliptical. This wave activity can be considered as a whistler wave train nested within the shock (Galeev et al. 1988; Galeev et al. 1989; Krasnoselskikh et al. 2002). Obviously, the presence of whistler oscillations, due to their high amplitude, has a considerable impact on the large-scale shock structure. Indeed, averaging of magnetic field data reveals two regions resembling overshoots for SC4 whilst only one maximum is observed for SC1. The profiles for the other spacecraft appear to be more complicated. It follows from these considerations that the concepts of both overshoot and ramp, which must precede it, become ambiguous for such nonstationary shocks. Instead, we can speak about short scale large-amplitude structures embedded into the shock transition, with the forward edge of one of these structures playing a role of the ramp. Figure 30 also shows that the magnetic field profiles measured onboard the different spacecraft differ considerably from each other. Obviously, the number of large-amplitude peaks, their amplitudes, as well the positions within the shock front, are different. The waves observed by different spacecraft in the foot region are also different. In particular, from Fig. 30 (left) it is easily seen that the time interval between the beginning of the wave activity at the forward edge of the shock and the ramp crossing may differ by 10–20 s. This difference is substantial compared to the duration of the crossing of typical elements of the shock structure. The distinctions found between observations from the different spacecraft are related to temporal rather than spatial variations in the structure of the shock front because the spacecraft separation is comparable with shock front thickness. Indeed, the distances between spacecraft lie within the range 380–980 km. The foot thickness estimated with the use of the theoretical formula derived by Schwartz et al. (1983) is equal to 550 km, in reasonable agreement with the observations, while the total shock front thickness is considerably larger. On the other hand, the maximum time lag between the crossings is about $3T_{Bi}$, where T_{Bi} is the ion gyroperiod $T_{Bi} = 15.5$ s. This time lag is larger than the period of the shock reformation. Relying on theoretical considerations and results of numerical simulations, Krasnoselskikh et al. (2002) argue that this type of nonstationarity is closely related to nonlinear whistler wave trains embedded into the shock front and that this is a typical property of quasiperpendicular high-Mach-number shocks. Further evidence for the existence of whistler waves embedded within the shock front can be seen from the rotational features of the magnetic field observed in the vicinity of the peaks, as shown in Fig. 31, that are typical of whistler mode waves.

The large-amplitude structures seen in the magnetic field profiles within the overshoot region and its vicinity have a characteristic time of about 2 s. To examine both the similarities and differences of these profiles, oscillations with frequencies higher than 2 Hz were removed by low pass filtering the data. The filtered data were then used to calculate a set of optimal cross-correlation coefficients for profile fragments that last 35 s and include a portion of foot and the entire overshoot region. The highest correlation was found between SC1 and SC2, while the lowest one was between SC3 and SC4, a result that is in accordance with visual observations of the shifted profiles shown in Fig. 30 (right). An additional analysis of the relative position of the spacecraft tetrahedron and the shock reveals that the

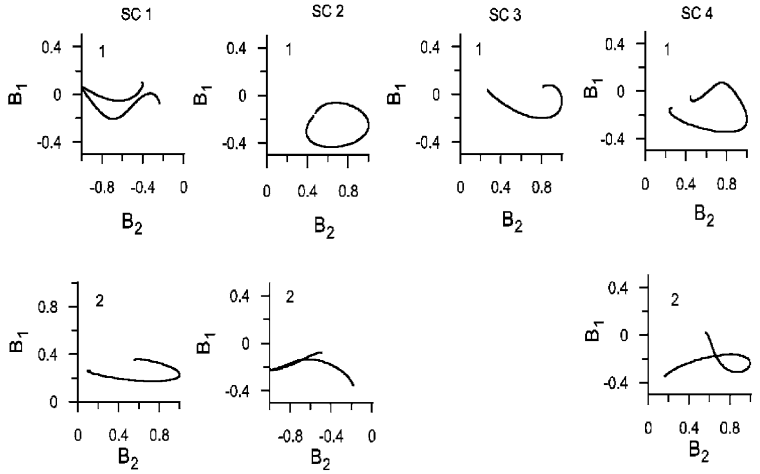

Fig. 31 Hodograms of magnetic field around their maxima for different satellites in the vicinity of supposed ramps

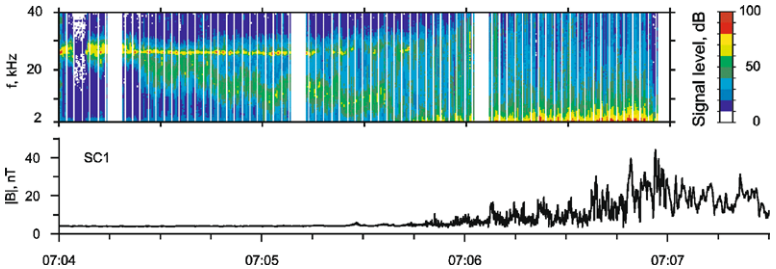

Fig. 32 (*top*) Electric field spectra and (*bottom*) magnetic field profile obtained during the Earth's bow shock crossing on 24th of January 2001 aboard SC1. The frequency-time spectrogram is measured by the Whisper experiment. The *vertical white bands* correspond to the time intervals when no data were obtained in the natural wave mode. The wave intensity is colour coded with the reference level of $10^{-7} V_{rms}/\mathrm{Hz}^{1/2}$, where rms is the root mean square to notify the averaged level of the fluctuating electric field variance. The magnetic field profile is obtained by FGM experiment. The time scales for the both panels are the same (Adapted from Lobzin et al. 2007)

similarity of the shock profiles seems to depend mainly on the time interval between the shock crossings and/or the spacecraft separation measured along the shock normal rather than on the distance along the shock surface which is in accordance with the interpretation that the observed variations are temporal rather than spatial.

Further evidence favoring the nonstationarity of this bow shock crossing comes from WHISPER measurements. In passive mode this experiment provides electric field spectra of natural emissions in the frequency range 2–80 kHz (Décréau et al. 1997). The frequency-time spectrogram obtained by WHISPER experiment aboard SC1 is shown in Fig. 32, together with the magnetic field profile with the same time scale. The bow shock crossing can be identified by a substantial enhancement in the electric field fluctuations within the frequency range 2–5 kHz. For SC1, maximum intensity for these oscillations is observed at 07:06:48 UT. One of the most obvious features of these spectra is the presence of intense waves in the vicinity of the plasma frequency, $f_{pe} = 27$ kHz, together with

downshifted oscillations. The most intense feature is a narrow-band Langmuir emission with a frequency in the vicinity of f_{pe}. As compared with Langmuir waves, the power density of downshifted oscillations is usually smaller, while the frequency band they occupy is considerably wider and can be as large as 15–20 % of the central frequency. Both the plasma waves and downshifted oscillations are considered to be typical of the electron foreshock region. It is commonly believed that Langmuir waves are generated by a plasma-beam instability, while for the downshifted oscillations two different mechanisms have been proposed, namely, the plasma-beam interaction, see (see Lacombe et al. 1985; Fuselier et al. 1985) and the loss-cone instability of electron cyclotron modes (Lobzin et al. 2005). The mean frequency of the downshifted oscillations is not constant but varies within the range 0.2–1.0 f_{pe}. In addition, there exists a tendency for a large shift to occur in the vicinity of the shock front, while near the edge of the electron foreshock the shifts are considerably smaller. However, this tendency exists only on large time scales of about 1.0–1.5 min. For smaller scales, 10–15 s, there are the large-amplitude variations of the mean frequency of the downshifted oscillations. The peculiarities of the spectra described above can be explained as follows. The downshifted oscillations are produced by energetic electrons, which are reflected by the bow shock and move almost along the magnetic field lines. Because the solar wind is quiet during the time interval considered (indeed, Figs. 30 and 31 show that there are no significant variations of the magnetic field; the plasma bulk velocity is also approximately constant in the foreshock), the observed evolution of the wave spectra can only be attributed to variations of the suprathermal electron fluxes which are reflected from the bow shock and form the "rabbit ears" in the electron distributions upstream of the shock as was shown by Lobzin et al. (2005). The reflection of electrons by a nearly perpendicular bow shock was studied by Leroy and Mangeney (1984) and Wu (1984). They argued that the main characteristics of the distribution function of the reflected electrons depend first of all on the angle between the shock normal and upstream magnetic field, θ_{B_n}, and to a lesser extent on the ratio of the maximum magnetic field to its upstream value and on the electrostatic potential jump in the de Hoffmann-Teller frame. Resulting from shock front nonstationarity, slow variations of the effective normal of the reflecting part of the shock will lead to considerable variations of number density, energy of reflected electrons, and/or loss-cone angle, thereby producing the observed variations of the downshifted wave spectra. Both theoretical considerations and numerical modeling show that a characteristic time of the shock front oscillations or reformation is comparable with the ion gyroperiod (see Leroy et al. 1982; Krasnoselskikh et al. 2002; Scholer et al. 2003). The time scale of the spectra variations is also comparable with ion gyroperiod T_{Bi}, in accordance with our interpretation.

7.2 Evidence for Shock Front Reformation

As noted above, the magnetic field profiles for the shock under consideration have several nonstationary features. In this section, we consider large-amplitude structures, with a characteristic time of about 1–2 s and present the arguments in favor of front reformation for this particular bow shock crossing. Figure 30 (right) shows the magnetic field profiles obtained after low-pass filtering and shifting the data in time to clearly show the correspondence between the elements observed aboard different spacecraft. For three spacecraft there are two large narrow peaks in the overshoot region and its vicinity, while for SC3 there is only one peak in the corresponding region (see Fig. 30 (right), where these peaks are shown by arrows and numbered). The amplitudes of these peaks, both absolute and relative, differ for different spacecraft. In addition, the distance between two adjacent peaks also varies, being the smallest for SC4 and the largest for SC2. Moreover, the single peak observed by

SC3, which largest amplitude and relatively large width, may be formed due to the coalescence of two separate peaks. The observed peaks in the overshoot region can be considered as a part of the nonstationary whistler wave packets since their rotational properties are clearly evident in Fig. 31. These properties were argued to be an intrinsic element of the quasiperpendicular supercritical shock front structure (Krasnoselskikh et al. 2002). In order to investigate these features further, an analysis of their polarization was performed using the minimum variance technique. The results provide additional evidence in favor of shock front nonstationarity. Indeed, the corresponding elements have different hodograms, which can be rather complicated. However, some of the elements have approximately circular polarization typical for large-amplitude whistlers as was stated in theoretical papers (Galeev et al. 1988, 1989; Krasnoselskikh et al. 2002) and is evidenced on Fig. 31. A comparison of the magnetic field profiles, shown in Fig. 30 with the results of numerical simulations of high-Mach-number shock reformation (Krasnoselskikh et al. 2002) reveals a doubtless resemblance between them. Indeed, for large Mach numbers, quasiperiodic reformation of the shock front was observed in the simulations, with whistler wave packets playing a crucial role. In the first stage of the reformation cycle, a small-amplitude whistler perturbation upstream of the ramp is formed This perturbation grows and moves towards the ramp. When its amplitude exceeds that of the ramp, this disturbance begins to play the role of a new ramp, while the old one moves away downstream. The experimental results shown in Figs. 30 and 31 resemble 4 different snapshots for the same shock undergoing the reformation. The strongest evidence favouring the shock reformation comes from the CIS experiment, which measures the ion composition and full three-dimensional distributions for major ions with energies up to 40 keV/e (Reme et al. 1997). The time resolution of these measurements is about one spacecraft spin, 4 s. Figure 33 shows 8 snapshots obtained at the upstream edge of the shock foot, where the disturbances of the solar wind magnetic field are still small. The figure shows the number of counts vs a function of V_x and V_y in the GSE coordinate system; with the data being integratedin the V_z direction. Reflected ions are observed for the first time at 07:05:16 (see the maximum of the number of counts in the quadrant corresponding to $V_x < 0$ and $V_y < 0$ in the first snapshot). In the time interval from 07:05:16 to 07:05:44, the position of this maximum in the velocity space does not change considerably. In addition, there exists a second population of reflected ions in the quadrant corresponding to $V_x < 0$ and $V_y > 0$. From the snapshots it is easily seen that the numbers of counts corresponding to the reflected ions show approximately periodic variations with a very large modulation depth and a period of about 8 s which corresponds to half of the proton gyroperiod T_{Bi}. To confirm this statement, we performed a summation of the number of counts corresponding to these populations, the results are approximately proportional to the corresponding number densities, n_r. The temporal evolution of these number densities normalized with respect to the corresponding maximum values for the time interval considered is shown in Fig. 33 (bottom). The quasiperiodic variations seem to be more pronounced for the first population (blue line), with the minimum-to-maximum ratio being as low as $\sim$3 %. The number of counts for the second population also varies with approximately the same period, in phase with that for the first one. It is worth noting that the minimum number of counts corresponding to the reflected ions in this region is greater than the 'background noise' by a factor of 5, far beyond experimental errors, while for the maximum number of counts this factor is as large as 30 if the 'noise' level is estimated in the unperturbed solar wind just before the shock crossing. The observed peculiarities of the ion dynamics resemble the features found in the numerical simulations of Krasnoselskikh et al. (2002), where a quasiperiodic front reformation was observed for quasiperpendicular shocks with high Mach numbers. In particular, when the leading wave train before the ramp attained a large enough amplitude, a new population of reflected ions appeared upstream of the precursor. In other words,

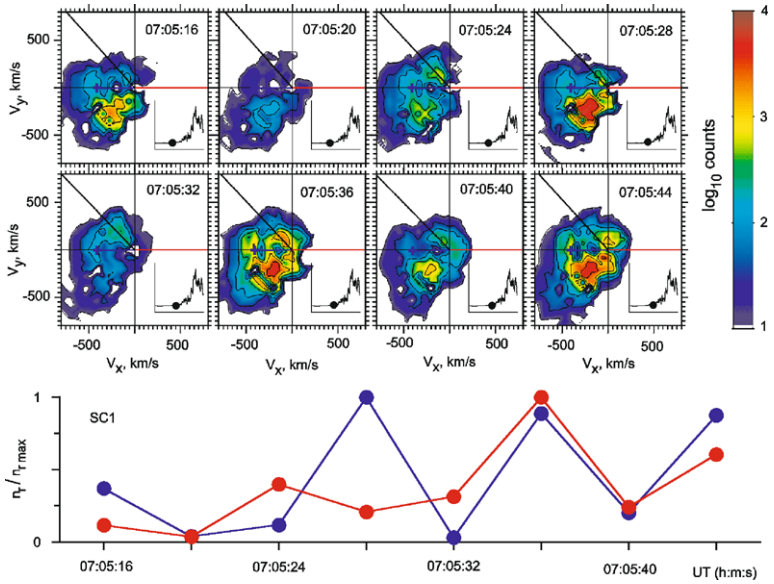

Fig. 33 (*Top*) Ion velocity distributions obtained from CIS measurements within the forward part of the foot for the Earth's bow shock crossing on 24th of January 2001 aboard SC1 and (*bottom*) temporal variations for the relative number of counts corresponding to reflected ions. The distributions were calculated in the GSE coordinates. In the *bottom panel*, a *blue line* corresponds to ions with $V_y < 0$, while a *red line* shows the data for $V_y > 0$. Strong variations of n_r, especially for $V_y < 0$, show that the reflection of ions is bursty. The relative positions where the measurements were made are indicated by the *dots* on the magnetic field profiles shown as *inserts* (Adapted from Lobzin et al. 2007)

the reflection of ions is not stationary. It is quasiperiodically modified during the reformation process. In this case a spacecraft that moves slowly across the shock, will observe the quasiperiodic appearance/disappearance of reflected ions, in accordance with experimental results outlined above.

7.3 Conclusions

In this section we have presented a set of experimental results for a high-Mach-number ($M_f = 5$) quasiperpendicular ($\theta_{Bn} = 81°$) bow shock crossing observed by Cluster spacecraft on 24th of January 2001 at 07:05–07:09 UT. The structure of this shock gives a clear evidence of its nonstationary behavior. In particular, the magnetic field profiles measured by FGM experiments onboard different spacecraft differ considerably from each other. This difference is clearly seen for large-amplitude oscillations, which have relatively short scales of about 1–2 s and resemble nonlinear whistler soliton-like structures that is confirmed by analysis of their hodograms. WHISPER measurements reveal the presence downshifted oscillations within the electron foreshock, with nonmonotonic variations of their central frequency, the characteristic time for these variations is comparable with the proton gyroperiod, $T_{Bi} = 15.5$ s. From the analysis of data from CIS experiment it follows that the reflection of ions from the shock are also highly nonstationary. Moreover, it is shown that the reflection is bursty and the characteristic time for this process is also comparable with the ion gyroperiod. From numerous numerical simulations of quasiperpendicular shocks it is well-known that for high Mach numbers the shock becomes nonstationary. Moreover, front reformation

can take place with a characteristic time comparable with the ion gyroperiod. The combination of the features outlined above for the bow shock crossing under consideration is the first convincing experimental evidence favoring the shock front reformation.

8 Conclusions

There exist several models of quasiperpendicular high Mach number shocks. Theoretical considerations and computer simulations on today's level are not capable to describe correctly all physical process that determine different aspects of shock physics. The only possibility to ensure that the theory or modelling correctly capture major physical effects is to rely on analysis of experimental data of direct in situ measurements onboard satellites. The best adapted for this goal are Cluster satellites since they allow one to distinguish spatial and temporal variations and during the mission they had different intersatellite distance that allows one to probe the shock on different scales. The difficult task in such investigation program consists in formulation of the right questions to be addressed to data and to their analysis. Our aim was to determine major physical processes that define characteristics of the most important part of the shock front, its ramp and wave activity around it. The problems closely related to this major problem are electron heating mechanisms and transition of shock behaviour from stationary to nonstationary. We left beyond the scope of our Review many questions. One can mention ripples, remote sensing of the shock by field aligned beam, instabilities behind the shock front. We restricted ourselves by the analysis of scales of magnetic and electric fields, the scale of electron heating, determination of the source and generation mechanism of precursor whistler wave train and direct observation of the shock front reformation by Cluster satellites. Huge collection of data of statistical analysis and of the studies of individual events (case studies) leads to the conclusion that the ramp region of supercritical quasiperpendicular shock is nothing more than an intrinsic element of nonlinear dispersive wave structure slightly modified by reflected ions. This interpretation allows one to explain in a natural way the whole collection of data that we reported in this Review and to understand the transition from stationary to nonstationary shock behaviour when the Mach number exceeds nonlinear whistler critical Mach number. The role of anomalous resistivity is shown to be relatively weak with respect to effects of dispersion. Our study also points out several important opened questions. Presumably the most important is what is detailed mechanism of the electron heating and isotropization. Certainly, the evaluation of the role of anomalous resistivity can not be considered as the solved problem, the data set used is too poor to come to definite conclusions, thus this study still waits new measurements. We did not address the problem of particle acceleration and new results presented here will certainly have an impact on re-consideration of this important problem.

Acknowledgements V.K. acknowledges ISSI for supporting team activities of the project High Mach Number Shocks, CNES for financial support of this work through the series of grants Cluster Co-I DWP. V.K. is also grateful to A. Spitkovsky for providing a figure and useful discussions of astrophysical shocks, A. Artemyev for assistance in preparation of the manuscript, and to R.Z. Sagdeev and A.A. Galeev, teachers who supported the interest to this topic for many years. The authors are grateful to A. Balogh for his kind support and encouragement during the compilation of this review. It is also our great pleasure to acknowledge the contribution of all Cluster PI's whose tireless efforts have provided the scientific community with a readily accessible, high quality, unique data collection without which this work could not have been completed. The authors are grateful to Referee who helped us to improve the manuscript.

Appendix A: Remark on Comparison of Computer Simulation Results with Experimental Data

Recently Comişel et al. (2011) made an attempt to perform computer simulations that can properly reproduce the realistic physical conditions corresponding to observations. They modelled the shock dynamics using 1D PIC code with the realistic ion to electron mass ratio under conditions corresponding to shock conditions on 24th of January 2001 that was observed by Lobzin et al. (2007). The only difference between the model and real plasma parameters is an unrealistic ratio of $(\omega_{pe}/\Omega_{ce})$. The modelling results clearly showed that the shock indeed is nonstationary. However, it was found that there are some important differences between the results of the simulations and observations. The major differences can be summarized as follows. The electric fields observed in simulations in the close vicinity of the shock front were much higher than the electric fields experimentally registered. The energy flux of waves observed in the foot region upstream of the shock front was found to be directed toward downstream that clearly indicates that the waves observed in simulations are generated by the beam of the reflected ions and not by the ramp region as the dispersive mechanism predicts. This gives an indication that the properties of waves observed are much closer to short scale lower hybrid or lower hybrid drift waves described in Sect. 6 and not to those described in Sects. 2 and 3. The question arises where does this difference come from. To answer this question one should consider some scaling properties of equations describing dynamics of the shock. In order to do that let us re-write our equations in dimensionless form making use of natural variables

$$\widetilde{v} = v/V_A, \qquad \widetilde{t} = t\Omega_{ci}, \qquad \widetilde{r} = r\Omega_{ci}/V_A, \qquad b = B/B_0, \qquad e = qE/\Omega_{ci}M_A V_A,$$
$$\widetilde{n} = n/n_0$$

The system have several dimensionless parameters that remain and should be taken into account. These are $\eta = \frac{m_e}{m_i}$ (the authors would prefer the letter μ but it is already used for magnetic permeability), $\chi = \frac{\omega_p}{\Omega_{ce}}$, and certainly $\beta_{e,i}$.

To account for the principal difference between the real physical conditions and simulations let us consider where the parameter χ may play an important role. In dimensionless variables it appears in two Maxwell equations

$$\mathrm{div}\,\overrightarrow{E} = \frac{\eta}{\chi^2}(\tilde{n}_i - \tilde{n}_e)$$
$$\mathrm{rot}\,\overrightarrow{B} = (\tilde{n}_i\overrightarrow{V}_i - \tilde{n}_e\overrightarrow{\tilde{v}_e}) + \frac{\eta}{\chi^2}\frac{\partial\overrightarrow{E}}{\partial\tilde{t}}.$$

To clarify its role one can consider the properties of linear waves. One can note that the ratio of electric to magnetic field is determined by the refractive index of waves. By definition it is

$$N = \frac{kc}{\omega}$$

and it is easy to see that it is exactly this ratio is used in determination of the electric to magnetic field ratio. In SI the system in dimensional variables reads

$$\mathrm{rot}\,\overrightarrow{E} = -\frac{\partial\overrightarrow{B}}{\partial t}$$

that leads to following estimate for linear waves:

$$[\overrightarrow{k} \times \overrightarrow{E}] = \omega\overrightarrow{B}.$$

This can be re-written as follows:

$$\frac{cB}{E_{k\perp}} = \frac{kc}{\omega} = N.$$

It can also be expressed in terms of phase velocity

$$N = \frac{c}{V_{ph}}.$$

If we take the waves having velocities close to the shock front velocity (approximately standing whistlers in a shock front reference frame) the velocity in the plasma reference frame is $V_{up} = V_{sw} = M_A V_A$, thus the refraction index is

$$N = \frac{c}{V_{sw}} = \frac{c}{M_A V_A} = \frac{\omega_{pi}}{M_A \Omega_{ci}} = \frac{\omega_{pe}}{M_A \Omega_{ce}} \frac{1}{\sqrt{\eta}}$$

$$N_{\exp} = \frac{Bc}{E_{k\perp}} = \frac{c}{V_{sw}} \left(\frac{\omega_p}{\Omega_{ce}} = \frac{2.7 \times 10^4}{1.2 \times 10^2} \sim 230 \right)$$

where $E_{k\perp}$ is the electric field component perpendicular to the k-vector.

On the 24th of January 2001 the solar wind velocity was $V_{swSW} = 440\ \mathrm{km\,s^{-1}}$.

$$N_{\exp} \approx 700.$$

The maximum value of ratio $\frac{\omega_p}{\Omega_c}$ in simulations is 8 thus

$$N_{sim} = 23$$

it is approximately 30 times smaller than in experiment, that means that for the same level of fluctuations of the magnetic field the electric field fluctuations are 30 times stronger than in experiment.

According to our analysis of dimensionless parameters another important difference consists in similar overestimate of electric fields due to even small deviations from quasi-neutrallity. One can suppose that this can lead to artificial increase of the role of quasi-electrostatic instabilities of short scale lower hybrid waves. As a result the dominant waves observed in simulations are similar to those reported in the section "Anomalous resistivity", namely drift lower hybrid type waves. Presumably, the overestimation of the role of the electric field and consequently of short scale oscillations and consequently underestimation of the role of lower frequency standing precursor whistler waves results in the difference between observations and simulation results. If so, the simulated shock is really resistive while the observed one is certainly dispersive. To evaluate the influence of this overestimate of the electric field let us evaluate the electric field needed to reflect upstream ion flow assuming that for efficient reflection the potential should be of the order of half energy of the incident ion. Reflecting potential in nonlinear wave on the scale about

$$L = 5\frac{c}{\omega_{pe}} = 0.9 \times 10^6\ \mathrm{cm}, \qquad E_{ions} = \frac{m_i V^2}{2} = 0.5 \times 10^9\ \mathrm{eV} \frac{V^2}{c^2} = 1\ \mathrm{keV}$$

This corresponds to the value of the electric field

$$E = \frac{0.5 \times 10^3 V}{2 \cdot 0.9 \times 10^4\ \mathrm{m}} = 30\ \mathrm{mV\,m^{-1}}$$

$$\delta B_{\exp} = \frac{N_{\exp} E}{c} = \frac{0.7 \times 10^3 \cdot 60\ \mathrm{V/m} \times 10^{-3}}{2 \cdot 2 \times 10^8} = 1.5 \times 10^{-4} \sim 15\ \mathrm{nT}$$

where $\delta B_{\exp}$ gives the idea of the magnetic field fluctuations really observed and obtained from the comparison with the electric field measurements. These effects are illustrated on the

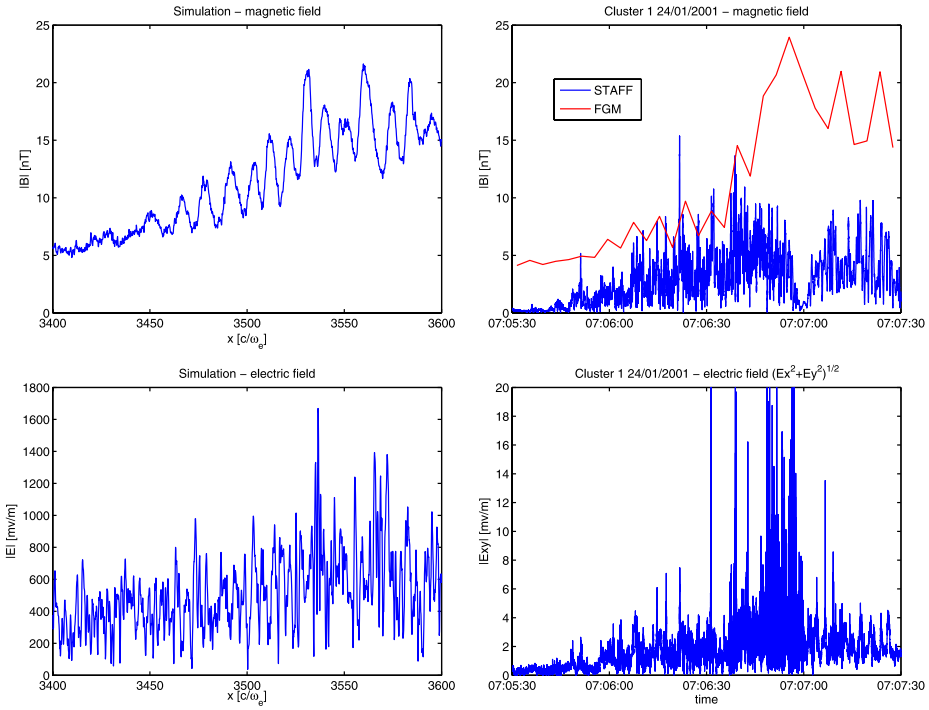

Fig. 34 Comparison of electric and magnetic fields observed on 24th of January 2001 by Cluster satellites and obtained in computer simulation by Comişel et al. (2011). *Both panels* show the fields in the vicinity of the foot/ramp regions. *Top panels* represent magnetic fields as measured by FGM instrument and STAFF search coil magnetometer (*right*), and obtained as a result of simulations (*left*). *Bottom panels* represent measured and simulated electric fields. One can see huge difference in amplitude of electric fields between measurements and simulations that results from artificial ratio of plasma to gyrofrequency and consequently unrealistic refractive index of waves (Figure is provided by J. Soucek and H. Comisel)

Fig. 34 where left hand panels show electric and magnetic field fluctuations in units similar to those experimentally observed, and right hand panels show the data obtained by Cluster satellites for similar parameters (Mach number, angle and β). The magnetic field fluctuations in simulations that will be associated with similar electric fields could be 30 times smaller. Thus electric fields capable to trap and reflect ions are associated with the magnetic field fluctuations that are quite small, namely, less than $\sim$1 nT. The ion trapping and reflection can occur in small amplitude oscillations in the foot region that can not happen in real shock. Crucial change of ion dynamics certainly results in change of the characteristics of the shock front and wave activity around.

The goal of this remark is not to understate the role and importance of computer simulations for the shock studies. We would like to point out that direct comparison of simulation results with the observations needs special attention and analysis of the simulation conditions to ensure that the process is properly described.

Appendix B: Table of Notations Used in the Article

Parameter	Interpretation
B	the magnitude of the magnetic field
B_0	upstream magnetic field
B_n	magnetic field component along the normal to the shock
$\beta = \frac{8\pi nT}{B^2}$	the ratio of total particle thermal pressure to the magnetic field pressure
ΔB	change of the magnetic field through inhomogeneous layer
Δt_{ij}	time difference of observation of shock front features such as electric field spikes by different satellites i and j
ΔE	an amplitude of the electric field spike feature
$E_{x,y,z}$	electric field components along corresponding axes
E_{spike}	maximum amplitude in electric field spike
E_{ij}	electric field as measured by means of probes i and j
$\mathbf{E}$	electric field vector
e_{ij}	electric potential difference between probes i and j onboard single satellite
$f = \omega/2\pi$	wave frequency
$f_e = \Omega_{ce}/2\pi$	electron gyrofrequency (in Hz)
γ_{LH}	growth rate of lower hybrid waves
$\mathbf{k}$	wave-vector of a wave
k_{ij}	an estimate of the $\mathbf{k}$-vector component from electric field probes i and j measurements onboard one single satellite
$k_{\parallel}$	parallel to the magnetic field component of the wave-vector
l_{gr}	characteristic gradient scale inside the inhomogeneous layer
L_d	dissipative scale
L_{disp}	dispersive scale
$L_{I,e} = c/\omega_{pi,pe}$	ion, electron inertial length
L_{Br}	thickness of the ramp region of the shock as seen in magnetic field measurements
L_ϕ	characteristic scale of the electrostatic potential variation in the shock front
L_{an}	characteristic scale of energy exchange due to anomalous resistivity
L_f	characteristic spatial size of the magnetic foot
L_r	width of the magnetic foot
$m_{i,e}$	ion, electron mass
$M_A = V_{up}/V_A$	Alfvenic Mach number, the ratio of the normal component of the upstream flow velocity to Alfven velocity
$M_{Ms} = V_{up}/V_{Ms}$	magnetosonic Mach number
$M_w = V_{w,max}/V_A$	nonlinear critical whistler Mach number
n_E	shock front normal determined from timing of electric field spikes measured onboard four satellites
n_B	shock front normal vector from magnetic field measurements
n	plasma density
$\hat{\mathbf{n}}$	shock front normal vector
n_r	number density of reflected ions
$R_{Li} = V_{up}/\Omega_{ci}$	convective ion gyroradius
R_{Le}	electron Larmor radius
$S_{\parallel}$	Poynting flux along the magnetic field

Parameter	Interpretation
T	total plasma temperature
$T_{i,e}$	ion, electron temperature
$T_{e\parallel}$	parallel to magnetic field electron temperature
$T_{e\perp}$	electron temperature perpendicular to the magnetic field
T_{Bi}	ion gyroperiod
$\overrightarrow{u}_{ed}$	the relative velocity of electrons carrying current
V_A	Alfven velocity
V_{up}	the normal component of the upstream velocity to the shock surface in its rest frame
V_{Ms}	velocity of the magnetosonic wave propagating in the same direction as the shock to the background magnetic field
$V_{w,max}$	highest possible velocity of nonlinear whistler wave that can stay in the upstream flow
V_{sw}	solar wind velocity
V_{ss}	relative shock spacecraft velocity
v_{ph}	phase velocity of ion sound wave
V_{ph}	phase velocity of wave
v_{is}	ion sound velocity
$V_{x,y,z}$	velocity components along corresponding axes
W_k	electric field energy density
λ	wavelength of precursor whistler wave
$\lambda_D = \epsilon_0 k_B T_e / ne^2$	Debye radius
ν_{eff}	effective collision frequency due to wave particle interaction
θ_{Bn}	the angle between the magnetic field and shock front normal
θ_{kB}	angle between the magnetic field vector and the wave vector
$\omega_{lh} \sim \sqrt{\Omega_{ci}\,\Omega_{ce}}$	lower hybrid frequency
ω_{pi}	ion plasma frequency
$\Omega_{ci,e} = eB/m_{i,e}$	ion, electron gyrofrequency
ω_p	electron plasma frequency

References

J.H. Adlam, J.E. Allen, The structure of strong collision-free hydromagnetic waves. Philos. Mag. **3**, 448–455 (1958). doi:10.1080/14786435808236833

U. Ascoli-Bartoli, S. Martellucci, M. Martone, Formation and development of hydromagnetic disturbances during the implosion phase of a preionized theta pinch (cariddi) (cn-21/75), in *Plasma Physics and Controlled Nuclear Fusion Research*, vol. I (1966), p. 275

H.U. Auster, K.H. Glassmeier, W. Magnes, O. Aydogar, D. Constantinescu, D. Fischer, K.H. Fornacon, E. Georgescu, P. Harvey, O. Hillenmaier, R. Kroth, M. Ludlam, Y. Narita, K. Okrafka, F. Plaschke, I. Richter, H. Schwarzl, B. Stoll, A. Valavanoglu, M. Wiedemann, The THEMIS fluxgate magnetometer. Space Sci. Rev. **135** (2008). doi:10.1007/s11214-008-9365-9

W.I. Axford, E. Leer, G. Skadron, The acceleration of cosmic rays by shock waves, in *International Cosmic Ray Conference*, vol. 11 (1977), pp. 132–137

S.D. Bale, F.S. Mozer, Measurement of large sale parallel and perpendicular electric fields on electron spatial scales in the terrestrial bow shock. Phys. Rev. Lett. **98**, 205001 (2007). doi:10.1103/PhysRevLett.98.205001

S.D. Bale, F.S. Mozer, T.S. Horbury, Density-transition scale at quasiperpendicular collisionless shocks. Phys. Rev. Lett. **91**(26), 265004 (2003). doi:10.1103/PhysRevLett.91.265004

S.D. Bale, F.S. Mozer, V.V. Krasnoselskikh, Direct measurement of the cross-shock electric potential at low plasma β, quasi-perpendicular bow shocks. ArXiv e-prints (2008)

S.D. Bale, P.J. Kellogg, D.E. Larson, R.P. Lin, K. Goetz, R.P. Lepping, Bipolar electrostatic structures in the shock transition region: evidence of electron phase space holes. Geophys. Res. Lett. **25**, 2929–2932 (1998). doi:10.1029/98GL02111

S.D. Bale, M.A. Balikhin, T.S. Horbury, V.V. Krasnoselskikh, H. Kucharek, E. Möbius, S.N. Walker, A. Balogh, D. Burgess, B. Lembége, E.A. Lucek, M. Scholer, S.J. Schwartz, M.F. Thomsen, Quasi-perpendicular shock structure and processes. Space Sci. Rev. **118**(1–4), 161–203 (2005). doi:10.1007/s11214-005-3827-0

M. Balikhin, M. Gedalin, Kinematic mechanism of electron heating in shocks: theory vs observations. Geophys. Res. Lett. **21**, 841–844 (1994). doi:10.1029/94GL00371

M. Balikhin, M. Gedalin, A. Petrukovich, New mechanism for heating in shocks. Phys. Rev. Lett. **70**, 1259–1262 (1993). doi:10.1103/PhysRevLett.70.1259

M. Balikhin, V. Krasnosselskikh, M. Gedalin, The scales in quasiperpendicular shocks. Adv. Space Res. **15**(8–9), 247–260 (1995). doi:10.1016/0273-1177(94)00105-A

M.A. Balikhin, T. Dudok de Wit, L.J.C. Woolliscroft, S.N. Walker, H. Alleyne, V. Krasnoselskikh, W.A.C. Mier–Jedrzejowicz, W. Baumjohann, Experimental determination of the dispersion of waves observed upstream of a quasi-perpendicular shock. Geophys. Res. Lett. **24**, 787–790 (1997a). doi:10.1029/97GL00671

M.A. Balikhin, S.N. Walker, T. Dudok de Witt, H.S.C. Alleyne, L.J.C. Woolliscroft, W.A.C. Mier-Jedrzejowicz, W. Baumjohann, Nonstationarity and low frequency turbulence at a quasi-perpendicular shock front. Adv. Space Res. **20**, 729–734 (1997b)

M.A. Balikhin, V. Krasnoselskikh, L.J.C. Woolliscroft, M. Gedalin, A study of the dispersion of the electron distribution in the presence of e and b gradients: application to electron heating at quasi-perpendicular shocks. J. Geophys. Res., Atmos. **103**, 2029–2040 (1998). doi:10.1029/97JA02463

M.A. Balikhin, M. Nozdrachev, M. Dunlop, V. Krasnoselskikh, S.N. Walker, H.S.C.K. Alleyne, V. Formisano, M. André, A. Balogh, A. Eriksson, K. Yearby, Observation of the terrestrial bow shock in quasi-electrostatic sub-shock regime. J. Geophys. Res., Atmos. **107**(8), 10 (2002). doi:10.1029/2001JA000327

M.A. Balikhin, O.A. Pokhotelov, S.N. Walker, E. Amata, M. Andre, M. Dunlop, H.S.C.K. Alleyne, Minimum variance free wave identification: application to cluster electric field data in the magnetosheath. Geophys. Res. Lett. **30**(10) (2003). doi:10.1029/2003GL016918

M. Balikhin, S. Walker, R. Treumann, H. Alleyne, V. Krasnoselskikh, M. Gedalin, M. Andre, M. Dunlop, A. Fazakerley, Ion sound wave packets at the quasiperpendicular shock front. Geophys. Res. Lett. **32**(24), 24106 (2005). doi:10.1029/2005GL024660

A. Balogh, M.W. Dunlop, S.W.H. Cowley, D.J. Southwood, J.G. Thomlinson, K.H. Glassmeier, G. Musmann, H. Lühr, S. Buchert, M.H. Acuña, D.H. Fairfield, J.A. Slavin, W. Riedler, K. Schwingenschuh, M.G. Kivelson, The cluster magnetic field investigation. Space Sci. Rev. **79**, 65–91 (1997). doi:10.1023/A:1004970907748

A. Bamba, R. Yamazaki, M. Ueno, K. Koyama, Small-scale structure of the sn 1006 shock with chandra observations. Astrophys. J. **589**, 827–837 (2003). doi:10.1086/374687

F. Begenal, J.W. Belcher, E.C. Sittler, R.P. Lepping, The uranian bow shock—Voyager 2 inbound observations of a high Mach number shock. J. Geophys. Res. **92**, 8603–8612 (1987). doi:10.1029/JA092iA08p08603

A.R. Bell, The acceleration of cosmic rays in shock fronts, I. Mon. Not. R. Astron. Soc. **182**, 147–156 (1978a)

A.R. Bell, The acceleration of cosmic rays in shock fronts, II. Mon. Not. R. Astron. Soc. **182**, 443–455 (1978b)

D. Biskamp, H. Welter, Ion heating in high-Mach-number, oblique, collisionless shock waves. Phys. Rev. Lett. **28**, 410–413 (1972). doi:10.1103/PhysRevLett.28.410

R.D. Blandford, J.P. Ostriker, Particle acceleration by astrophysical shocks. Astrophys. J. Lett. **221**, 29–32 (1978). doi:10.1086/182658

K.D. Cole, Effects of crossed magnetic and /spatially dependent/ electric fields on charged particle motion. Planet. Space Sci. **24**, 515–518 (1976). doi:10.1016/0032-0633(76)90096-9

H. Comişel, M. Scholer, J. Soucek, S. Matsukiyo, Non-stationarity of the quasi-perpendicular bow shock: comparison between cluster observations and simulations. Ann. Geophys. **29**, 263–274 (2011). doi:10.5194/angeo-29-263-2011

N. Cornilleau-Wehrlin, P. Chauveau, S. Louis, A. Meyer, J.M. Nappa, S. Perraut, L. Rezeau, P. Robert, A. Roux, C. De Villedary, Y. de Conchy, L. Friel, C.C. Harvey, D. Hubert, C. Lacombe, R. Manning, F. Wouters, F. Lefeuvre, M. Parrot, J.L. Pinçon, B. Poirier, W. Kofman, P. Louarn, The STAFF investigator team, the cluster spatio-temporal analysis of field fluctuations (staff) experiment. Space Sci. Rev. **79**, 107–136 (1997)

F.V. Coroniti, Dissipation discontinuities in hydromagnetic shock waves. J. Plasma Phys. **4**, 265 (1970)

R.C. Davidson, N.T. Gladd, C.S. Wu, J.D. Huba, Effects of finite beta plasma on the lower hybrid instability. Phys. Fluids **20**, 301 (1977)
L. Davis, R. Lüst, A. Schlüter, The structure of hydromagnetic shock waves, I: nonlinear hydromagnetic waves in a cold plasma. Z. Naturforsch. Teil A **13**, 916 (1958)
F. de Hoffmann, E. Teller, Magneto-hydrodynamic shocks. Phys. Rev. **80**, 692–703 (1950). doi:10.1103/PhysRev.80.692
P.M.E. Décréau, P. Fergeau, V. Krannosels'kikh, M. Leveque, P. Martin, O. Randriamboarison, F.X. Sene, J.G. Trotignon, P. Canu, P.B. Mogensen, Whisper, a resonance sounder and wave analyser: performances and perspectives for the cluster mission. Space Sci. Rev. **79**, 157–193 (1997). doi:10.1023/A:1004931326404
A.P. Dimmock, M.A. Balikhin, V.V. Krasnoselskikh, S.N. Walker, S.D. Bale, Y. Hobara, A statistical study of the cross-shock electric potential at low Mach number, quasi-perpendicular bow shock crossings using cluster data. J. Geophys. Res., Space Phys. **117**(A2), 2210 (2012). doi:10.1029/2011JA017089
C.P. Escoubet, R. Schmidt, M.L. Goldstein, Cluster—science and mission overview. Space Sci. Rev. **79**, 11–32 (1997)
V.G. Eselevich, A.G. Eskov, R.C. Kurtmullaev, A.I. Malyutin, Isomagnetic discontinuity in a collisionless shock wave. Sov. Phys. JETP **33**, 1120 (1971)
M.H. Farris, S.M. Petrinec, C.T. Russell, The thickness of the magnetosheath: constraints on the polytropic index. Geophys. Res. Lett. **18**, 1821 (1991). doi:10.1029/91GL02090
M.H. Farris, C.T. Russell, M.F. Thomsen, Magnetic structure of the low beta, quasi-perpendicular shock. J. Geophys. Res., Atmos. **98**, 15285–15294 (1993). doi:10.1029/93JA00958
W.C. Feldman, R.C. Anderson, J.R. Asbridge, S.J. Bame, J.T. Gosling, R.D. Zwickl, Plasma electron signature of magnetic connection to the Earth's bow shock—isee 3. J. Geophys. Res., Atmos. **87**(A2), 632–642 (1982)
W.C. Feldman, R.C. Anderson, S.J. Bame, S.P. Gary, J.T. Gosling, D.J. McComas, M.F. Thomsen, G. Paschmann, M.M. Hoppe, Electron velocity distributions near the Earth's bow shock. J. Geophys. Res., Atmos. **88**, 96–110 (1983)
V. Formisano, Measurement of the potential drop across the Earth's collisionless bow shock. Geophys. Res. Lett. **9**, 1033 (1982)
V. Formisano, Collisionless shock waves in space and astrophysical plasmas, in *Proc. ESA Workshop on Future Missions in Solar, Heliospheric and Space Plasma Physics*, vol. ESA SP-235 (1985), p. 83
V. Formisano, R. Torbert, Ion acoustic wave forms generated by ion-ion streams at the Earth's bow shock. Geophys. Res. Lett. **9**, 207 (1982)
S.A. Fuselier, D.A. Gurnett, R.J. Fitzenreiter, The downshift of electron plasma oscillations in the electron foreshock region. J. Geophys. Res. **90**, 3935–3946 (1985). doi:10.1029/JA090iA05p03935
A.A. Galeev, Collisionless shocks, in *Physics of Solar Planetary Environment; Proceedings of the International Symposium on Solar-Terrestrial Physics*, Boulder, CO, June 7–18, 1976, ed. by D.J. Williams (AGU, Washington, 1976), pp. 464–490
A.A. Galeev, R.Z. Sagdeev, Current instabilities and anomalous resistivity of plasma, in *Basic Plasma Physics: Selected Chapters, Handbook of Plasma Physics*, vol. 1, ed. by A.A. Galeev, R.N. Sudan (1984), p. 271
A.A. Galeev, R.N. Sudan, *Basic Plasma Physics. Selected Chapters. Handbook of Plasma Physics*, vols. 1 and 2 (1989)
A.A. Galeev, V.V. Krasnoselskikh, V.V. Lobzin, Fine structure of the front of a quasi-perpendicular supercritical collisionless shock wave. Sov. J. Plasma Phys. **14**, 1192–1200 (1988)
A.A. Galeev, C.F. Kennel, V.V. Krasnoselskikh, V.V. Lobzin, The role of whistler oscillations in the formation of the structure of high Mach number collisionless shock, in *Plasma Astrophysics* (1989), pp. 165–171
M. Gedalin, Ion reflection at the shock front revisited. J. Geophys. Res. **101**, 4871 (1996). doi:10.1029/95JA03669
M. Gedalin, Ion heating in oblique low-Mach number shocks. Geophys. Res. Lett. **24**, 2511 (1997)
M. Gedalin, K. Gedalin, M. Balikhin, V. Krasnosselskikh, L.J.C. Woolliscroft, Demagnetization of electrons in inhomogeneous $E_{\perp}B$: implications for electron heating in shocks. J. Geophys. Res. **100**, 19911–19918 (1995a). doi:10.1029/95JA01399
M. Gedalin, K. Gedalin, M. Balikhin, V. Krasnosselskikh, Demagnetization of electrons in the electromagnetic field structure, typical for quasi-perpendicular collisionless shock front. J. Geophys. Res. **100**, 9481–9488 (1995b). doi:10.1029/94JA03369
G. Goldenbaum, E. Hintz, Experimental study of shock wave formation in an almost collisionfree plasma. Phys. Plasmas **8**, 2111–2112 (1965). doi:10.1063/1.1761164
C.C. Goodrich, J.D. Scudder, The adiabatic energy change of plasma electrons and the frame dependence of the cross shock potential at collisionless magnetosonic shock waves. J. Geophys. Res., Atmos. **89**, 6654–6662 (1984)

E.W. Greenstadt, R.W. Fredricks, Shock systems in collisionless space plasmas, in *Solar System Plasma Physics*, vol. 3, ed. by L.J. Lanzerotti, C.F. Kennel, E.N. Parker (North Holland, Amsterdam, 1979), pp. 3–43

D.A. Gurnett, Plasma waves and instabilities, in *Collisionless Shocks in the Heliosphere: Reviews of Current Research*, ed. by B.T. Tsurutani, R.G. Stone Geophysical Monograph (AGU, Washington, 1985), pp. 207–224

G. Gustafsson, R. Bostrom, B. Holback, G. Holmgren, A. Lundgren, K. Stasiewicz, L. Ahlen, F.S. Mozer, D. Pankow, P. Harvey, P. Berg, R. Ulrich, A. Pedersen, R. Schmidt, A. Butler, A.W.C. Fransen, D. Klinge, C.-G. Falthammar, P.-A. Lindqvist, S. Christenson, J. Holtet, B. Lybekk, T.A. Sten, P. Tanskanen, K. Lappalainen, J. Wygant, The electric field and wave experiment for the cluster mission. Space Sci. Rev. **79**, 137–156 (1997)

P. Hellinger, A. Mangeney, Upstream whistlers generated by protons reflected from a quasi-perpendicular shock. J. Geophys. Res., Space Phys. **102**(A5), 9809–9819 (1997). doi:10.1029/96JA03826

P. Hellinger, P. Trávníček, H. Matsumoto, Reformation of perpendicular shocks: hybrid simulations. Geophys. Res. Lett. **29**(24), 240000 (2002). doi:10.1029/2002GL015915

P. Hellinger, P. Trávníček, B. Lembège, P. Savoini, Emission of nonlinear whistler waves at the front of perpendicular supercritical shocks: hybrid versus full particle simulations. Geophys. Res. Lett. **34**, 14109 (2007). doi:10.1029/2007GL030239

J.P. Heppner, N.C. Maynard, T.L. Aggson, Early results from isee-1 electric field measurements. Space Sci. Rev. **22**, 777–789 (1978)

Y. Hobara, S.N. Walker, M. Balikhin, O.A. Pokhotelov, M. Gedalin, V. Krasnoselskikh, M. Hayakawa, M. André, M. Dunlop, H. Rème, A. Fazakerley, Cluster observations of electrostatic solitary waves near the Earth's bow shock. J. Geophys. Res., Atmos. **113**, 05211 (2008). doi:10.1029/2007JA012789

Y. Hobara, M. Balikhin, V. Krasnoselskikh, M. Gedalin, H. Yamagishi, Statistical study of the quasi-perpendicular shock ramp widths. J. Geophys. Res. **115**, 11106 (2010). doi:10.1029/2010JA015659

T.S. Horbury, P.J. Cargill, E.A. Lucek, A. Balogh, M.W. Dunlop, T.M. Oddy, C. Carr, P. Brown, A. Szabo, K.-H. Fornaçon, Cluster magnetic field observations of the bowshock: orientation, motion and structure. Ann. Geophys. **19**, 1399–1409 (2001). doi:10.5194/angeo-19-1399-2001

T.S. Horbury, P.J. Cargill, E.A. Lucek, J. Eastwood, A. Balogh, M.W. Dunlop, K.-H. Fornaçon, E. Georgescu, Four spacecraft measurements of the quasi-perpendicular terrestrial bowshock: orientation and motion. J. Geophys. Res., Atmos. **107**(A8), 10–11 (2002). doi:10.1029/2001JA000273

V.I. Karpman, Structure of the shock front propagating at an angle of the magnetic field in a low density plasma. Sov. Phys. Tech. Phys. Engl. Transl. **8**, 715 (1964)

V.I. Karpman, J.K. Alekhin, N.D. Borisov, N.A. Rjabova, Electrostatic waves with frequencies exceeding gyrofrequency in magnetosphere. Astrophys. Space Sci. **22**(2), 267–278 (1973). doi:10.1007/BF00647426

C.F. Kennel, J.P. Edmiston, T. Hada, A quarter century of collisionless shock research, in *Collisionless Shocks in the Heliosphere: A Tutorial Review*, ed. by R.G. Stone, B.T. Tsurutani Geophysical Monograph, vol. 34 (American Geophysical Union, Washington, 1985), pp. 1–36

S. Klimov, S. Savin, Y. Aleksevich, G. Avanesova, V. Balebanov, M. Balikhin, A. Galeev, B. Gribov, M. Nozdrachev, V. Smirnov, A. Sokolov, O. Vaisberg, P. Oberc, Z. Krawczyk, S. Grzedzielski, J. Juchniewicz, K. Nowak, D. Orlowski, B. Parfianovich, D. Wozniak, Z. Zbyszynski, Y. Voita, P. Triska, Extremely-low-frequency plasma waves in the environment of comet Halley. Nature **321**, 292–293 (1986)

K. Koyama, R. Petre, E.V. Gotthelf, U. Hwang, M. Matsuura, M. Ozaki, S.S. Holt, Evidence for shock acceleration of high-energy electrons in the supernova Remnant sn1006. Nature **378**, 255–258 (1995). doi:10.1038/378255a0

V. Krasnoselskikh, Nonlinear motions of a plasma across a magnetic field. Sov. Phys. JETP **62**, 282–294 (1985)

V.V. Krasnoselskikh, E.N. Kruchina, A.S. Volokitin, G. Thejappa, Fast electron generation in quasiperpendicular shocks and type II solar radiobursts. Astron. Astrophys. **149**, 323–329 (1985)

V.V. Krasnoselskikh, M.A. Balikhin, H.S.C. Alleyne, S.I. Klimov, W.A.C. Mier-Jedrzejowicz, A.K. Pardaens, A. Petrukovich, D.J. Southwood, T. Vinogradova, L.J.C. Woolliscroft, On the nature of low frequency turbulence in the foot of strong quasi-perpendicular shocks. Adv. Space Res. **11**(9), 15–18 (1991)

V.V. Krasnoselskikh, B. Lembége, P. Savoini, V.V. Lobzin, Nonstationarity of strong collisionless quasiperpendicular shocks: theory and full particle numerical simulations. Phys. Plasmas **9**(4), 1192–1209 (2002). doi:10.1063/1.1457465

G.F. Krymskii, A regular mechanism for the acceleration of charged particles on the front of a shock wave. Dokl. Akad. Nauk SSSR **234**, 1306–1308 (1977)

R.H. Kurtmullaev, J.E. Nesterikhin, V.I. Pilsky, Shock waves in partially ionized plasma, in *Phenomena in Ionized Gases, VIII International Conference* (1967), p. 459

R.K. Kurtmullaev, V.K. Malinovskii, Y.E. Nesterikhin, A.G. Ponomarenko, Excitation of strong collisionless shock waves in a plasma. J. Appl. Mech. Tech. Phys. **6**, 68–73 (1965). doi:10.1007/BF00915616
C. Lacombe, A. Mangeney, C. Harvey, J. Scudder, Electron plasma waves upstream of the Earth's bow shock. J. Geophys. Res. **90**, 73–94 (1985). doi:10.1029/JA090iA01p00073
J.M. Laming, Accelerated electrons in Cassiopeia A: an explaination for the hard x-ray tail. Astrophys. J. **546**, 1149–1158 (2001)
B. Lefebvre, S.J. Schwartz, A.F. Fazakerley, P. Décréau, Electron dynamics and cross-shock potential at the quasi-perpendicular Earth's bow shock. J. Geophys. Res. **112**, 09212 (2007). doi:10.1029/2007JA012277
B. Lembège, S.N. Walker, P. Savoini, M.A. Balikhin, V. Krasnoselskikh, The spatial sizes of electric and magnetic field gradients in a simulated shock. Adv. Space Res. **24**, 109–112 (1999)
B. Lembège, J. Giacalone, M. Scholer, T. Hada, M. Hoshino, V. Krasnoselskikh, H. Kucharek, P. Savoini, T. Terasawa, Selected problems in collisionless-shock physics. Space Sci. Rev. **110**, 161–226 (2004). doi:10.1023/B:SPAC.0000023372.12232.b7
M.M. Leroy, A. Mangeney, A theory of energization of solar wind electrons by the Earth's bow shock. Ann. Geophys. **2**, 449–456 (1984)
M.M. Leroy, D. Winske, C.C. Goodrich, C.S. Wu, K. Papadopoulos, The structure of perpendicular bow shocks. J. Geophys. Res. **87**(A7), 5081–5094 (1982). doi:10.1029/JA087iA07p05081
P.C. Liewer, V.K. Decyk, J.M. Dawson, B. Lembège, Numerical studies of electron dynamics in oblique quasi-perpendicular collisionless shock waves. J. Geophys. Res., Atmos. **96**(A6), 9455 (1991)
W.A. Livesey, C.T. Russell, C.F. Kennel, A comparison of specularly reflected gyrating ion orbits with observed shock foot thicknesses. J. Geophys. Res., Atmos. **89**(A8), 6824–6828 (1984)
V.V. Lobzin, V.V. Krasnoselskikh, S.J. Schwartz, I. Cairns, B. Lefebvre, P. Décréau, A. Fazakerley, Generation of downshifted oscillations in the electron foreshock: a loss-cone instability. Geophys. Res. Lett. **32**, 18101 (2005). doi:10.1029/2005GL023563
V.V. Lobzin, V.V. Krasnoselskikh, J.-M. Bosqued, J.-L. Pinçon, S.J. Schwartz, M. Dunlop, Nonstationarity and reformation of high-Mach-number quasiperpendicular shocks: cluster observations. Geophys. Res. Lett. **34**, 5107 (2007). doi:10.1029/2006GL029095
E. Mach, J. Arbes, Einige versuche über totale Reflexion und anomale Dispersion. Ann. Phys. **263**, 436–444 (1886). doi:10.1002/andp.18862630307
E. Mach, P. Salcher, Photographische fixirung der durch Projectile in der Luft eingeleiteten Vorgänge. Ann. Phys. **268**, 277–291 (1887). doi:10.1002/andp.18872681008
S. Matsukiyo, M. Scholer, On microinstabilities in the foot of high Mach number perpendicular shocks. J. Geophys. Res., Space Phys. **111**(A6), 6104 (2006). doi:10.1029/2005JA011409
C. Mazelle, B. Lembége, A. Morgenthaler, K. Meziane, T.S. Horbury, V. Génot, E.A. Lucek, I. Dandouras, Self-reformation of the quasi-perpendicular shock: cluster observations, in *Twelfth International Solar Wind Conference*, vol. 1216 (2010), pp. 471–474. doi:10.1063/1.3395905
J.D. Means, Use of the three-dimensional covariance matrix in analyzing the polarization properties of plane waves. J. Geophys. Res. **77**, 5551–5559 (1972)
M.M. Mellott, Subcritical collisionless shock waves, in *Washington DC American Geophysical Union Geophysical Monograph Series*, vol. 35 (1985), pp. 131–140
J.J. Mitchell, S.J. Schwartz, U. Auster, Electron cross talk and asymmetric electron distributions near the Earth's bow shock. Ann. Geophys. **30**, 503–513 (2012). doi:10.5194/angeo-30-503-2012
D.L. Morse, W.W. Destler, P.L. Auer, Nonstationary behavior of collisionless shocks. Phys. Rev. Lett. **28**, 13–16 (1972). doi:10.1103/PhysRevLett.28.13
N.F. Ness, K.W. Behannon, R.P. Lepping, Y.C. Whang, K.H. Schatten, Magnetic field observations near venus: preliminary results from Mariner 10. Science **183**, 1301–1306 (1974). doi:10.1126/science.183.4131.1301
N.F. Ness, M.H. Acuna, R.P. Lepping, J.E.P. Connerney, K.W. Behannon, L.F. Burlaga, F.M. Neubauer, Magnetic field studies by Voyager 1—preliminary results at saturn. Science **212**, 211–217 (1981). doi:10.1126/science.212.4491.211
J.A. Newbury, C.T. Russell, Observations of a very thin collisionless shock. Geophys. Res. Lett. **23**, 781 (1996). doi:10.1029/96GL00700
J.A. Newbury, C.T. Russell, M. Gedalin, The ramp widths of high-Mach-number, quasi-perpendicular collisionless shocks. J. Geophys. Res., Atmos. **103**(A12), 29581–29593 (1998). doi:10.1029/1998JA900024
M. Oka, T. Terasawa, Y. Seki, M. Fujimoto, Y. Kasaba, H. Kojima, I. Shinohara, H. Matsui, H. Matsumoto, Y. Saito, T. Mukai, Whistler critical Mach number and electron acceleration at the bow shock: geotail observation. Geophys. Res. Lett. **33**, 24104 (2006). doi:10.1029/2006GL028156
K. Papadopoulos, Electron acceleration in magnetosonic shock fronts. Technical report, 1981
K. Papadopoulos, Microinstabilities and anomalous transport in collisionless shocks, in *Advances in Space Plasma Physics*, ed. by W. Grossmann, E.M. Campbell, B. Buti (1985a), p. 289

K. Papadopoulos, Microinstabilities and anomolous transport, in *Collisionless Shocks in the Heliosphere: A Tutorial Review*, ed. by R.G. Stone, B.T. Tsurutani Geophysical Monograph, vol. 34 (American Geophysical Union, Washington, 1985b), pp. 59–90

G. Paschmann, P.W. Daly, *Analysis Methods for Multi-spacecraft Data*. ISSI Scientific Reports Series sr-001, esa/issi, vol. 1 (1998). ISSN:1608-280x

J.W.M. Paul, L.S. Holmes, M.J. Parkinson, J. Sheffield, Experimental observations on the structure of collisionless shock waves in a magnetized plasma. Nature **208**, 133–135 (1965). doi:10.1038/208133a0

J.W.M. Paul, G.C. Goldenbaum, A. Iiyoshi, L.S. Holmes, R.A. Hardcastle, Measurement of electron temperatures produced by collisionless shock waves in a magnetized plasma. Nature **216**, 363–364 (1967). doi:10.1038/216363a0

J.-L. Pinçon, K.-H. Glassmeier, Multi-spacecraft methods of wave field characterisation, in *ISSI Scientific Reports Series*, vol. 8 (2008), pp. 47–54

J.-L. Pinçon, P.M. Kintner, P.W. Schuck, C.E. Seyler, Observation and analysis of lower hybrid solitary structures as rotating eigenmodes. J. Geophys. Res., Atmos. **102**, 17283–17296 (1997)

T. Piran, Magnetic fields in gamma-ray bursts: a short overview. in *American Institute of Physics Conference Series*, vol. 784, ed. by E.M. de Gouveia dal Pino, G. Lugones, A. Lazarian, 2005, pp. 164–174. doi:10.1063/1.2077181

K.B. Quest, Simulations of high mach number perpendicular shocks with resistive electrons. J. Geophys. Res., Atmos. **91**(A8), 8805–8815 (1986)

H. Reme, J.M. Bosqued, J.A. Sauvaud, A. Cros, J. Dandouras, C. Aoustin, J. Bouyssou, T. Camus, J. Cuvilo, C. Martz, J.L. Médale, H. Perrier, D. Romefort, J. Rouzaud, D. D'Uston, E. Möbius, K. Crocker, M. Granoff, L.M. Kistler, M. Popecki, D. Hovestadt, B. Klecker, G. Paschmann, M. Scholer, C.W. Carlson, D.W. Curtis, R.P. Lin, J.P. McFadden, V. Formisano, E. Amata, M.B. Bavassano-Cattaneo, P. Baldetti, G. Belluci, R. Bruno, G. Chionchio, A. di Lellis, E.G. Shelley, A.G. Ghielmetti, W. Lennartsson, A. Korth, U. Rosenbauer, R. Lundin, S. Olsen, G.K. Parks, M. McCarthy, H. Balsiger, The cluster ion spectrometry (cis) experiment. Space Sci. Rev. **79**, 303–350 (1997)

C.T. Russell, On the relative locations of the bow shocks of the terrestrial planets. Geophys. Res. Lett. **4**, 387–390 (1977). doi:10.1029/GL004i010p00387

C.T. Russell, Planetary bow shocks, in *Washington DC American Geophysical Union Geophysical Monograph Series*, vol. 35 (1985), pp. 109–130

C.T. Russell, M.M. Mellot, E.J. Smith, J.H. King, Multiple spacecraft observations on interplanetary shocks: four spacecraft determination of shock normals. J. Geophys. Res., Atmos. **88**, 4739–4748 (1983)

R.Z. Sagdeev, Asymptotic methods in the hydrodynamic theory of stability, in *Lectures Presented at the Trieste Seminar on Plasma Physics* (1965a), p. 625

R.Z. Sagdeev, Landau damping and finite resistivity instability in plasmas, in *Lectures Presented at the Trieste Seminar on Plasma Physics* (1965b), p. 555

R.Z. Sagdeev, Cooperative phenomena and shock waves in collisionless plasmas. Rev. Plasma Phys. **4**, 23 (1966)

R.Z. Sagdeyev, "Shock" waves in rarefied plasma, in *Ionization Phenomena in Gases*, vol. II, ed. by N.R. Nilsson (1960), p. 1081

J.C. Samson, J.V. Olson, Some comments on the descriptions of the polarization states of waves. Geophys. J. R. Astron. Soc. **61**, 115–129 (1980). doi:10.1111/j.1365-246X.1980.tb04308.x

M. Scholer, D. Burgess, Transition scale at quasiperpendicular collisionless shocks: full particle electromagnetic simulations. Phys. Plasmas **13**(6), 062101 (2006). doi:10.1063/1.2207126

M. Scholer, S. Matsukiyo, Nonstationarity of quasi-perpendicular shocks: a comparison of full particle simulations with different ion to electron mass ratio. Ann. Geophys. **22**, 2345–2353 (2004)

M. Scholer, I. Shinohara, S. Matsukiyo, Quasi-perpendicular shocks: length scale of the cross-shock potential, shock reformation, and implication for shock surfing. J. Geophys. Res., Space Phys. **108**, 1014 (2003). doi:10.1029/2002JA009515

S.J. Schwartz, Shock and discontinuity normals, mach numbers, and related parameters, in *ISSI Scientific Reports Series*, vol. 1 (1998), pp. 249–270

S.J. Schwartz, M.F. Thomsen, J.T. Gosling, Ions upstream of the Earth's bow shock—a theoretical comparison of alternative source populations. J. Geophys. Res. **88**, 2039–2047 (1983). doi:10.1029/JA088iA03p02039

S.J. Schwartz, M.F. Thomsen, S.J. Bame, J. Stansberry, Electron heating and the potential jump across fast mode shocks. J. Geophys. Res. **93**(A11), 12923–12931 (1988). doi:10.1029/JA093iA11p12923

S.J. Schwartz, E. Henley, J. Mitchell, V. Krasnoselskikh, Electron temperature gradient scale at collisionless shocks. Phys. Rev. Lett. **107**(21), 215002 (2011). doi:10.1103/PhysRevLett.107.215002

N. Sckopke, G. Paschmann, S.J. Bame, J.T. Gosling, C.T. Russell, Evolution of ion distributions across the nearly perpendicular bow shock—specularly and non-specularly reflected-gyrating ions. J. Geophys. Res., Atmos. **88**(A8), 6121–6136 (1983)

J.D. Scudder, A review of the physics of electron heating at collisionless shocks. Adv. Space Res. **15**, 181 (1995)
J.D. Scudder, A. Mangeney, C. Lacombe, C.C. Harvey, T.L. Aggson, R.R. Anderson, J.T. Gosling, G. Paschmann, C.T. Russell, The resolved layer of a collisionless high β supercritical quasi-perpendicular shock wave, 1: Rankine–Hugoniot geometry currents and stationarity. J. Geophys. Res., Atmos. **91**, 11019–11052 (1986a)
J.D. Scudder, A. Mangeney, C. Lacombe, C.C. Harvey, T.L. Aggson, The resolved layer of a collisionless high β supercritical quasi-perpendicular shock wave, 2: dissipative fluid electrodynamics. J. Geophys. Res., Atmos. **91**, 11053 (1986b)
J.D. Scudder, A. Mangeney, C. Lacombe, C.C. Harvey, C.S. Wu, R.R. Anderson, The resolved layer of a collisionless high β supercritical quasi-perpendicular shock wave, 3: Vlasov electrodynamics. J. Geophys. Res., Atmos. **91**, 11075 (1986c)
V. Smirnov, O. Vaisberg, Evidence of the nonlinear structure at the bow shock front, in *Collisionless Shocks*, Budapest, ed. by K. Szego (1987), pp. 70–76
D. Sundkvist, V. Krasnoselskikh, S.D. Bale, S.J. Schwartz, J. Soucek, F. Mozer, Dispersive nature of high mach number collisionless plasma shocks: Poynting flux of oblique whistler waves. Phys. Rev. Lett. **108**(2), 025002 (2012). doi:10.1103/PhysRevLett.108.025002
M.F. Thomsen, J.T. Gosling, S.J. Bame, K.B. Quest, D. Winske, On the noncoplanarity of the magnetic field within a fast collisionless shock. J. Geophys. Res., Atmos. **92**(A3), 2305–2314 (1987)
D.A. Tidman, N.A. Krall, *Shockwaves in Collisionless Plasmas* (Wiley, New York, 1971)
A. Tjulin, A.I. Eriksson, M. André, Lower hybrid cavities in the inner magnetosphere. Geophys. Res. Lett. **30**, 17–21 (2003). doi:10.1029/2003GL016915
O.L. Vaisberg, A.A. Galeev, G.N. Zastenker, S.I. Klimov, M.N. Nozdrachev, R.Z. Sagdeev, A.I. Sokolov, V.D. Shapiro, Electron acceleration at the front of strong collisionless shock waves. Zh. Èksp. Teor. Fiz. **85**, 1232–1243 (1983)
O. Vaisberg, S. Klimov, G. Zastenker, M. Nozdrachev, A. Sokolov, V. Smirnov, S. Savin, L. Avanov, Relaxation of plasma at the shock front. Adv. Space Res. **4**, 265–275 (1984). doi:10.1016/0273-1177(84)90320-X
P. Veltri, G. Zimbardo, Electron whistler interaction at the Earths bow shock, 2: electron pitch-angle diffusion. J. Geophys. Res. **98**(A8), 13335–13346 (1993)
S.N. Walker, M.A. Balikhin, M.N. Nozdrachev, Ramp nonstationarity and the generation of whistler waves upstream of a strong quasiperpendicular shock. Geophys. Res. Lett. **26**(10), 1357–1360 (1999a). doi:10.1029/1999GL900210
S.N. Walker, M.A. Balikhin, H.S.C.K. Alleyne, W. Baumjohann, M. Dunlop, Observations of a very thin shock. Adv. Space Res. **24**, 47–50 (1999b)
S.N. Walker, M.A. Balikhin, H.S.C.K. Alleyne, Y. Hobara, M. André, M.W. Dunlop, Lower hybrid waves at the shock front: a reassessment. Ann. Geophys. **26**, 699–707 (2008). http://www.ann-geophys.net/26/699/2008/
S. Walker, H. Alleyne, M. Balikhin, M. André, T. Horbury, Electric field scales at quasi-perpendicular shocks. Ann. Geophys. **22**(7), 2291–2300 (2004). http://www.ann-geophys.net/22/2291/2004/
L.B. Wilson III, A. Koval, A. Szabo, A. Breneman, C.A. Cattell, K. Goetz, P.J. Kellogg, K. Kersten, J.C. Kasper, B.A. Maruca, M. Pulupa, Observations of electromagnetic whistler precursors at supercritical interplanetary shocks. Geophys. Res. Lett. **39**, 8109 (2012). doi:10.1029/2012GL051581
L.C. Woods, On the structure of collisionless magneto-plasma shock waves at super-critical Alfvèn-Mach numbers. J. Plasma Phys. **3**(3), 435–447 (1969)
L.C. Woods, On double-structured, perpendicular, magneto-plasma shock waves. Plasma Phys. **13**, 289–302 (1971). doi:10.1088/0032-1028/13/4/302
L.J.C. Woolliscroft, H.S.C. Alleyne, C.M. Dunford, A. Sumner, J.A. Thompson, S.N. Walker, K.H. Yearby, A. Buckley, S. Chapman, M.P. Gough, The digital wave-processing experiment on cluster. Space Sci. Rev. **79**, 209–231 (1997)
C.S. Wu, A fast Fermi process—energetic electrons accelerated by a nearly perpendicular bow shock. J. Geophys. Res. **89**, 8857–8862 (1984). doi:10.1029/JA089iA10p08857
J.R. Wygant, M. Bensadoun, F.S. Mozer, Electric field measurements at subcritical, oblique bow shock crossings. J. Geophys. Res., Atmos. **92**(A10), 11109–11121 (1987)
G. Zank, H. Pauls, I. Cairns, G. Webb, Interstellar pickup ions and quasi-perpendicular shocks: implications for the termination shock and interplanetary shocks. J. Geophys. Res. **101**, 457–477 (1996)